10 Nucleon matrix elements

Authors: S. Collins, R. Gupta, A. Nicholson, H. Wittig

A large number of experiments testing the Standard Model (SM) and searching for physics Beyond the Standard Model (BSM) involve either free nucleons (proton and neutron beams) or the scattering of electrons, muons, neutrinos and dark matter off nuclear targets. Necessary ingredients in the analysis of the experimental results are the matrix elements of various probes (fundamental currents or operators in a low-energy effective theory) between nucleon or nuclear states. The goal of lattice-QCD calculations in this context is to provide high-precision predictions of these matrix elements, the simplest of which give the nucleon charges and form factors. Determinations of the charges, the first Mellin moments of parton distribution functions, are the most mature and in this review we update results for twelve quantities, the isovector and flavour-diagonal axial vector, scalar and tensor charges, given in the two previous FLAG reports in 2019 and 2021 [1, 2]. In this edition in Sec. 10.5, we also add a review of the second Mellin moments for the vector, axial and tensor currents that give the momentum fraction, the helicity moment and the transversity moment as a sufficient number of calculations have been performed and the results are considered robust.

Other quantities that are not being reviewed but for which significant progress has been made in the last five years are the nucleon axial vector and electromagnetic form factors [3–17] and parton distribution functions from matrix elements of nonlocal operators [18–22]. The more challenging calculations of nuclear matrix elements that are needed, for example, to calculate the cross-sections of neutrinos or dark matter scattering off nuclear targets, are proceeding along three paths. The first is based on direct evaluations of matrix elements calculated with initial and final states consisting of multiple nucleons [23, 24]. The second proceeds by matching few-nucleon observables computed in lattice QCD to nuclear effective field theories and extrapolating in the mass number A, while the third strategy uses the HAL QCD method [25] or the direct method [26] to extract nuclear forces and currents from lattice calculations as input for *ab initio* many-body methods. We expect future FLAG reviews to include results on these quantities once a sufficient level of control over all the systematics is reached.

10.1 Isovector and flavour-diagonal charges of the nucleon

The simplest nucleon matrix elements are composed of local quark-bilinear operators, $\overline{q_i}\Gamma_\alpha q_j$, where Γ_α can be any of the sixteen Dirac matrices. In this report, we consider two types of flavour structures: (a) when $i = u$ and $j = d$. These $\overline{u}\Gamma_\alpha d$ operators arise in $W^\pm$ mediated weak interactions such as in neutron or pion decay. We restrict the discussion to the matrix elements of the axial-vector (A), scalar (S) and tensor (T) currents, which give the isovector charges, $g^{u-d}_{A,S,T}$.[1] (b) When $i = j$ for $j \in \{u, d, s\}$, there is no change of flavour, e.g., in processes mediated via the electromagnetic or weak neutral interaction or dark matter. These γ or Z^0 or possible dark matter mediated processes couple to all flavours with their corresponding charges. Since these probes interact with nucleons within nuclear targets, one has to include the effects of QCD (to go from the couplings defined at the quark and gluon

[1] In the isospin-symmetric limit $\langle p|\bar{u}\Gamma d|n\rangle = \langle p|\bar{u}\Gamma u - \bar{d}\Gamma d|p\rangle = \langle n|\bar{d}\Gamma d - \bar{u}\Gamma u|n\rangle$ for nucleon and proton states $|p\rangle$ and $|n\rangle$, respectively. The latter two (equivalent) isovector matrix elements are computed on the lattice.

level to those for nucleons) and nuclear forces in order to make contact with experiments. The isovector and flavour-diagonal charges, given by the matrix elements of the corresponding operators calculated between nucleon states, are these nucleon level couplings. Here we review results for the light and strange flavours, $g^u_{A,S,T}$, $g^d_{A,S,T}$, and $g^s_{A,S,T}$ and the isovector charges $g^{u-d}_{A,S,T}$.

The isovector and flavour-diagonal operators also arise in BSM theories due to the exchange of novel force carriers or as effective interactions due to loop effects. The associated couplings are defined at the energy scale $\Lambda_{\rm BSM}$, while lattice-QCD calculations of matrix elements are carried out at a hadronic scale, μ, of a few GeV. The tool for connecting the couplings at the two scales is the renormalization group. Since the operators of interest are composed of quark fields (and more generally also of gluon fields), the predominant change in the corresponding couplings under a scale transformation is due to QCD. To define the operators and their couplings at the hadronic scale μ, one constructs renormalized operators, whose matrix elements are finite in the continuum limit. This requires calculating both multiplicative renormalization factors, including the anomalous dimensions and finite terms, and the mixing with other operators. We discuss the details of the renormalization factors needed for each of the six operators reviewed in this report in Sec. 10.1.3.

Once renormalized operators are defined, the nucleon matrix elements of interest are extracted using expectation values of two-point and three-point correlation functions illustrated in Fig. 41, where the latter can have both quark-line connected and disconnected contributions. In order to isolate the ground-state matrix element, these correlation functions are analyzed using their spectral decomposition. The current practice is to fit the n-point correlation functions (or ratios involving three- and two-point functions) including contributions from one or two excited states. In some cases, such as axial and vector operators, Ward identities provide relations between correlation functions, or ground-state matrix elements, or facilitate the calculation of renormalization factors. It is important to ensure that all such Ward identities are satisfied in lattice calculations, especially as in the case of axial form factors where they provide checks of whether excited-state contamination has been removed in obtaining matrix elements within ground-state nucleons [14, 27, 28].

The ideal situation occurs if the time separation τ between the nucleon source and sink positions, and the distance of the operator-insertion time from the source and the sink, t and $\tau - t$, respectively, are large enough such that the contribution of all excited states is negligible. In the limit of large τ, the ratio of noise to signal in the nucleon two- and three-point correlation functions grows exponentially as $e^{(M_N - \frac{3}{2}M_\pi)\tau}$ [29, 30], where M_N and M_π are the masses of the nucleon and the pion, respectively. Therefore, in particular at small pion masses, maintaining reasonable errors for large τ is challenging, with most current calculations limited to $\tau \lesssim 1.5$ fm. In addition, the mass gap between the ground and excited (including multi-particle) states is smaller than in the meson sector and at these separations, excited-state effects can be significant. The approach commonly taken is to first obtain results with high statistics at multiple values of τ, using the methods described in Sec. 10.1.1. Then, as mentioned above, excited-state contamination is removed by fitting the data using a fit form involving one or two excited states. The different strategies that have been employed to minimize excited-state contamination are discussed in Sec. 10.1.2.

Usually, the quark-connected part of the three-point function (corresponding to the plot in the centre of Fig. 41) is computed via the so-called "sequential propagator method", which uses the product of two quark propagators between the positions of the initial and the final

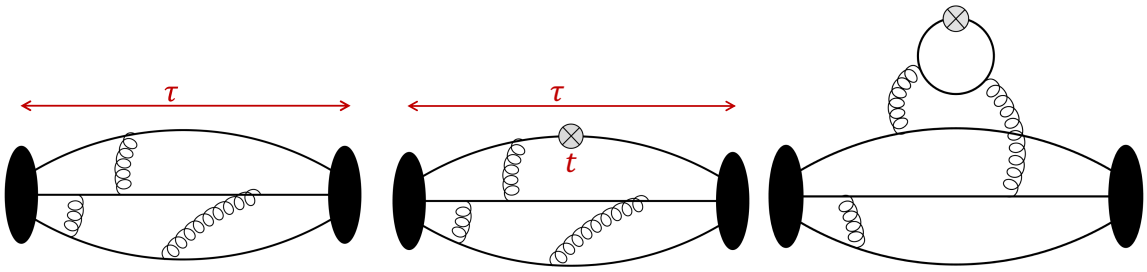

Figure 41: The two- and three-point correlation functions (illustrated by Feynman diagrams) that need to be calculated to extract the ground-state nucleon matrix elements. (Left) the nucleon two-point function. (Middle) the connected three-point function with source-sink separation τ and operator-insertion time slice t. (Right) the quark-disconnected three-point function with operator insertion at t.

nucleons as a source term for another inversion of the lattice Dirac operator. This implies that the position of the sink timeslice is fixed at some chosen value. Varying the value of the source-sink separation τ then requires the calculation of another sequential propagator.

The evaluation of quark-disconnected contributions is computationally more challenging as the disconnected loop (which contains the operator insertion, as illustrated in Fig. 41 right) is needed at all points on a particular timeslice or, in general, over the whole lattice. The quark loop is computed stochastically and then correlated with the nucleon two-point function before averaging this three-point function over the ensemble of gauge configurations. The associated statistical error, therefore, is a combination of that due to the stochastic evaluation (on each configuration) and that from the gauge average. The number of stochastic sources employed on each configuration is, typically, optimized to reduce the overall error for a given computational cost. The statistical errors of the connected contributions, in contrast, usually come only from the ensemble average since they are often evaluated exactly on each configuration, for a small number of source positions. If these positions are well-separated in space and time, then each measurement is statistically independent. The methodology applied for these calculations and the variance reduction techniques are summarized in Sec. 10.1.1. By construction, arbitrary values of τ across the entire temporal extent of the lattice can be realized when computing the quark-disconnected contribution, since the source-sink separation is determined by the part of the diagram that corresponds to the two-point nucleon correlator. However, in practice, statistical fluctuations of both the connected and disconnected contributions increase sharply, so that the signal is lost in the statistical noise for $\tau \gtrsim 1.5\,\text{fm}$.

The lattice calculation is performed for a given number of quark flavours and at a number of values of the lattice spacing a, the pion mass M_π, and the lattice size, represented by $M_\pi L$. The results need to be extrapolated to the physical point defined by $a = 0$, $M_\pi = 135$ MeV and $M_\pi L \to \infty$. This is done by fitting the data simultaneously in these three variables using a theoretically motivated ansatz. The ansätze used and the fitting strategy are described in Sec. 10.1.4.

The procedure for rating the various calculations and the criteria specific to this chapter are discussed in Sec. 10.2, which also includes a brief description of how the final averages are constructed. The physics motivation for computing the isovector charges, $g_{A,S,T}^{u-d}$, and the review of the lattice results are presented in Sec. 10.3. This is followed by a discussion of the

relevance of the flavour-diagonal charges, $g_{A,S,T}^{u,d,s}$, and a presentation of the lattice results in Sec. 10.4.

10.1.1 Technical aspects of the calculations of nucleon matrix elements

The calculation of n-point functions needed to extract nucleon matrix elements requires making four essential choices. The first involves choosing between the suite of background gauge field ensembles one has access to. The range of lattice parameters should be large enough to facilitate the extrapolation to the continuum and infinite-volume limits, and, ideally, the evaluation at the physical pion mass taken to be $M_\pi = 135$ MeV. Such ensembles have been generated with a variety of discretization schemes for the gauge and fermion actions that have different levels of improvement and preservation of continuum symmetries. The actions employed at present include (i) Wilson gauge with nonperturbatively improved Sheikholeslami-Wohlert fermions (nonperturbatively improved clover fermions) [31–37], (ii) Iwasaki gauge with nonperturbatively improved clover fermions [11, 38], (iii) Iwasaki gauge with twisted-mass fermions with a clover term [39–43], (iv) tadpole Symanzik improved gauge with highly improved staggered quarks (HISQ) [44–52], (v) Iwasaki gauge with domain-wall fermions (DW) [27, 53–58] and (vi) Iwasaki gauge with overlap fermions [59–61]. For details of the lattice actions, see the glossary in the Appendix A.1 of FLAG 19 [2].

The second choice is of the valence-quark action. Here there are two choices, to maintain a unitary formulation by choosing exactly the same action as is used in the generation of gauge configurations or to choose a different action and tune the quark masses to match the pseudoscalar meson spectrum in the two theories. Such mixed-action formulations are nonunitary but are expected to have the same continuum limit as QCD. The reason for choosing a mixed-action approach is expediency. For example, the generation of 2+1+1 flavour HISQ and 2+1 flavour DW ensembles with physical quark masses has been possible even at the coarse lattice spacing of $a = 0.15$ fm and there are indications that cut-off effects are reasonably small. These ensembles have been analyzed using clover-improved Wilson fermions, DW and overlap fermions since the construction of baryon correlation functions with definite spin and parity is much simpler compared to staggered fermions.

The third choice is the combination of the algorithm for inverting the Dirac matrix and variance reduction techniques. Efficient inversion and variance reduction techniques are needed for the calculation of nucleon correlation functions with high precision because the signal-to-noise ratio degrades exponentially as $e^{(\frac{3}{2}M_\pi - M_N)\tau}$ with the source-sink separation τ. Thus, the number of measurements needed for high precision is much larger than in the meson sector. Commonly used inversion algorithms include the multigrid [62] and the deflation-accelerated Krylov solvers [63], which can handle linear systems with large condition numbers very efficiently, thereby enabling calculations of correlation functions at the physical pion mass.

The sampling of the path integral is limited by the number $N_{\rm conf}$ of gauge configurations generated. One requires sufficiently large $N_{\rm conf}$ such that the phase space (for example, different topological sectors) has been adequately sampled and all the correlation functions satisfy the expected lattice symmetries such as C, P, T, momentum and translation invariance. Thus, one needs gauge field generation algorithms that give decorrelated large-volume configurations cost-effectively. On such large lattices, to reduce errors one can exploit the fact that the volume is large enough to allow multiple measurements of nucleon correlation functions that are essentially statistically independent. Two other common variance reduc-

tion techniques that reduce the cost of multiple measurements on each configuration are: the truncated solver with bias correction method [64] and deflation of the Dirac matrix for the low-lying modes followed by sloppy solution with bias correction for the residual matrix consisting predominately of the high-frequency modes [64, 65].

A number of other variance reduction methods are also being used and developed. These include deflation with hierarchical probing for disconnected diagrams [66, 67], the coherent source sequential propagator method [68, 69], low-mode averaging [70, 71], the hopping-parameter expansion [72, 73] and partitioning [74] (also known as dilution [75]).

The final choice is of the interpolating operator used to create and annihilate the nucleon state, and of the operator used to calculate the matrix element. Along with the choice of the interpolating operator (or operators if a variational method is used) one also chooses a "smearing" of the source used to construct the quark propagator. By tuning the width of the smearing, one can optimize the spatial extent of the nucleon interpolating operator to reduce the overlap with the excited states. Two common smearing algorithms that are equally performant are Gaussian (Wuppertal) [76] and Jacobi [77] smearing. Specific smearing techniques for hadrons boosted to (large) nonzero momentum have also been designed [78–80].

Having made all the above choices, for which a reasonable recipe exists, one calculates a statistical sample of correlation functions from which the desired ground-state nucleon matrix element is extracted. Excited states, unfortunately, contribute significantly to nucleon correlation functions in present studies. To remove their contributions, calculations are performed with multiple source-sink separations τ and fits are made to the correlation functions using their spectral decomposition as discussed in the next section.

10.1.2 Controlling excited-state contamination

Nucleon matrix elements are determined from a combination of two- and three-point correlation functions. To be more specific, let $B^\alpha(\vec{x},t)$ denote an interpolating operator for the nucleon. Placing the initial state at time slice $t=0$, the two-point correlation function of a nucleon with momentum $\vec{p}$ reads

$$C_2(\vec{p};\tau) = \sum_{\vec{x},\vec{y}} e^{i\vec{p}\cdot(\vec{x}-\vec{y})}\, \mathbb{P}_{\beta\alpha} \left\langle B^\alpha(\vec{x},\tau)\, \overline{B}^\beta(\vec{y},0) \right\rangle , \tag{407}$$

where the projector $\mathbb{P}$ selects the polarization, and α,β denote Dirac indices. The three-point function of two nucleons and a quark-bilinear operator O_Γ is defined as

$$C_3^\Gamma(\vec{q};t,\tau) = \sum_{\vec{x},\vec{y},\vec{z}} e^{i\vec{p}'\cdot(\vec{x}-\vec{z})}\, e^{-i\vec{p}\cdot(\vec{y}-\vec{z})}\, \mathbb{P}_{\beta\alpha} \left\langle B^\alpha(\vec{x},\tau)\, O_\Gamma(\vec{z},t)\, \overline{B}^\beta(\vec{y},0) \right\rangle , \tag{408}$$

where $\vec{p}$, $\vec{p}\,'$ denote the momenta of the nucleons at the source and sink, respectively, and $\vec{q}\equiv\vec{p}\,'-\vec{p}$ is the momentum transfer. The bilinear operator is inserted at time slice t, and τ denotes the source-sink separation. The corresponding quark-line diagrams for both C_2 and C_3^Γ, in terms of the nonperturbative quark propagators, $D^{-1}(y,x)$ where D denotes the lattice Dirac operator, are shown in Fig. 41.

The framework for the analysis of excited-state contamination is based on spectral decomposition. After inserting complete sets of eigenstates of the transfer matrix, the expressions

for the correlators C_2 and C_3^Γ read

$$C_2(\vec{p};\tau) = \frac{1}{L^3}\sum_n \mathbb{P}_{\beta\alpha}\,\langle\Omega|B^\alpha|n\rangle\langle n|\overline{B}^\beta|\Omega\rangle\, e^{-E_n\tau}, \tag{409}$$

$$C_3^\Gamma(\vec{q};t,\tau) = \frac{1}{L^3}\sum_{n,m} \mathbb{P}_{\beta\alpha}\,\langle\Omega|B^\alpha|n\rangle\,\langle n|O_\Gamma|m\rangle\,\langle m|\overline{B}^\beta|\Omega\rangle\, e^{-E_n(\tau-t)}\, e^{-E_m t}, \tag{410}$$

where $|\Omega\rangle$ denotes the vacuum state, and E_n represents the energy of the n^{th} eigenstate $|n\rangle$ in the nucleon channel. Here we restrict the discussion to vanishing momentum transfer, i.e., the forward limit $\vec{q}=0$, and label the ground state by $n=0$. The matrix element of interest $g_\Gamma \equiv \langle 0|O_\Gamma|0\rangle$ can, for instance, be obtained from the asymptotic behaviour of the ratio

$$R_\Gamma(t,\tau) \equiv \frac{C_3^\Gamma(\vec{q}=0;t,\tau)}{C_2(\vec{p}=0;\tau)} \overset{t,(\tau-t)\to\infty}{\longrightarrow} g_\Gamma + \mathrm{O}(e^{-\Delta t},\, e^{-\Delta(\tau-t)},\, e^{-\Delta\tau}), \tag{411}$$

where $\Delta \equiv E_1 - E_0$ denotes the energy gap between the ground state and the first excitation. We also assume that the bilinear operator O_Γ is appropriately renormalized (see Sec. 10.1.3).

Excited states with the same quantum numbers as the nucleon include resonances such as a Roper-like state with a mass of about 1.5 GeV, or multi-particle states consisting of a nucleon and one or more pions [81, 82]. The latter can provide significant contributions to the two- and three-point correlators in Eqs. (407) and (408) or their ratios (411) as the pion mass approaches its physical value. Ignoring the interactions between the individual hadrons, one can easily identify the lowest-lying multi-particle states: they include the $N\pi\pi$ state with all three particles at rest at ~ 1.2 GeV, as well as $N\pi$ states with both hadrons having nonzero and opposite momentum. Depending on the spatial box size L in physical units (with the smallest nonzero momentum equal to $2\pi/L$), there may be a dense spectrum of $N\pi$ states before the first nucleon resonance is encountered. Corrections to nucleon correlation functions due to the pion continuum have been studied using chiral effective theory [81–84] and Lüscher's finite-volume quantization condition [85].

The well-known noise problem of baryonic correlation functions implies that the long-distance regime, $t, (\tau - t) \to \infty$, where the correlators are dominated by the ground state, is difficult to reach. Current lattice calculations of baryonic three-point functions are typically confined to source-sink separations of $\tau \lesssim 1.5$ fm, despite the availability of efficient noise reduction methods. In view of the dense excitation spectrum encountered in the nucleon channel, one has to demonstrate that the contributions from excited states are sufficiently suppressed to guarantee an unbiased determination of nucleon matrix elements. There are several strategies to address this problem:

- Multi-state fits to correlator ratios or individual two- and three-point functions;
- Three-point correlation functions summed over the operator-insertion time t;
- Increasing the projection of the interpolator B^α onto the ground state.

The first of the above methods includes excited state contributions explicitly when fitting to the spectral decomposition of the correlation functions, Eqs. (409, 410) or, alternatively, their ratio (see Eq. (411)). In its simplest form, the resulting expression for R_Γ includes the contributions from the first excited state, i.e.,

$$R_\Gamma(t,\tau) = g_\Gamma + c_{01}\, e^{-\Delta t} + c_{10}\, e^{-\Delta(\tau-t)} + c_{11}\, e^{-\Delta\tau} + \ldots, \tag{412}$$

where c_{01}, c_{10}, c_{11} and Δ are treated as additional parameters when fitting $R_\Gamma(t,\tau)$ simultaneously over intervals in the source-sink separation τ and the operator-insertion timeslice t. Multi-exponential fits become more difficult to stabilize for a growing number of excited states, since an increasing number of free parameters must be sufficiently constrained by the data. Therefore, a high level of comparable statistical precision over several source-sink separations is required. One common way to address this issue is to introduce Bayesian constraints, as described in [86]. Alternatively, one may try to reduce the number of free parameters, for instance, by determining the energy gap Δ from nucleon two-point function and/or using a common gap for several different nucleon matrix elements [87].

Ignoring the explicit contributions from excited states and fitting $R_\Gamma(t,\tau)$ to a constant in t for fixed τ amounts to applying what is called the "plateau method". The name derives from the ideal situation that sufficiently large source-sink separations τ can be realized, which would cause $R_\Gamma(t,\tau)$ to exhibit a plateau in t independent of τ. The ability to control excited-state contamination is rather limited in this approach, since the only option is to check for consistency in the estimate of the plateau as τ is varied. In view of the exponential degradation of the statistical signal for increasing τ, such stability checks are difficult to perform reliably.

Summed operator insertions, originally proposed in Ref. [88], have also emerged as a widely used method to address the problem of excited-state contamination. One way to implement this method [89, 90] proceeds by summing $R_\Gamma(t,\tau)$ over the insertion time t, resulting in the correlator ratio $S_\Gamma(\tau)$,

$$S_\Gamma(\tau) \equiv \sum_{t=a}^{\tau-a} R_\Gamma(t,\tau). \tag{413}$$

The asymptotic behaviour of $S_\Gamma(\tau)$, including sub-leading terms, for large source-sink separations τ can be easily derived from the spectral decomposition of the correlators and is given by [91]

$$S_\Gamma(\tau) \overset{\tau\gg 1/\Delta}{\longrightarrow} K_\Gamma + (\tau-a)\, g_\Gamma + (\tau-a)\, e^{-\Delta\tau} d_\Gamma + e^{-\Delta\tau} f_\Gamma + \ldots, \tag{414}$$

where K_Γ is a constant, and the coefficients d_Γ and f_Γ contain linear combinations of transition matrix elements involving the ground and first excited states. Thus, the matrix element of interest g_Γ is obtained from the linear slope of $S_\Gamma(\tau)$ with respect to the source-sink separation τ. While the leading corrections from excited states $e^{-\Delta\tau}$ are smaller than those of the original ratio $R_\Gamma(t,\tau)$ (see Eq. (411)), extracting the slope from a linear fit to $S_\Gamma(\tau)$ typically results in relatively large statistical errors. In principle, one could include the contributions from excited states explicitly in the expression for $S_\Gamma(\tau)$. However, in practice it is often difficult to constrain an enlarged set of parameters reliably, in particular if one cannot afford to determine $S_\Gamma(\tau)$ except for a handful of source-sink separations.

The original summed operator-insertion technique described in Refs. [76, 88, 92, 93] avoids the explicit summation over the operator-insertion time t at every fixed value of τ. Instead, one replaces one of the quark propagators that appear in the representation of the two-point correlation function $C_2(t)$ by a "sequential" propagator, according to

$$D^{-1}(y,x) \to D_\Gamma^{-1}(y,x) = \sum_z D^{-1}(y,z)\Gamma D^{-1}(z,x). \tag{415}$$

In this expression, the position $z \equiv (\vec{z},t)$ of the insertion of the quark-bilinear operator is implicitly summed over, by inverting the lattice Dirac operator D on the source field $\Gamma D^{-1}(z,x)$. While this gives access to all source-sink separations $0 \le \tau \le T$, where T is the

temporal extent of the lattice, the resulting correlator also contains contact terms, as well as contributions from $\tau < t < T$ that must be controlled. This method has been adopted recently by the CalLat collaboration in their calculation of the isovector axial charge [48, 52].[2]

As in the case of explicitly summing over the operator-insertion time, the matrix element of interest is determined from the slope of the summed correlator. For instance, in Ref. [52], the axial charge was determined from the summed three-point correlation function, by fitting to its asymptotic behaviour [94] including sub-leading terms.

In practice, one often uses several methods simultaneously, e.g., multi-state fits and the summation method based on Eq. (414), in order to check the robustness of the result. All of the approaches for controlling excited-state contributions proceed by fitting data obtained in a finite interval in τ to a function that describes the approach to the asymptotic behaviour derived from the spectral decomposition. Obviously, the accessible values of τ must be large enough so that the model function provides a good representation of the data that enter such a fit. It is then reasonable to impose a lower threshold on τ above which the fit model is deemed reliable. We will return to this issue when explaining our quality criteria in Sec. 10.2.

The third method for controlling excited-state contamination aims at optimizing the projection onto the ground state in the two-point and three-point correlation functions [35, 69, 97, 98]. The RQCD collaboration has chosen to optimize the parameters in the Gaussian smearing procedure, so that the overlap of the nucleon interpolating operator onto the ground state is maximized [35]. In this way it may be possible to use shorter source-sink separations without incurring a bias due to excited states.

The variational method, originally designed to provide detailed information on energy levels of the ground and excited states in a given channel [99–102], has also been adapted to the determination of hadron-to-hadron transition elements [91]. In the case of nucleon matrix elements, the authors of Ref. [97] have employed a basis of operators to construct interpolators that couple to individual eigenstates in the nucleon channel. The method has produced promising results when applied to calculations of the axial and other forward matrix elements at a fixed value of the pion mass [69, 97, 98, 103]. However, a more comprehensive study aimed at providing an estimate at the physical point has, until now, not been performed.

The investigation of excited-state effects is an active subfield in calculations of nucleon matrix elements, and many refinements and extensions have been implemented since the first edition of the FLAG report. For instance, it has been shown that the previously observed failure of the axial and pseudoscalar form factors to satisfy the PCAC relation linking them could be avoided by including the enhanced contribution of $N\pi$ excitations, either by including additional information on the nucleon excitation spectrum extracted from the three-point function of the axial current [28], or with guidance from chiral effective field theory analyses of nucleon three-point functions [14]. Following this, in Refs. [104, 105] it has been demonstrated that this enhanced $N\pi$ contribution can be significantly reduced when performing a GEVP analysis with a basis that includes a five-quark/antiquark interpolator with the quantum numbers of the nucleon in addition to a three-quark interpolator. For the flavour-diagonal u- and d-quark scalar operators, a χPT study of excited-state corrections [106] suggests that there is a significant enhancement of the disconnected contribution, which impacts the calculation of the pion-nucleon sigma term $\sigma_{\pi N}$ as discussed in Sec. 10.4.2.

[2] In Ref. [94] it is shown that the method can be linked to the Feynman-Hellmann theorem. A direct implementation of the Feynman-Hellmann theorem by means of a modification of the lattice action is discussed and applied in Refs. [95, 96].

The variety of methods that are employed to address the problem of excited-state contamination has greatly improved our understanding of and control over excited-state effects in calculations of nucleon matrix elements. However, there is still room for further improvement: For instance, dedicated calculations of the excitation spectrum using the variational method could replace the often rudimentary spectral information gained from multi-state fits to the two- and three-point functions used primarily for the determination of the matrix elements. In general, the development of methods to explicitly include multi-particle states, such as $N\pi$ and $N\pi\pi$ with appropriate momentum configurations, coupled with the determination of the associated (transition) matrix elements, is needed to significantly enhance the precision of a variety of nucleon matrix elements. Such approaches would, to some extent, eliminate the need to extend the source-sink separation τ into a regime that is currently inaccessible due to the signal-to-noise problem.

Since the ongoing efforts to study excited-state contamination are producing deeper insights, we have decided to follow a more cautious approach in the assessment of available calculations of nucleon matrix elements. This is reflected in a modification of the quality criterion for excited-state contamination that is described and discussed in Sec. 10.2.

10.1.3 Renormalization and Symanzik improvement of local currents

and their matching to a continuum reference scheme such as $\overline{\text{MS}}$, and the application of Symanzik improvement to remove $\mathcal{O}(a)$ contributions. For the charges, the relevant operators are the axial (A_μ), tensor ($T_{\mu\nu}$) and scalar (S) local operators of the form $\mathcal{O}_\Gamma = \bar{q}\Gamma q$, with $\Gamma = \gamma_\mu\gamma_5$, $i\sigma_{\mu\nu}$ and $\mathbf{1}$, respectively, whose matrix elements are evaluated in the forward limit. The steps in the renormalization of the 1-link operators, defined in Section 10.5, used to calculate the second Mellin moments of distribution functions are similar to those for the charges and we refer readers to Refs. [87, 107].

For the charges, the general form for renormalized operators in the isovector flavour combination, at a scale μ, reads

$$\mathcal{O}_\Gamma^{\overline{\text{MS}}}(\mu) = Z_{\mathcal{O}}^{\overline{\text{MS}},\text{Latt}}(\mu a, g^2)\left[\mathcal{O}_\Gamma(a) + ab_{\mathcal{O}} m\mathcal{O}_\Gamma(a) + ac_{\mathcal{O}}\mathcal{O}_\Gamma^{\text{imp}}(a)\right] + \mathcal{O}(a^2), \tag{416}$$

where $Z_{\mathcal{O}}^{\overline{\text{MS}},\text{Latt}}(\mu a, g^2)$ denotes the multiplicative renormalization factor determined in the chiral limit, $m \to 0$, and the second and third terms represent all possible quark-mass-dependent and -independent Symanzik improvement terms, respectively, at $\mathcal{O}(a)$.[3] The chiral properties of overlap, domain-wall fermions (with improvement up to $\mathcal{O}(m_{\text{res}}^n)$ where m_{res} is the residual mass) and twisted-mass fermions (at maximal twist [112, 113]) mean that the $\mathcal{O}(a)$-improvement terms are absent, while for nonperturbatively improved Sheikholeslami-Wohlert-Wilson (nonperturbatively improved clover) fermions all terms appear in principle. For the operators of interest here there are several mass-dependent terms but at most one dimension-four $\mathcal{O}_\Gamma^{\text{imp}}$; see, e.g., Refs. [114, 115]. However, the latter involve external derivatives whose corresponding matrix elements vanish in the forward limit. Note that no mention is made of staggered fermions as they are not, currently, widely employed as valence quarks in nucleon matrix element calculations.

[3] Here, $a(g^2)$ refers to the lattice spacing in the chiral limit, however, lattice simulations are usually carried out by fixing the value of g^2 while varying the quark masses. This means $a = a(\tilde{g}^2)$ where $\tilde{g}^2 = g^2(1 + b_g a m_q)$ [108, 109] is the improved coupling that varies with the average sea-quark mass m_q. The difference between the renormalization factors calculated with respect to g^2 and $\tilde{g}^2$ can effectively be absorbed into the $b_{\mathcal{O}}$ coefficients [110, 111].

In order to illustrate the above remarks we consider the renormalization and improvement of the isovector axial current. This current has no anomalous dimension and hence the renormalization factor, $Z_A = Z_A^{\overline{\rm MS},{\rm Latt}}(g^2)$, is independent of the scale. The factor is usually computed nonperturbatively via the axial Ward identity [116] or the Rome-Southampton method [117] (see Sec. A.3 of FLAG 19 [2] for details). In some studies, the ratio with the corresponding vector renormalization factor, Z_A/Z_V, is determined for which some of the systematics cancel. In this case, one constructs the combination $Z_A g_A/(Z_V g_V)$, where $Z_V g_V = 1$ and g_A and g_V are the lattice forward matrix elements, to arrive at the renormalized axial charge [47]. For domain-wall fermions the ratio is employed in order to remove $\mathcal{O}(am_{\rm res})$ terms and achieve leading discretization effects starting at $\mathcal{O}(a^2)$ [118]. Thus, as mentioned above, $\mathcal{O}(a)$-improvement terms are only present for nonperturbatively improved clover fermions. For the axial current, Eq. (416) takes the explicit form,

$$A_\mu^{\overline{\rm MS}}(\mu) = Z_A^{\overline{\rm MS},{\rm Latt}}(g^2)\left[\left(1 + ab_A m_{\rm val} + 3a\tilde{b}_A m_{\rm sea}\right) A_\mu(a) + ac_A \partial_\mu P(a)\right] + \mathcal{O}(a^2), \quad (417)$$

where $m_{\rm val}$ and $m_{\rm sea}$ are the average valence- and sea-quark masses derived from the vector Ward identity [109, 115, 116], and P is the pseudoscalar operator $\overline{q}\gamma_5 q$. The matrix element of the derivative term is equivalent to $q_\mu \langle N(p')|P|N(p)\rangle$ and hence vanishes in the forward limit when the momentum transfer $q_\mu = 0$. The improvement coefficients b_A and $\tilde{b}_A$ are known perturbatively for a variety of gauge actions [114, 119, 120] and nonperturbatively for the tree-level Symanzik-improved gauge action for $N_f = 2 + 1$ [121].

Turning to operators for individual quark flavours, these can mix under renormalization and the singlet and nonsinglet renormalization factors can differ. For the axial current, such mixing occurs for all fermion formulations just like in the continuum, where the singlet combination acquires an anomalous dimension due to the $U_A(1)$ anomaly. The ratio of singlet to nonsinglet renormalization factors, $r_{\mathcal{O}} = Z_{\mathcal{O}}^{\rm s.}/Z_{\mathcal{O}}^{\rm n.s.}$ for $\mathcal{O} = A$ differs from 1 at $\mathcal{O}(\alpha_s^2)$ in perturbation theory (due to quark loops), suggesting that the mixing is a small effect. The nonperturbative determinations performed so far find $r_A \approx 1$ [7, 41], supporting this. For the tensor current the disconnected diagram vanishes in the continuum due to chirality and consequently on the lattice $r_T = 1$ holds for overlap and DW fermions (assuming $m_{\rm res} = 0$ for the latter). For twisted-mass and clover fermions the mixing is expected to be small with $r_T = 1 + \mathcal{O}(\alpha_s^3)$ [122] and this is confirmed by the nonperturbative studies of Refs. [43, 123].

The scalar operators for the individual quark flavours, $\overline{q}q$, are relevant not only for the corresponding scalar charges, but also for the sigma terms $\sigma_q = m_q \langle N|\overline{q}q|N\rangle$ when combined with the quark masses m_q. For overlap and DW fermions $r_S = 1$, like in the continuum and all $\overline{q}q$ renormalize multiplicatively with the isovector Z_S. The latter is equal to the inverse of the mass renormalization and hence $m_q\overline{q}q$ is renormalization group (RG) invariant. For twisted-mass fermions, through the use of Osterwalder-Seiler valence fermions, the operators $m_{ud}(\overline{u}u + \overline{d}d)$ and $m_s\overline{s}s$ are also invariant [124].[4] In contrast, the lack of good chiral properties leads to significant mixing between quark flavours for clover fermions. Nonperturbative determinations via the axial Ward identity [36, 125] have found the ratio r_S to be much larger than the perturbative expectation $1+\mathcal{O}(\alpha_s^2)$ [122] may suggest. While the sum over the quark flavours which appear in the action $\sum_q^{N_f} m_q\overline{q}q$ is RG invariant, large cancellations between

[4]Note that for twisted-mass fermions the pseudoscalar renormalization factor is the relevant factor for the scalar operator. The isovector (isosinglet) scalar current in the physical basis becomes the isosinglet (isovector) pseudoscalar current in the twisted basis. Perturbatively $r_P = 1 + \mathcal{O}(\alpha_s^3)$ and nonperturbative determinations have found $r_P \approx 1$ [43].

the contributions from individual flavours can occur when evaluating, e.g., the strange sigma term. Note that for twisted-mass and clover fermions there is also an additive contribution $\propto a^{-3}\mathbf{1}$ (or $\propto \mu a^{-2}\mathbf{1}$) to the scalar operator. This contribution is removed from the nucleon scalar matrix elements by working with the subtracted current, $\overline{q}q - \langle\overline{q}q\rangle$, where $\langle\overline{q}q\rangle$ is the vacuum expectation value of the current [115].

Symanzik improvement for the singlet currents follows the same pattern as in the isovector case with $\mathcal{O}(a)$ terms only appearing for nonperturbatively improved clover fermions. For the axial and tensor operators only mass-dependent terms are relevant in the forward limit while for the scalar there is an additional gluonic operator $\mathcal{O}_S^{\rm imp} = \mathrm{Tr}(F_{\mu\nu}F_{\mu\nu})$ with a coefficient of $\mathcal{O}(\alpha_s)$ in perturbation theory. When constructing the sigma terms from the quark masses and the scalar operator, the improvement terms remain and they must be included to remove all $\mathcal{O}(a)$ effects for nonperturbatively improved clover fermions, see Ref. [115] for a discussion.

10.1.4 Extrapolations in a, M_π and $M_\pi L$

To obtain physical results that can be used to compare to or make predictions for experiment, all quantities must be extrapolated to the continuum and infinite-volume limits. In general, either a chiral extrapolation or interpolation must also be made to the physical pion mass. These extrapolations need to be performed simultaneously since discretization and finite-volume effects are themselves dependent upon the pion mass. Furthermore, in practice it is not possible to hold the pion mass fixed while the lattice spacing is varied, as some variation in a occurs when tuning the quark masses at fixed gauge coupling. Thus, one performs a simultaneous extrapolation in all three variables using a theoretically motivated formula of the form,

$$g(M_\pi, a, L) = g_{\rm phys} + \delta_{M_\pi} + \delta_a + \delta_L \ , \tag{418}$$

where $g_{\rm phys}$ is the desired extrapolated result, and δ_{M_π}, δ_a, δ_L are the deviations due to the pion mass, the lattice spacing, and the volume, respectively. Below we outline the forms for each of these terms.

All observables discussed in this section are dimensionless, therefore the extrapolation formulae may be parameterized by a set of dimensionless variables:

$$\epsilon_\pi = \frac{M_\pi}{\Lambda_\chi} \ , \qquad M_\pi L \ , \qquad \epsilon_a = \Lambda_a a \ . \tag{419}$$

Here, $\Lambda_\chi \sim 1$ GeV is a chiral symmetry breaking scale, which, for example, can be set to $\Lambda_\chi = 4\pi F_\pi$, where $F_\pi = 92.2$ MeV is the pion decay constant, and Λ_a is a discretization scale, e.g., $\Lambda_a = \frac{1}{4\pi w_0}$, where w_0 is a gradient-flow scale [126].

Effective field theory methods may be used to determine the form of each of these extrapolations. For the single nucleon charges, Heavy-Baryon χPT (HBχPT) is a common choice [127, 128], however, other variants, such as unitarized [129] or covariant χPT [130, 131], are also employed. Various formulations of HBχPT exist, including those for two- and three-flavours, as well as with and without explicit Δ baryon degrees of freedom. Two-flavour HBχPT is typically used due to issues with convergence of the three-flavour theory [38, 132–135]. The convergence properties of all known formulations for baryon χPT, even at the physical pion mass, have not been well-established.

To $\mathcal{O}(\epsilon_\pi^2)$, the two-flavour chiral expansion for the nucleon charges is known to be of the form [136],

$$g = g_0 + g_1\epsilon_\pi + g_2\epsilon_\pi^2 + \tilde{g}_2\epsilon_\pi^2 \ln\left(\epsilon_\pi^2\right) \ , \tag{420}$$

where $g_1 = 0$ for all charges g except $g_S^{u,d}$. The dimensionless coefficients $g_{0,1,2}, \tilde{g}_2$ are assumed to be different for each of the different charges. The coefficients in front of the logarithms, $\tilde{g}_2$, are known functions of the low-energy constants (LECs), and do not represent new, independent LECs. Mixed-action calculations will have further dependence upon the mixed valence-sea pion mass, m_{vs}.

Given the potential difficulties with convergence of the chiral expansion, known values of the $\tilde{g}_2$ in terms of LECs are not typically used, but are left as free fit parameters. Furthermore, many quantities have been found to display mild pion-mass dependence, such that Taylor expansions, i.e., neglecting logarithms in the above expressions, are also often employed. The lack of a rigorously established theoretical basis for the extrapolation in the pion mass thus requires data close to the physical pion mass for obtaining high-precision extrapolated/interpolated results.

Discretization effects depend upon the lattice action used in a particular calculation, and their form may be determined using the standard Symanzik power counting. In general, for an unimproved action, the corrections due to discretization effects δ_a include terms of the form,

$$\delta_a = c_1\epsilon_a + c_2\epsilon_a^2 + \cdots \ , \tag{421}$$

where $c_{1,2}$ are dimensionless coefficients. Additional terms of the form $\tilde{c}_n\left(\epsilon_\pi\epsilon_a\right)^n$, where n is an integer whose lowest value depends on the combined discretization and chiral properties, will also appear. Improved actions systematically remove correction terms, e.g., an $\mathcal{O}(a)$-improved action, combined with a similarly improved operator, will contain terms in the extrapolation ansatz beginning at ϵ_a^2 (see Sec. 10.1.3).

Finite volume corrections δ_L may be determined in the usual way from effective field theory, by replacing loop integrals over continuous momenta with discrete sums. Finite volume effects therefore introduce no new undetermined parameters to the extrapolation. For example, at next-to-leading order, and neglecting contributions from intermediate Δ baryons, the finite-volume corrections for the axial charge in two-flavour HBχPT take the form [137],

$$\delta_L \equiv g_A(L) - g_A(\infty) = \frac{8}{3}\epsilon_\pi^2\left[g_{A,0}^3 F_1\left(M_\pi L\right) + g_{A,0}F_3\left(M_\pi L\right)\right] \ , \tag{422}$$

where

$$\begin{aligned} F_1\left(mL\right) &= \sum_{\mathbf{n}\neq\mathbf{0}}\left[K_0\left(mL|\mathbf{n}|\right) - \frac{K_1\left(mL|\mathbf{n}|\right)}{mL|\mathbf{n}|}\right] \ , \\ F_3\left(mL\right) &= -\frac{3}{2}\sum_{\mathbf{n}\neq 0}\frac{K_1\left(mL|\mathbf{n}|\right)}{mL|\mathbf{n}|} \ , \end{aligned} \tag{423}$$

and $K_\nu(z)$ are the modified Bessel functions of the second kind. Some extrapolations are performed using the form for asymptotically large $M_\pi L$,

$$K_0(z) \to \frac{e^{-z}}{\sqrt{z}} \ , \tag{424}$$

and neglecting contributions due to K_1. Care must, however, be taken to establish that these corrections are negligible for all included values of $M_\pi L$. The numerical coefficients, for example, 8/3 in Eq. (422), are often taken to be additional free fit parameters, due to the question of convergence of the theory discussed above.

Given the lack of knowledge about the convergence of the expansions and the resulting plethora of possibilities for extrapolation models at differing orders, it is important to include statistical tests of model selection for a given set of data. Bayesian model averaging [138] or use of the Akaike Information Criterion [139] are common choices which penalize over-parameterized models.

10.2 Quality criteria for nucleon matrix elements and averaging procedure

There are two specific issues that call for a modification and extension of the FLAG quality criteria listed in Sec. 2. The first concerns the rating of the chiral extrapolation: The FLAG criteria reflect the ability of χPT to provide accurate descriptions of the pion-mass dependence of observables. Clearly, this ability is linked to the convergence properties of χPT in a particular mass range. Quantities extracted from nucleon matrix elements are extrapolated to the physical pion mass using some variant of baryonic χPT, whose convergence is not well established as compared to the mesonic sector. Therefore, we have opted for stricter quality criteria, 200 MeV $\leq M_{\pi,\min} \leq$ 300 MeV, for a green circle in the chiral extrapolation of nucleon matrix elements, i.e.,

- ★ $M_{\pi,\min} <$ 200 MeV with three or more pion masses used in the extrapolation
  or two values of M_π with one lying within 10 MeV of 135 MeV (the physical neutral pion mass) and the other one below 200 MeV
- ○ 200 MeV $\leq M_{\pi,\min} \leq$ 300 MeV with three or more pion masses used in the extrapolation;
  or two values of M_π with $M_{\pi,\min} <$ 200 MeV;
  or a single value of M_π lying within 10 MeV of 135 MeV (the physical neutral pion mass)
- ■ Otherwise

In Sec. 10.1.2 we have discussed that insufficient control over excited-state contributions, arising from the noise problem in baryonic correlation functions, may lead to a systematic bias in the determination of nucleon matrix elements. We therefore introduce an additional criterion that rates the efforts to suppress excited-state contamination in the final result. As described in Sec. 10.1.2, the applied methodology to control excited-state contamination is quite diverse. Since a broad consensus on the question which procedures should be followed has yet to emerge, our criterion is expressed in terms of simulation parameters that can be straightforwardly extracted on the basis of publications. Furthermore, the criterion must also be readily applicable to a variety of different local operators whose matrix elements are discussed in this chapter. These requirements are satisfied by the source-sink separation τ, i.e., the Euclidean distance between the initial and final nucleons. The discussion at the end of Sec. 10.1.2 shows that there is room for improvement in the ability to control excited-state contamination. Hence, we have reverted to a binary system, based on the range of source-sink separations of a given calculations. While we do not award the highest category—a green star—in this edition, we stress that the adoption of the modified criterion for excited-state contamination has not led to a situation where calculations that were previously rated with

a green star are now excluded from FLAG averages. The rating scale concerning control over excited-state contributions is thus

- ○ Three or more source-sink separations τ, at least two of which must be above 1.0 fm.
- ■ Otherwise

We will continue to monitor the situation concerning excited-state contamination and, if necessary, adapt the criteria further in future editions of the FLAG report.

As explained in Sec. 2, FLAG averages are distinguished by the sea-quark content. Hence, for a given configuration of the quark sea (i.e., for $N_f = 2$, 2+1, 2+1+1, or 1+1+1+1), we first identify those calculations that pass the FLAG and the additional quality criteria defined in this section, i.e., excluding any calculation that has a red tag in one or more of the categories. We then add statistical and systematic errors in quadrature and perform a weighted average. If the fit is of bad quality (i.e., if $\chi^2_{\rm min}/{\rm dof} > 1$), the errors of the input quantities are scaled by $\sqrt{\chi^2/{\rm dof}}$. In the following step, correlations among different calculations are taken into account in the error estimate by applying Schmelling's procedure [140].

10.3 Isovector charges

The axial, scalar and tensor isovector charges are needed to interpret the results of many experiments and phenomena mediated by weak interactions, including probes of new physics. The most natural process from which isovector charges can be measured is neutron beta decay ($n \to p^+ e^- \overline{\nu}_e$). At the quark level, this process occurs when a down quark in a neutron transforms into an up quark due to weak interactions, in particular due to the axial-current interaction. While scalar and tensor currents have not been observed in nature, effective scalar and tensor interactions arise in the SM due to loop effects. At the TeV and higher scales, contributions to these three currents could arise due to new interactions and/or loop effects in BSM theories. These super-weak corrections to standard weak decays can be probed through high-precision measurements of the neutron decay distribution by examining deviations from SM predictions as described in Ref. [141]. The lattice-QCD methodology for the calculation of isovector charges is well established, and the control over statistical and systematic uncertainties has become quite robust since the first edition of the FLAG report that featured nucleon matrix elements [2].

The axial charge g_A^{u-d} is an important parameter that encapsulates the strength of weak interactions of nucleons. It enters in many analyses of nucleon structure and of SM and BSM physics. For example, it enters in (i) the extraction of V_{ud} and tests of the unitarity of the Cabibbo-Kobayashi-Maskawa (CKM) matrix; (ii) the analysis of neutrinoless double-beta decay, (iii) neutrino-nucleus quasi-elastic scattering cross-section; (iv) the rate of proton-proton fusion, the first step in the thermonuclear reaction chains that power low-mass hydrogen-burning stars like the Sun; (v) solar and reactor neutrino fluxes; (vi) muon capture rates, etc. Currently the best determination of the ratio of the axial to the vector charge, g_A/g_V, comes from measurement of neutron beta decay using polarized ultracold neutrons by the UCNA collaboration, 1.2772(20) [142, 143], and by PERKEO II, 1.2761^{+14}_{-17} [144]. Note that, in the SM, $g_V = 1$ up to second-order corrections in isospin breaking [145, 146] as a result of the conservation of the vector current. The percent-level contributions of radiative corrections discussed in Ref. [147] will need to be considered once the accuracy of the lattice-QCD calculations reaches that of g_A^{u-d} measured in experiments. The current goal is to calculate it

directly with $\mathcal{O}(1\%)$ accuracy using lattice QCD.

Isovector scalar or tensor interactions contribute to the helicity-flip parameters, called b and B, in the neutron decay distribution. By combining the calculation of the scalar and tensor charges with the measurements of b and B, one can put constraints on novel scalar and tensor interactions at the TeV scale as described in Ref. [141]. To optimally bound such scalar and tensor interactions using measurements of b and B parameters in planned experiments targeting 10^{-3} precision [148–150], we need to determine g_S^{u-d} and g_T^{u-d} at the 10% level as explained in Refs. [47, 141]. Future higher-precision measurements of b and B would require correspondingly higher-precision calculations of the matrix elements to place even more stringent bounds on these couplings at the TeV-scale.

One can estimate g_S^{u-d} via the conserved vector current (CVC) relation, $g_S/g_V = (M_{\text{neutron}} - M_{\text{proton}})^{\text{QCD}}/(m_d - m_u)^{\text{QCD}}$, as done by Gonzalez-Alonso *et al.* [151]. In their analysis, they took estimates of the two mass differences on the right-hand side from the global lattice-QCD data [152] and obtained $g_S^{u-d} = 1.02(8)(7)$.

The tensor charge g_T^{u-d} can be extracted experimentally from semi-inclusive deep-inelastic scattering (SIDIS) data [153–156]. A sample of these phenomenological estimates is shown in Fig. 44, and the noteworthy feature is that the current uncertainty in these phenomenological estimates is large.

10.3.1 Results for g_A^{u-d}, g_S^{u-d} and g_T^{u-d}

Results for the isovector axial, scalar and tensor charges are presented in Tabs. 67, 68 and 69, respectively. Compared with previous editions of the FLAG report, we have made two changes: First, we have stopped listing results for isovector charges from simulations in two-flavour QCD, since no new results have been reported since 2018. Secondly, for simulations using 2+1 or 2+1+1 flavours of dynamical quarks, we have imposed a cutoff to focus on results published after 2014. For full listings, including results obtained in two-flavour QCD [31, 33–35, 37, 39, 41, 43, 168] or published prior to our cutoff date [44, 53–55, 68, 169–171], we refer to earlier editions of the FLAG report.

For the sake of brevity, only calculations completed after FLAG 21 and calculations that meet the criteria for inclusion in averages are described below. For detailed descriptions of past calculations and those that do not meet the criteria, the reader is again referred to earlier editions of FLAG. The final results for the scalar and tensor charges, g_S^{u-d} and g_T^{u-d}, are presented in the $\overline{\text{MS}}$-scheme at a reference scale of 2 GeV by all collaborations.

The $2+1$-flavour calculation of the scalar and tensor charges by χQCD 21A [172] was performed using a mixed-action approach with domain-wall fermion gauge configurations generated by the RBC/UKQCD collaboration and overlap valence quarks. They include five pion masses ranging from $m_\pi \sim 140$ MeV to 370 MeV, four lattice spacings ($a \sim 0.06$, 0.08, 0.11, and 0.14 fm), thereby considerably extending the parameter range in their earlier calculation of the axial charge in χQCD 18 [27]. Matrix elements are computed for three to six different valence-quark masses on each ensemble. The extrapolation to the physical pion mass, continuum and infinite-volume limits is obtained by a global fit of all data to a partially quenched chiral perturbation theory ansatz. Excited-state contamination is assessed using three to five sink-source separations and multi-state fits. Renormalization factors were determined nonperturbatively using the RI/MOM prescription.

The NME 21 [167] $2+1$-flavour calculation utilized seven ensembles of $\mathcal{O}(a)$-improved Wilson fermions. Three lattice spacings, ranging from $a \sim 0.07$ fm to 0.13 fm, several pion

Collaboration	Ref.	N_f	publication status	continuum extrapolation	chiral extrapolation	finite volume	renormalization	excited states	g_A^{u-d}
ETM 23	[157]	2+1+1	A	★	★	★	★	○	1.245(28)(14)[c]
PNDME 23[a]	[158]	2+1+1	A	★‡	★	★	★	○	1.292(53)(24)[c]
CalLat 19	[159]	2+1+1	C	○	★	★	★	○	1.2642(93)
ETM 19	[160]	2+1+1	A	■	○	★	★	○	1.286(23)
PNDME 18[a]	[51]	2+1+1	A	★‡	★	★	★	○	1.218(25)(30)
CalLat 18	[52]	2+1+1	A	○	★	★	★	○	1.271(10)(7)
CalLat 17	[48]	2+1+1	P	○	★	★	★	○	1.278(21)(26)
PNDME 16[a]	[47]	2+1+1	A	○‡	★	★	★	○	1.195(33)(20)
Mainz 24	[161]	2+1	A	★	★	★	★	○	1.254(19)(15)
PACS 23	[162]	2+1	A	■	○	★	★	○	1.264(14)(3)
RQCD 23	[163]	2+1	A	★	★	★	★	○	$1.284(^{+0.028}_{-0.027})$
QCDSF/UKQCD/CSSM 23	[164]	2+1	A	★	○	★	★	○	1.253(63)(41)[d]
PACS 22B	[165]	2+1	A	■	○	★	★	○	1.288(14)(9)
Mainz 22	[166]	2+1	A	★	★	★	★	○	1.225(39)(25)[c]
NME 21[a]	[167]	2+1	A	○‡	★	★	★	○	1.31(6)(5)
RQCD 19	[14]	2+1	A	★	★	★	★	○	1.302(45)(73)[c]
LHPC 19	[15]	2+1	A	■‡	★	★	★	○	1.265(49)
Mainz 19	[87]	2+1	A	★	○	★	★	○	$1.242(25)(^{+0}_{-0.030})$
PACS 18A	[13]	2+1	A	■	★	★	★	○	1.273(24)(5)(9)
PACS 18	[11]	2+1	A	■	■	★	★	■	1.163(75)(14)
χQCD 18	[27]	2+1	A	○	★	★	★	○	1.254(16)(30)[$]
JLQCD 18	[61]	2+1	A	■	○	○	★	○	1.123(28)(29)(90)

[a] The improvement coefficient in the valence-quark action is set to its tadpole-improved tree-level value.
[b] The quark action is tree-level improved.
[c] Determination includes data for nonforward matrix elements.
[d] Feynman-Hellmann theorem is used to determine the matrix element.
[‡] The rating takes into account that the action is not fully $\mathcal{O}(a)$-improved by requiring an additional lattice spacing.
[$] For this partially quenched analysis the criteria are applied to the unitary points.

Table 67: Overview of results for g_A^{u-d}.

masses, $m_\pi \sim 165$ MeV to 285 MeV, and volumes corresponding to $m_\pi L \sim 3.75$ to 6.15 were used. Combined continuum, chiral, and infinite-volume extrapolations were performed to the physical point using leading-order fit functions. Several fitting strategies were explored using four to six source-sink separations ranging from 0.7–1.8 fm. Final results are quoted

Collaboration	Ref.	N_f	publication status	continuum extrapolation	chiral extrapolation	finite volume	renormalization	excited states	g_S^{u-d}
PNDME 23	[158]	2+1+1	A	★‡	★	★	★	○	1.085(50)(103)
ETM 19	[160]	2+1+1	A	■	○	★	★	○	1.35(17)
PNDME 18	[51]	2+1+1	A	★‡	★	★	★	○	1.022(80)(60)
PNDME 16	[47]	2+1+1	A	○‡	★	★	★	○	0.97(12)(6)
Mainz 24	[161]	2+1	A	★	★	★	★	○	1.203(77)(81)
RQCD 23	[163]	2+1	A	★	★	★	★	○	1.11^{+14}_{-16}
QCDSF/UKQCD/CSSM 23	[164]	2+1	A	★	○	★	★	○[d]	1.08(21)(03)[d]
PACS 22B	[165]	2+1	A	■	○	★	★	○	0.927(83)(22)
NME 21	[167]	2+1	A	○‡	★	★	★	○	1.06(9)(6)
χQCD 21A	[172]	2+1	A	★	★	★	★	○	0.94(10)(08)[$]
RBC/UKQCD 19	[173]	2+1	A	■	○	★	★	■	0.9(3)
Mainz 19	[87]	2+1	A	★	○	★	★	○	$1.13(11)(^{7}_{6})$
LHPC 19	[15]	2+1	A	■‡	★	★	★	○	0.927(303)
JLQCD 18	[61]	2+1	A	■	○	○	★	○	0.88(8)(3)(7)

[d] Feynman-Hellmann theorem is used.
‡ The rating takes into account that the action is not fully $\mathcal{O}(a)$-improved by requiring an additional lattice spacing.
[$] For this partially quenched analysis the criteria are applied to the unitary points.

Table 68: Overview of results for g_S^{u-d}.

by averaging results from two of these fitting strategies, in which the excited-state energy for the three-point function is fixed using two alternative choices of priors. Renormalization is nonperturbative (RI-SMOM) using two strategies.

PACS 22B [165] reports estimates for the scalar and tensor charges, computed on two ensembles with nonperturbatively improved Wilson quark and Iwasaki gauge action at a single lattice spacing of 0.085 fm, pion mass near physical value, and two volumes with $m_\pi L \sim 3.7$ and 7.4. Two to four source-sink separations ranging from 0.85–1.36 fm were used to estimate contributions from excited states. They employ the RI-SMOM$_{\gamma_\mu}$ renormalization procedure. Due to the use of only a single lattice spacing, this calculation does not meet the criteria for inclusion in the average. In PACS 23 [162], another ensemble was considered for the calculation of the axial charge and form factors, which features a smaller lattice spacing of 0.063 fm, a 10 fm spatial box size and a near-physical pion mass of 138 MeV. The range of source-sink separations matches the choice in PACS 22B. The size of discretization effects is estimated by the difference between results at fine and coarser lattice spacings. Since these

Collaboration	Ref.	N_f	publication status	continuum extrapolation	chiral extrapolation	finite volume	renormalization	excited states	g_T^{u-d}
PNDME 23	[158]	2+1+1	A	★‡	★	★	★	○	0.991(21)(10)
ETM 22	[174]	2+1+1	A	★	★	★	★	○	0.924(54)
ETM 19	[160]	2+1+1	A	■	○	★	★	○	0.936(25)
PNDME 18	[51]	2+1+1	A	★‡	★	★	★	○	0.989(32)(10)
PNDME 16	[47]	2+1+1	A	○‡	★	★	★	○	0.987(51)(20)
PNDME 15, 15A	[45, 46]	2+1+1	A	○‡	★	★	★	○	1.020(76)
Mainz 24	[161]	2+1	A	★	★	★	★	○	0.993(15)(05)
RQCD 23	[163]	2+1	A	★	★	★	★	○	0.984^{+19}_{-29}
QCDSF/UKQCD/CSSM 23	[164]	2+1	A	★	○	★	★	○[d]	1.010(21)(12)
PACS 22B	[165]	2+1	A	■	○	★	★	○	1.036(6)(20)
NME 21	[167]	2+1	A	○‡	★	★	★	○	0.95(5)(2)
RBC/UKQCD 19	[173]	2+1	A	■	○	★	★	■	1.04(5)
Mainz 19	[87]	2+1	A	★	○	★	★	○	$0.965(38)(^{13}_{41})$
LHPC 19	[15]	2+1	A	■‡	★	★	★	○	0.972(41)
JLQCD 18	[61]	2+1	A	■	○	○	★	○	1.08(3)(3)(9)

[d] Feynman-Hellmann theorem is used.
‡ The rating takes into account that the action is not fully $\mathcal{O}(a)$-improved by requiring an additional lattice spacing.

Table 69: Overview of results for g_T^{u-d}.

results are based on only two lattice spacings, they do not qualify for an average.

The calculation of all three isovector charges by QCDSF/UKQCD/CSSM 23 [164] used a Feynman-Hellmann approach to determine matrix elements from derivatives of energies produced via a variation of the action. These energies were determined from fits to two-point correlation functions, where a weighted average is taken of the results obtained when varying the fitting range. The computations utilized the 2 + 1-flavour stout-link nonperturbative clover action with Wilson-clover valence quarks. Pion masses range from 220–468 MeV, using a flavour-breaking expansion around the flavour SU(3) point to extrapolate to physical pion mass. Combined pion-mass, lattice-spacing, and volume extrapolations were performed, using multiple volumes ranging from $m_\pi L \sim 3.2$–9, and five lattice spacings, 0.052–0.082 fm. Only the leading discretization effects and asymptotic form of the volume extrapolation, Eq. (424), were included. They employ the RI'-MOM prescription for nonperturbative renormalization.

The calculations of g_A^{u-d}, g_S^{u-d} and g_T^{u-d} published by RQCD 23 [163] and Mainz 24 [161] are both based on 2+1-flavour ensembles generated by the CLS effort using nonperturbatively

improved Wilson fermions. The subsets of ensembles used in the two calculations partly overlap. The 48 ensembles used by RQCD 23 [163] span six values of the lattice spacing, from 0.039–0.098 fm, pion masses from 130 MeV up to 430 MeV, and volumes corresponding to $m_\pi L \sim 3$–6.5. Excited states are controlled using simultaneous two- and three-state fits of up to four different observables using four time separations, $t \approx 0.7$–1.2 fm, with a number of fit strategies employed. Extrapolations to the physical point were performed using leading-order chiral expressions for the pion mass, the leading asymptotic form for finite-volume corrections, and terms up to a^2 in the lattice spacing. Renormalization uses the nonperturbative RI'-SMOM scheme. In an earlier paper (RQCD 19 [14]), the Regensburg group computed the axial form factor on a subset of the ensembles that enter RQCD 23. The estimate for g_A^{u-d} from an analysis including matrix elements for nonforward kinematics is also listed in Tab. 67 but has been superseded by the result in RQCD 23.

The Mainz 24 [161] calculation, which supersedes Mainz 19 [87], uses four lattice spacings ($a \sim 0.05$ fm to 0.086 fm) from the CLS set of ensembles, pion masses ranging from ~ 130 MeV to ~ 350 MeV, and volumes corresponding to $m_\pi L \sim 3$–5.4. Physical-point extrapolations were performed simultaneously in the lattice spacing, pion mass, and volume. In Mainz 24, the range of source-sink separations used was enlarged to 0.2–1.4 fm, which allowed for the inclusion of sub-leading terms in the summation method for improved control over excited-state effects. Renormalization was performed nonperturbatively using the RI-SMOM scheme. The Mainz group has also performed a calculation of the axial form factor (Mainz 22 [166]) on the same set of ensembles, by incorporating the summation method directly into the z-expansion used to describe the Q^2-dependence. The corresponding estimate for g_A^{u-d} from an analysis including nonforward matrix elements has larger errors than the most recent result [161].

New results for $N_f = 2+1+1$ flavours of dynamical fermions have been published by PNDME [158] and ETM [157, 174]. The mixed-action calculation by PNDME 23 [158], which supersedes PNDME 18 [51] and PNDME 16 [47], was performed using the MILC HISQ ensembles, with a clover valence action. As in PNDME 18 [51], the 11 ensembles used include three pion-mass values, $M_\pi \sim 135$, 225, 320 MeV, and four lattice spacings, $a \sim 0.06$, 0.09, 0.12, 0.15 fm. Note that four lattice spacings are required to meet the green star criteria, as this calculation is not fully $\mathcal{O}(a)$-improved. Lattice size ranges between $3.3 \lesssim M_\pi L \lesssim 5.5$. Physical-point extrapolations were performed simultaneously, keeping only the leading-order terms in the various expansion parameters. For the finite-volume extrapolation, the asymptotic limit of the χPT prediction, Eq. (424), was used. PNDME 23 [158] adds a study of sensitivity to excited-state contamination using between three and five source-sink time separations from $0.72 \lesssim \tau \lesssim 1.68$ fm, and several strategies, including removing $N\pi$ contributions. Renormalization was performed nonperturbatively using the RI-SMOM scheme.

The ETM collaboration has presented new results for the tensor charge (ETM 22 [174]) and for the axial charge (ETM 23 [157]). Both calculations use three ensembles with $2+1+1$-flavour twisted-mass fermions with close-to-physical pion masses at $a = 0.057$, 0.069 and 0.080 fm, with volumes corresponding to $m_\pi L \sim 3.6$–3.9. These results supersede those in [160] based on the single ensemble at $a = 0.080$ fm. To control excited-state effects, they compared results from the plateau, summation method and two-state fits. After applying nonperturbative renormalization via the RI'-MOM method supplemented by a perturbative subtraction of lattice artefacts [175, 176], they perform the extrapolation to the continuum limit via a fit which is linear in a^2.

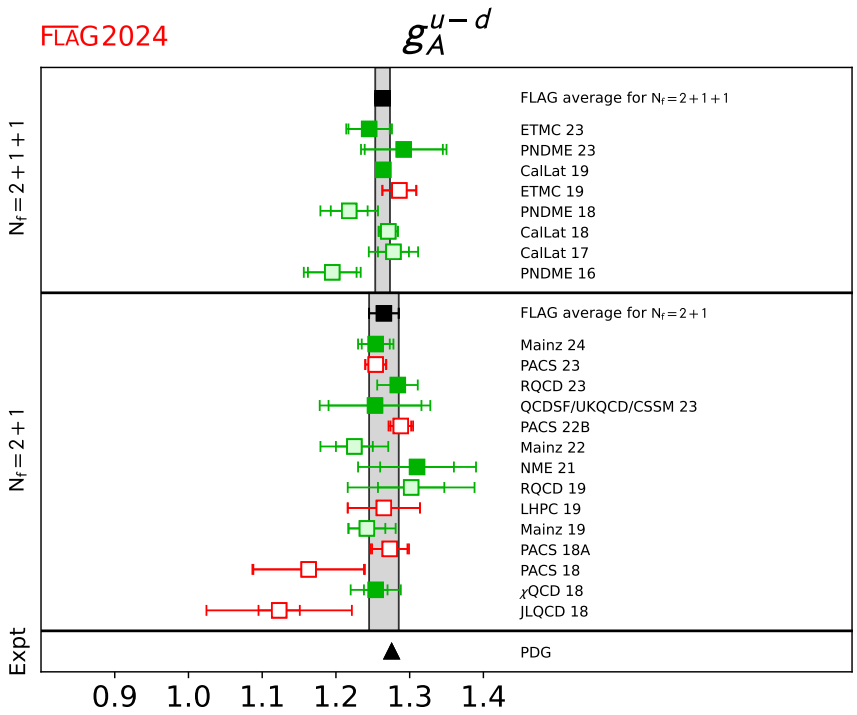

Figure 42: Lattice results and FLAG averages for the isovector axial charge g_A^{u-d} $2+1$ and $2+1+1$ flavour calculations. Also shown is the experimental result as quoted in the PDG [177].

We now proceed to discussing global averages for the isovector charges. The compilation of results for the axial charge g_A^{u-d}, plotted in Fig. 42, shows that the situation has greatly improved in terms of stability and precision thanks to several new calculations that have been added since FLAG 21. For QCD with $N_f = 2+1+1$ dynamical quarks, the latest calculations by ETM 23 [157], PNDME 23 [158] and CalLat 19 [159] pass all quality criteria. Since PNDME and CalLat both use gauge ensembles produced by MILC, we assume that the quoted errors are 100% correlated, even though the range of pion masses and lattice spacings explored in Refs. [158] and [52, 159] is not exactly identical. The two results are fully consistent within errors, which is an improvement, since FLAG 21 reported a slight tension between CalLat 19 [159] and PNDME 18 [51]. The calculation by ETM 23 [157] uses an independent set of ensembles. Performing a weighted average yields $g_A^{u-d} = 1.2633(100)$ with $\chi^2/\text{dof} = 0.30$. The result by CalLat dominates the $2+1+1$ weighted average due to its smaller error. Values for $\delta(a_{\min})$ for the two $N_f = 2+1+1$ calculations that enter the averages vary between 1.0–1.5 (PNDME 23: 1.0, CalLat 19: 1.5).

For QCD with $N_f = 2+1$ dynamical quarks, we compute a weighted average from the results χQCD 18 [27], NME 21 [167], QCDSF/UKQCD/CSSM 23 [164], RQCD 23 [163] and Mainz 24 [161]. Since the calculations by the Mainz group and RQCD were both performed on ensembles generated by the CLS effort, we treat the results RQCD 23 [163] and Mainz 24 [161] as 100% correlated. This yields $g_A^{u-d} = 1.265(20)$ with $\chi^2/\text{dof} = 0.28$. Values for $\delta(a_{\min})$ for the qualified calculations for $N_f = 2+1$ suggest that discretization effects are under good control (NME 21: 0.15, QCDSF/UKQCD/CSSM 23: 0.6, RQCD 23: 2.0, Mainz 24: 2.3). From the information provided in the paper, it is not possible to infer $\delta(a_{\min})$ for χQCD 18.

To summarize, the FLAG averages for the axial charge read

$$N_f = 2+1+1: \qquad g_A^{u-d} = 1.263(10) \qquad \text{Refs. [52, 157–159]}, \tag{425}$$

$$N_f = 2+1: \qquad g_A^{u-d} = 1.265(20) \qquad \text{Refs. [27, 161, 163, 164, 167]}. \tag{426}$$

The averages computed for QCD with $N_f = 2+1+1$ and $N_f = 2+1$ flavours are in excellent agreement, with a relative precision of 0.8% and 1.5%, respectively. The average for $2+1+1$ flavours exhibits a mild tension of 1.25σ with the experimental value of $g_A^{u-d} = 1.2756(13)$ quoted by the PDG. While lattice QCD is able to determine the axial charge with a total relative uncertainty at the percent level, the experimental result is more precise by an order of magnitude. We conclude with the remark that there has been enormous progress in calculating this important benchmark quantity in lattice QCD over the course of the past 10–15 years, owing to a variety of methods to control excited-state effects, higher statistical precision, as well as much better control over the extrapolation to the physical point.

Turning now to the isovector scalar charge, we note that—in addition to the direct three-point method—its value can also be determined indirectly via the conserved vector current (CVC) relation from results for the neutron-proton mass difference [178–186] and the down- and up-quark-mass difference (see Sec. 4.1.3). For comparison, the compilation in Fig. 43 also shows the indirect determination by Gonzalez-Alonso *et al.* [151] obtained using lattice and phenomenological input.

For $2+1+1$ flavours, only PNDME 23 [158], which supersedes PNDME 18 [51] and PNDME 16 [47], meets all the criteria for inclusion in the average. Consequently we identify the result from PNDME 23 with the global average.

There are five $2+1$-flavour calculations which satisfy all criteria required for inclusion in the average, i.e., χQCD 21A [172], NME 21 [167], QCDSF/UKQCD/CSSM 23 [164], RQCD 23 [163] and Mainz 24 [161]. The calculations by PACS 22B [165] and LHP 19 [15] have been performed at fewer than three lattice spacings and therefore do not meet the criteria. As in the case of the isovector charge, we assume 100% correlation between the results reported by Mainz 24 and RQCD 23, since the calculations were both performed on the CLS set of ensembles. Values of $\delta(a_{\min})$ for the qualified calculations range from 0.4–2.4 (PNDME 23: 1.6, NME 21: 2.4, RQCD 23: 0.4, Mainz 24: 0.5). It is not possible based on the information given to determine $\delta(a_{\min})$ for χQCD 21 or QCDSF/UKQCD/CSSM 23, however, in the former calculation it is noted that all data on the finest lattice spacing is within one sigma of the quoted final result, while for the latter extrapolations performed without accounting for discretization effects give results within one sigma of the final quoted result. Thus it is likely that in these cases $\delta(a_{\min})$ is within a reasonable range.

The final FLAG values for g_S^{u-d} are

$$N_f = 2+1+1: \qquad g_S^{u-d} = 1.085(114) \qquad \text{Ref. [158]}, \tag{427}$$

$$N_f = 2+1: \qquad g_S^{u-d} = 1.083(69) \qquad \text{Refs. [161, 163, 164, 167, 172]}, \tag{428}$$

so that the total relative error for $N_f = 2+1+1$ and $2+1$ is about 10.5% and 6.4%, respectively. This implies that the relevant precision target for current experimental searches for new scalar interactions has been met.

Estimates of the isovector tensor charge are generally at a high level of precision, with values that are stable over time, as can be seen from the compilation given in Tab. 69 and plotted in Fig. 44. This is a consequence of the smaller statistical fluctuations in the raw

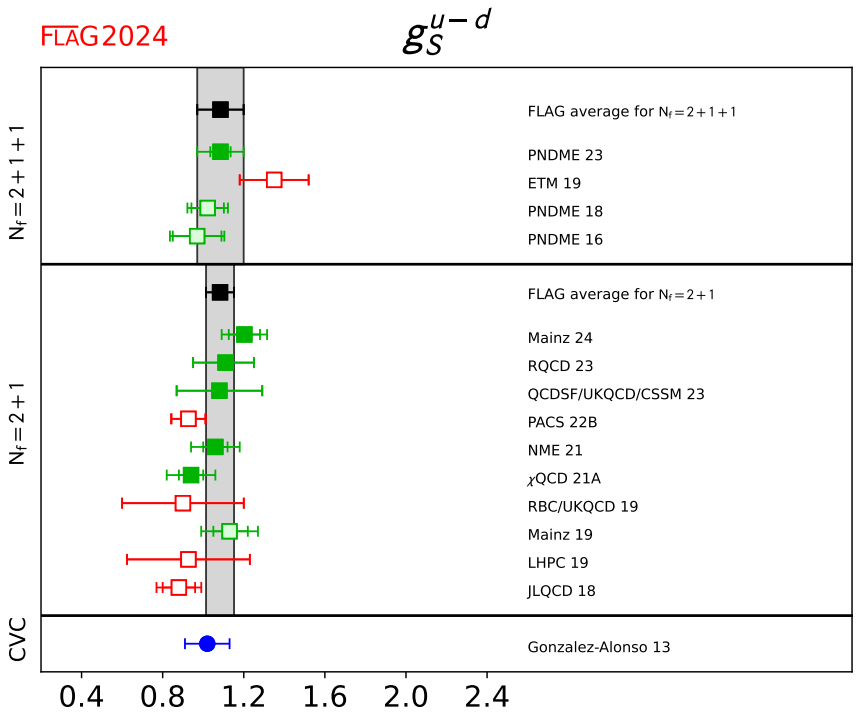

Figure 43: Lattice results and FLAG averages for the isovector scalar charge g_S^{u-d} for $N_f = 2$, $2+1$, and $2+1+1$ flavour calculations. Also shown is a phenomenological result obtained using the conserved vector current (CVC) relation [151] (circle).

data and the very mild dependence on a, M_π, and the lattice size $M_\pi L$. As a result, the uncertainty due to the various extrapolations is small. Also shown for comparison in Fig. 44 are phenomenological results using measures of transversity [187–194].

For $N_f = 2{+}1{+}1$ flavours, two calculations meet all the criteria for inclusion in the average: PNDME 23 [158], which supersedes PNDME 18 [51] and PNDME 16 [47], and ETM 22 [174]. Computational details for PNDME 23 and ETM 22 have already been described above.

Using $N_f = 2+1$ flavours, four calculations meet all criteria for inclusion in the average: NME 21[167], QCDSF/UKQCD/CSSM 23 [164], RQCD 23 [163], and Mainz 24 [161] calculation, which supersedes Mainz 19 [87]. Details of these calculations, as well as the PACS 22B [165] calculation which does not meet all criteria for inclusion in the average, have been described above. As in the cases of the axial and scalar charge, we assume 100% correlation between the Mainz 24 and RQCD 23 calculations. Values of $\delta(a_{\min})$ for the qualified calculations range from 0.03–2 (PNDME 23: 2, NME 21: 0.5, RQCD 23: 0.03, Mainz 24: 0.5). Similarly to the case for g_S, it is not possible based on the information given to determine $\delta(a_{\min})$ for χQCD 21 or QCDSF/UKQCD/CSSM 23. However, in the former calculation it is noted that all data on the finest lattice spacing is within one sigma of the quoted final result, while for the latter extrapolations performed without accounting for discretization give results within one sigma of the final quoted result. Thus, it is likely that in these cases $\delta(a_{\min})$ is within a reasonable range.

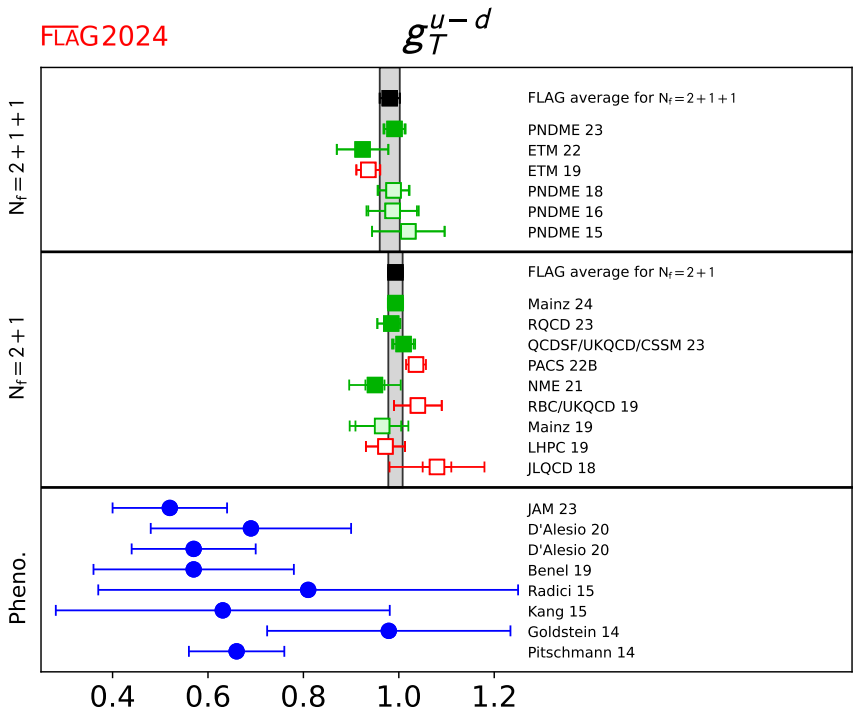

Figure 44: Lattice results and FLAG averages for the isovector tensor charge g_T^{u-d} for $N_f = 2$, 2+1, and 2+1+1 flavour calculations. Also shown are phenomenological results using measures of transversity [187–194] (circles).

The final FLAG values for g_T^{u-d} are

$$N_f = 2+1+1: \qquad g_T^{u-d} = 0.981(21) \qquad \text{Ref. [158, 174]}, \tag{429}$$

$$N_f = 2+1: \qquad g_T^{u-d} = 0.993(15) \qquad \text{Refs. [161, 163, 164, 167]}, \tag{430}$$

which implies that the isovector tensor charge is determined at the level of 1.5–2.0% relative precision.

10.4 Flavour-diagonal charges

Three examples of interactions for which matrix elements of flavour-diagonal operators ($q\Gamma q$ where Γ defines the Lorentz structure of the bilinear quark operator) are needed are the neutral-current interactions of neutrinos, elastic scattering of electrons off nuclei, and the scattering of dark matter off nuclei. In addition, these matrix elements also probe intrinsic properties of nucleons (the spin, the nucleon sigma term and strangeness content, and the contribution of the electric dipole moment (EDM) of the quarks to the nucleon EDM) as explained below. For brevity, all operators are assumed to be appropriately renormalized as discussed in Sec. 10.1.3.

The matrix elements of the scalar operator $\bar{q}q$ with flavour q give the rate of change in the nucleon mass due to nonzero values of the corresponding quark mass. This relationship is given by the Feynman-Hellmann theorem. The quantities of interest are the nucleon σ-term,

$\sigma_{\pi N}$, and the strange and charm content of the nucleon, σ_s and σ_c,

$$\sigma_{\pi N} = m_{ud}\langle N|\overline{u}u + \overline{d}d|N\rangle\,, \tag{431}$$
$$\sigma_s = m_s\langle N|\overline{s}s|N\rangle\,, \tag{432}$$
$$\sigma_c = m_c\langle N|\overline{c}c|N\rangle\,. \tag{433}$$

Here, m_{ud} is the average of the up- and down-quark masses and m_s, m_c are the strange- and charm-quark masses. The $\sigma_{\pi N,s,c}$ give the shift in M_N due to nonzero light-, strange- and charm-quark masses. The same matrix elements are also needed to quantify the spin-independent interaction of dark matter with nucleons. Note that, while σ_b and σ_t are also phenomenologically interesting, they are unlikely to be calculated on the lattice due to the expected tiny signal in the matrix elements. In principle, the heavy sigma terms can be estimated using $\sigma_{u,d,s}$ by exploiting the heavy-quark limit [195–197].

The matrix elements of the axial operator $\overline{q}\gamma_\mu\gamma_5 q$ give the contribution Δq of quarks of flavour q to the spin of the nucleon:

$$\begin{aligned}\langle N|\overline{q}\gamma_\mu\gamma_5 q|N\rangle &= g_A^q\overline{u}_N\gamma_\mu\gamma_5 u_N,\\ g_A^q \equiv \Delta q &= \int_0^1 dx(\Delta q(x) + \Delta\overline{q}(x))\,.\end{aligned} \tag{434}$$

The charge g_A^q is thus the contribution of the spin of a quark of flavour q to the spin of the nucleon. It is also related to the first Mellin moment of the polarized parton distribution function (PDF) Δq as shown in the second line in Eq. (434). Measurements by the European Muon collaboration in 1987 of the spin asymmetry in polarized deep inelastic scattering showed that the sum of the spins of the quarks contributes less than half of the total spin of the proton [198]. To understand this unexpected result, called the "proton spin crisis", it is common to start with Ji's sum rule [199], which provides a gauge invariant decomposition of the nucleon's total spin, as

$$\frac{1}{2} = \sum_{q=u,d,s,c,\cdot}\left(\frac{1}{2}\Delta q + L_q\right) + J_g\,, \tag{435}$$

where $\Delta q/2 \equiv g_A^q/2$ is the contribution of the intrinsic spin of a quark with flavour q; L_q is the orbital angular momentum of that quark; and J_g is the total angular momentum of the gluons. Thus, to obtain the spin of the proton starting from QCD requires calculating the contributions of the three terms: the spin and orbital angular momentum of the quarks, and the angular momentum of the gluons. Lattice-QCD calculations of the various matrix elements needed to extract the three contributions are underway. An alternate decomposition of the spin of the proton has been provided by Jaffe and Manohar [200]. The two formulations differ in the decomposition of the contributions of the quark orbital angular momentum and of the gluons. The contribution of the quark spin, which is the subject of this review and given in Eq. (434), is the same in both formulations.

The tensor charges are defined as the matrix elements of the tensor operator $\overline{q}\sigma^{\mu\nu}q$ with $\sigma^{\mu\nu} = \{\gamma_\mu, \gamma_\nu\}/2$:

$$g_T^q\overline{u}_N\sigma_{\mu\nu}u_N = \langle N|\overline{q}\sigma_{\mu\nu}q|N\rangle\,. \tag{436}$$

These flavour-diagonal tensor charges $g_T^{u,d,s,c}$ quantify the contributions of the u, d, s, c quark EDM to the neutron electric dipole moment (nEDM) [45, 201]. Since particles can

have an EDM only due to P- and T- (or CP- assuming CPT is a good symmetry) violating interactions, the nEDM is a very sensitive probe of new sources of CP violation that arise in most extensions of the SM designed to explain nature at the TeV scale. The current experimental bound on the nEDM is $d_n < 1.8 \times 10^{-26}$ e cm [202, 203], while the known CP violation in the SM implies $d_n < 10^{-31}$ e cm [204]. A nonzero result over the intervening five orders of magnitude would signal new physics. Planned experiments aim to reduce the bound to around 10^{-28} e cm. A discovery or reduction in the bound from these experiments will put stringent constraints on many BSM theories, provided the matrix elements of novel CP-violating interactions, of which the quark EDM is one, are calculated with the required precision.

One can also extract these tensor charges from the zeroth moment of the transversity distributions that are measured in many experiments including Drell-Yan and semi-inclusive deep inelastic scattering (SIDIS). Of particular importance is the active program at Jefferson Lab (JLab) to measure them [153, 154]. Transversity distributions describe the net transverse polarization of quarks in a transversely polarized nucleon. Their extraction from the data taken over a limited range of Q^2 and Bjorken x is, however, not straightforward and requires additional phenomenological modeling. At present, lattice-QCD estimates of $g_T^{u,d,s}$, presented in the next section, are more accurate than these phenomenological estimates [187–194]. Future experiments will significantly improve the extraction of the transversity distributions. Thus, accurate calculations of the tensor charges using lattice QCD will continue to help elucidate the structure of the nucleon in terms of quarks and gluons and provide a benchmark against which phenomenological estimates utilizing measurements at JLab and other experimental facilities worldwide can be compared.

The methodology for the calculation of flavour-diagonal charges is well-established. The major challenges are the much larger statistical errors in the disconnected contributions for the same computational cost and the need for the additional calculations of the isosinglet renormalization factors. In this report, we present results for the axial and tensor charges in the same section 10.4.1 since they are mostly calculated together and because the statistical and systematic uncertainties are similar. The calculation of the scalar charges can, however, be done in two ways and the results are therefore presented separately in section 10.4.2.

10.4.1 Results for $g_A^{u,d,s}$ and $g_T^{u,d,s}$

A compilation of results for the flavour-diagonal axial (tensor) charges for the proton is given in Tab. 70 (Tab. 71), and are plotted in Fig. 45. Results for the neutron can be obtained by interchanging the u- and d-flavour indices. To keep the report current, publications from before 2014 that do not satisfy one or more of the FLAG criteria and the $N_f = 2$ results have been removed. They can be obtained from the FLAG 19 [2] and FLAG 21 [1] reports.

There are no new results that qualify for FLAG averages, so the FLAG values for the proton in the $\overline{\text{MS}}$ scheme at 2 GeV remain the same as in FLAG 19 [2] and FLAG 21 [1]. For $g_A^{u,d,s}$, only the PNDME 18A [50] calculation qualifies for the 2+1+1-flavour theory, and only the χQCD 18 [27] for 2+1 flavours.

The PNDME 18A [50] results were obtained using the 2+1+1-flavour clover-on-HISQ formulation. The connected contributions were obtained on 11 HISQ ensembles generated by the MILC collaboration with $a \approx 0.057$, 0.87, 0.12 and 0.15 fm, $M_\pi \approx 135$, 220 and 320 MeV, and $3.3 < M_\pi L < 5.5$. The light disconnected contributions were obtained on six of these ensembles with the lowest pion mass $M_\pi \approx 220$ MeV, while the strange discon-

Collaboration	Ref.	N_f	publication status	continuum extrapolation	chiral extrapolation	finite volume	renormalization	excited states	g_A^u	g_A^d
PNDME 20	[205]	2+1+1	C	★‡	★	★	★	○	0.790(23)(30)	−0.425(15)(30)
ETM 19	[160]	2+1+1	A	■	○	★	★	○	0.862(17)	−0.424(16)
PNDME 18A	[50]	2+1+1	A	★‡	★	★	★	○	0.777(25)(30)#	−0.438(18)(30)#
Mainz 19A	[206]	2+1	C	★	○	★	★	○	0.84(3)(4)	−0.40(3)(4)
χQCD 18	[27]	2+1	A	○	★	★	★	○	0.847(18)(32)$	−0.407(16)(18)$
									g_A^s	
PNDME 20	[205]	2+1+1	C	★‡	★	★	★	○	−0.053(7)	
ETM 19	[160]	2+1+1	A	■	○	★	★	○	−0.0458(73)	
PNDME 18A	[50]	2+1+1	A	★‡	★	★	★	○	−0.053(8)#	
Mainz 19A	[206]	2+1	C	★	○	★	★	○	−0.044(4)(5)	
χQCD 18	[27]	2+1	A	○	★	★	★	○	−0.035(6)(7)$	
JLQCD 18	[61]	2+1	A	■	○	○	★	○	−0.046(26)(9)#	
χQCD 15	[58]	2+1	A	■	○	■	★	○	−0.0403(44)(78)#	

Assumed that $Z_A^{n.s.} = Z_A^s$.

‡ The rating takes into account that the action is not fully $\mathcal{O}(a)$-improved by requiring an additional lattice spacing.

$ For this partially quenched analysis the criteria are applied to the unitary points.

Table 70: Overview of results for g_A^q.

nected contributions were obtained on seven ensembles, i.e., including an additional one at $a \approx 0.087$ fm and $M_\pi \approx 135$ MeV. The excited-state and the chiral-continuum fits were done separately for the connected and disconnected contributions, which introduces a systematic that is hypothesied to be small as explained in Ref. [50]. The analysis of the excited-state contamination, discussed in Sec. 10.1.2, was done using three-state fits for the connected contribution and two-state fits for the disconnected contributions. Isovector renormalization factors, calculated on the lattice in the RI-SMOM scheme and converted to $\overline{\text{MS}}$, are used for the flavour-diagonal operators, i.e., assuming $Z_{A,S,T}^{u-d} = Z_{A,S,T}^{u,d,s}$. The chiral-continuum extrapolation was done keeping the leading correction terms proportional to M_π^2 and a, and the leading finite-volume correction in $M_\pi L$ was included in the analysis of the connected contributions. The continuum-limit criteria, $\delta(a_{\text{min}})$, can only be extracted for g_A^s from PNDME

Collaboration	Ref.	N_f	publication status	continuum extrapolation	chiral extrapolation	finite volume	renormalization	excited states	g_T^u	g_T^d
PNDME 20	[205]	2+1+1	C	★‡	★	★	★	○	0.783(27)(10)	−0.205(10)(10)
ETM 19	[160]	2+1+1	A	■	○	★	★	○	0.729(22)	−0.2075(75)
PNDME 18B	[49]	2+1+1	A	★‡	★	★	★	○	0.784(28)(10)#	−0.204(11)(10)#
PNDME 16	[47]	2+1+1	A	○‡	★	★	★	○	0.792(42)#&	−0.194(14)#&
PNDME 15	[45, 46]	2+1+1	A	○‡	★	★	★	○	0.774(66)#	−0.233(28)#
Mainz 19A	[206]	2+1	C	★	○	★	★	○	0.77(4)(6)	−0.19(4)(6)
JLQCD 18	[61]	2+1	A	■	○	○	★	○	0.85(3)(2)(7)	−0.24(2)(0)(2)

Collaboration	Ref.	N_f	publication status	continuum extrapolation	chiral extrapolation	finite volume	renormalization	excited states	g_T^s
PNDME 20	[205]	2+1+1	C	★‡	★	★	★	○	−0.0022(12)
ETM 19	[160]	2+1+1	A	■	○	★	★	○	−0.00268(58)
PNDME 18B	[49]	2+1+1	A	★‡	★	★	★	○	−0.0027(16)#
PNDME 15	[45, 46]	2+1+1	A	○‡	★	★	★	○	0.008(9)#
Mainz 19A	[206]	2+1	C	★	○	★	★	○	−0.0026(73)(42)
JLQCD 18	[61]	2+1	A	■	○	○	★	○	−0.012(16)(8)

‡ The rating takes into account that the action is not fully $\mathcal{O}(a)$-improved by requiring an additional lattice spacing.
# Assumed that $Z_T^{n.s.} = Z_T^s$.
& Disconnected terms omitted.

Table 71: Overview of results for g_T^q.

18A and is 0.3.

The PNDME 20 [205] and the more recent conference proceedings, [207] and [208], are updates. They extend the disconnected calculations to eight ensembles, perform fits to the sum of the connected and disconnected contributions, and also show, through explicit calculations, that flavour mixing in the calculation of renormalization factors in the RI-sMOM scheme is small, and the isovector renormalization factor is a good approximation for renormalizing flavour-diagonal axial and tensor charges as discussed in Sec. 10.1.3. These updates are, however, not included in Tab. 71 as they are preliminary.

The ETM 19 [160] results for $g_A^{u,d,s,c}$ are from a single ensemble with 2+1+1-flavour twisted-mass fermions with a clover term at $a = 0.0801(4)$ fm and $M_\pi = 139.3(7)$ MeV. These are not considered for the averages as they do not satisfy the criteria for the continuum

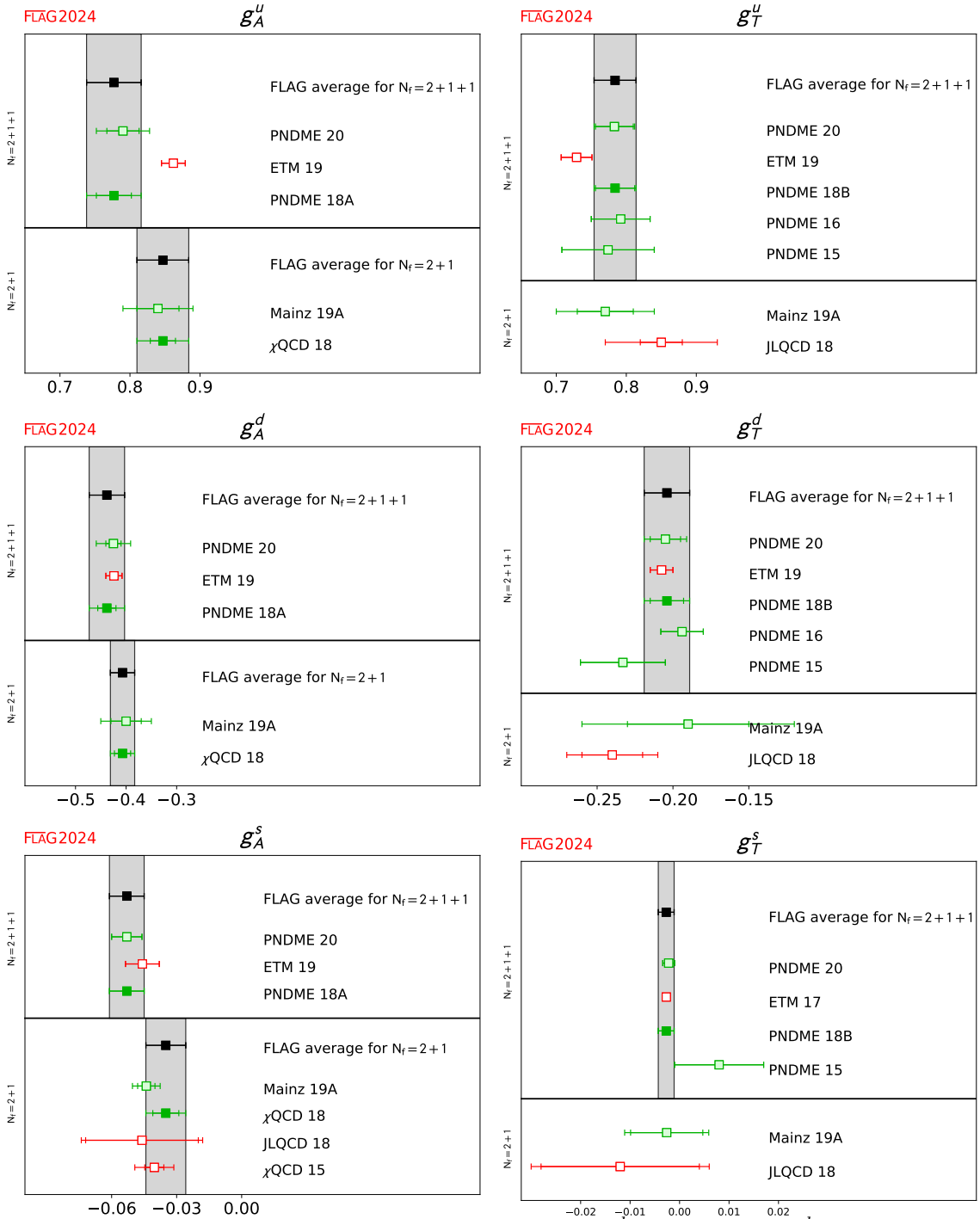

Figure 45: Lattice results and FLAG averages for $g_A^{u,d,s}$ (left) and $g_T^{u,d,s}$ (right) for the $N_f = 2+1$ and $2+1+1$-flavour calculations.

extrapolation.

The 2+1+1-flavour FLAG values for the axial charges $g_A^{u,d,s}$ of the proton are the PNDME

18A results given in Tab. 70:

$$N_f = 2+1+1: \qquad g_A^u = \quad 0.777(25)(30) \qquad \text{Ref. [50]}, \tag{437}$$
$$N_f = 2+1+1: \qquad g_A^d = -0.438(18)(30) \qquad \text{Ref. [50]}, \tag{438}$$
$$N_f = 2+1+1: \qquad g_A^s = -0.053(8) \qquad \text{Ref. [50]}. \tag{439}$$

The 2+1-flavour FLAG results from χQCD 18 [27] were obtained using the overlap-on-domain-wall formalism. Three domain-wall ensembles with lattice spacings 0.143, 0.11 and 0.083 fm and sea-quark pion masses M_π = 171, 337 and 302 MeV, respectively, were analyzed. In addition to the three approximately unitary points, the paper presents data for an additional 4–5 valence-quark masses on each ensemble, i.e., partially quenched data. Separate excited-state fits were done for the connected and disconnected contributions. The continuum, chiral and volume extrapolation to the combined unitary and nonunitary data is made including terms proportional to both $M^2_{\pi,\text{valence}}$ and $M^2_{\pi,\text{sea}}$, and two $\mathcal{O}(a^2)$ discretization terms for the two different domain-wall actions. With just three unitary points, not all the coefficients are well constrained. The $M_{\pi,sea}$-dependence is omitted and considered as a systematic, and a prior is used for the coefficients of the a^2-terms to stabilize the fit. The continuum-limit criteria, $\delta(a_{\min})$, could not be extracted for these results from χQCD 18.

These χQCD 18 2+1-flavour results for the proton, which supersede the χQCD 15 [58] analysis, are

$$N_f = 2+1: \qquad g_A^u = \quad 0.847(18)(32) \qquad \text{Ref. [27]}, \tag{440}$$
$$N_f = 2+1: \qquad g_A^d = -0.407(16)(18) \qquad \text{Ref. [27]}, \tag{441}$$
$$N_f = 2+1: \qquad g_A^s = -0.035(6)(7) \qquad \text{Ref. [27]}. \tag{442}$$

The results for $g_A^{u,d,s}$ from Mainz 19A [206] satisfy all the criteria, however, they are not included in the averages as [206] is a conference proceeding. The JLQCD 18 [61], ETM 17C [42] and Engelhardt 12 [209] calculations were not considered for the averages as they did not satisfy the criteria for the continuum extrapolation. All three calculations were done at a single lattice spacing. The JLQCD 18 calculation used overlap fermions and the Iwasaki gauge action. They perform a chiral fit using data at four pion masses in the range 290–540 MeV. Finite-volume corrections are assumed to be negligible since each of the two pairs of points on different lattice volumes satisfy $M_\pi L \geq 4$. The ETM 17C calculation is based on a single twisted-mass ensemble with M_π = 130 MeV, a = 0.094 and a relatively small $M_\pi L$ = 2.98. Engelhardt 12 [209] calculation was done on three asqtad ensembles with M_π = 293, 356 and 495 MeV, but all at a single lattice spacing a = 0.124 fm.

Results for g_A^s are also presented by LHPC in Ref. [7]. However, this calculation is not included in Tab. 70 as it has been performed on a single ensemble with a = 0.114 fm and a heavy pion mass, $M_\pi \approx 317$ MeV.

Switching to the tensor charges, $g_T^{u,d,s}$, only one calculation, the PNDME 18B [49], qualifies for the FLAG averaging. These 2+1+1-flavour theory results, which use the same ensembles already discussed for $g_A^{u,d,s}$, supersede those in PNDME 16 [47] and PNDME 15 [45]. The continuum-limit criteria, $\delta(a_{\min})$, can only be extracted for g_T^s from PNDME 18B and is 0.5. Again, results in the more recent conference proceedings, [207] and [208], are not discussed here as they are preliminary.

The FLAG values for the proton in the $\overline{\text{MS}}$ scheme at 2 GeV, which remain the same as in FLAG 19 and FLAG 21, are:

$$N_f = 2+1+1: \qquad g_T^u = \quad 0.784(28)(10) \qquad \text{Ref. [49]}, \tag{443}$$
$$N_f = 2+1+1: \qquad g_T^d = -0.204(11)(10) \qquad \text{Ref. [49]}, \tag{444}$$
$$N_f = 2+1+1: \qquad g_T^s = -0.0027(16) \qquad \text{Ref. [49]}. \tag{445}$$

The ensembles and the analysis strategy used in PNDME 18B is the same as described in PNDME 18A for $g_A^{u,d,s}$. The only difference for the tensor charges was that a one-state (constant) fit was used for the disconnected contributions as the data did not show significant excited-state contamination. The isovector renormalization factors, used for all three flavour-diagonal tensor operators, were calculated on the lattice in the RI-SMOM scheme and converted to $\overline{\text{MS}}$ at 2 GeV using 2-loop perturbation theory [210]. The proceeding [208] extends the calculation to eight ensembles and reports that flavour mixing in the calculation of renormalization factors is small, and the isovector renormalization factor, which was used for renormalizing the flavour-diagonal tensor charges in PNDME 18B, is a good approximation.

The ETM 19 [160] results for $g_T^{u,d,s,c}$ are from a single ensemble with 2+1+1-flavour twisted-mass fermions with a clover term at $a = 0.0801(4)$ fm and $M_\pi = 139.3(7)$ MeV. It was not considered for the final averages because it did not satisfy the criteria for the continuum extrapolation. The same applies to the JLQCD 18 [61] and ETM 17 [43] calculations. The Mainz 19A [206] results with 2+1-flavour ensembles of clover fermions are not included in the averages as Ref. [206] is a conference proceeding.

10.4.2 Results for $g_S^{u,d,s}$ from direct and hybrid calculations of the matrix elements

The sigma terms $\sigma_q = m_q\langle N|\bar{q}q|N\rangle = m_q g_S^q$ or the quark-mass fractions $f_{T_q} = \sigma_q/M_N$ are normally computed rather than g_S^q. These combinations have the advantage of being renormalization group invariant in the continuum, and this holds on the lattice for actions with good chiral properties, see Sec. 10.1.3 for a discussion. In order to aid comparison with phenomenological estimates, e.g., from π-N scattering [214–216], the light-quark sigma terms are usually added to give the πN sigma term, $\sigma_{\pi N} = \sigma_u + \sigma_d$. The direct evaluation of the sigma terms involves the calculation of the corresponding three-point correlation functions for different source-sink separations τ. For $\sigma_{\pi N}$ there are both connected and disconnected contributions, while for most lattice fermion formulations only disconnected contributions are needed for σ_s. The techniques typically employed lead to the availability of a wider range of τ for the disconnected contributions compared to the connected ones (both, however, suffer from signal-to-noise problems for large τ, as discussed in Sec. 10.1) and we only comment on the range of τ computed for the latter in the following.

Recent $N_f = 2+1$ and $N_f = 2+1+1$ results for $\sigma_{\pi N}$ and σ_s from the direct approach are compiled in Tab. 72. In the following, we summarize new results that have appeared since the last FLAG report and previous studies that enter the averages. Details of ETM 19 [160] and JLQCD 18 [61] can be found in the FLAG 21 report. As there have been no new $N_f = 2$ studies of the sigma terms since the introduction of the section on nucleon matrix elements [36, 40], we also refer the reader to the previous report for a discussion of these results and other early three- and four-flavour works with at least one red square [56, 60, 209].

Collaboration	Ref.	N_f	publication status	continuum extrapolation	chiral extrapolation	finite volume	renormalization	excited states	$\sigma_{\pi N}$ [MeV]	σ_s [MeV]
PNDME 21	[106]	2+1+1	A	○ ‡	★	★	[a]/–	○	59.6(7.4)	–
ETM 19	[160]	2+1+1	A	■	○	★	na/na	○	41.6(3.8)	45.6(6.2)
Mainz 23	[211]	2+1	A	★ [b]	★	★	★/★	○	43.7(3.6)	28.6(9.3)
JLQCD 18	[61]	2+1	A	■	○	○	na/na	○	26(3)(5)(2)	17(18)(9)
χQCD 15A	[57]	2+1	A	○	★	★	na/na	○	45.9(7.4)(2.8)[$]	40.2(11.7)(3.5)[$]
MILC 12C	[212]	2+1+1	A	★	★	★	–/○	○	–	0.44(8)(5)×m_s [¶§]
MILC 12C	[212]	2+1	A	★	○	★	–/○	○	–	0.637(55)(74)×m_s [¶§]
MILC 09D	[213]	2+1	A	★	○	★	–/na	○	–	59(6)(8)[§]

The renormalization criteria is given for $\sigma_{\pi N}$ (first) and σ_s (second). The label 'na' indicates that no renormalization is required.

- *a* Mixing between quark flavours is found to be small and is neglected.
- ‡ The rating takes into account that the action is not fully $\mathcal{O}(a)$-improved by requiring an additional lattice spacing.
- *b* The rating takes into account that the scalar current is not fully $\mathcal{O}(a)$-improved by requiring an additional lattice spacing. The gluonic operator that appears in the $\mathcal{O}(a)$ improvement for Wilson fermions is not implemented. The effect of this term is expected to be small.
- $ For this partially quenched analysis the criteria are applied to the unitary points.
- § This study employs a hybrid method, see Ref. [213].
- ¶ The matrix element $\langle N|\bar{s}s|N\rangle$ at the scale $\mu = 2$ GeV in the $\overline{\text{MS}}$ scheme is computed.

Table 72: Overview of results for $\sigma_{\pi N}$ and σ_s from the direct approach (above) and σ_s from the hybrid approach (below).

Starting with $N_f = 2 + 1 + 1$, there is a new study from PNDME [106]. This calculation is based on a mixed-action set-up of $\mathcal{O}(a)$-improved Wilson valence fermions on top of staggered (HISQ) gauge ensembles generated by the MILC collaboration. Six ensembles are utilized with lattice spacings, $a \approx 0.12, 0.09$ and 0.06 fm and pion masses $M_\pi \approx 315, 230$ and 138 MeV. The two-point and three-point correlation functions are fitted simultaneously including contributions from four and three states, respectively, where wide-width priors are used for the excited-state masses entering the fits. Four to five values of the source-sink separation are utilized with the largest $\tau \approx 1.5$ fm. The fitting procedure is repeated using a narrow-width prior for the first excited state which is set to the energy of the lowest multi-hadron state ($N\pi$ or $N\pi\pi$, see Sec. 10.1.2). This choice is motivated by a χPT analysis [106],

which indicates that excited-state contributions arising from low-lying $N\pi$ and $N\pi\pi$ states can be significant on close-to-physical pion mass ensembles. In particular, there is a significant enhancement of the disconnected contribution due to the large QCD condensate. The quality of the fits is, however, similar for both a narrow- and wide-width prior for the first excited state. Combined continuum- and chiral-limit fits are performed with a parameterization composed of a term linear in the lattice spacing and the NNLO SU(2) baryon χPT expression for the pion-mass dependence. Finite-volume effects are not resolved. The result from the narrow-width first-excited-state prior analysis is chosen as the final value, while the wide-width prior analysis (which has a first-excited-state energy significantly above the lowest $N\pi$ or $N\pi\pi$ noninteracting level) gives $\sigma_{\pi N} \approx 42$ MeV.

Moving on to the $N_f = 2+1$ results, Mainz 23 [211] is a new study employing 16 nonperturbatively $\mathcal{O}(a)$-improved Wilson fermion ensembles from the CLS consortium. The flavour average of the light- and strange-quark mass is held constant in the simulations as the pion mass varies in the range $350 \gtrsim M_\pi \gtrsim 130$ MeV. Four lattice spacings are realized, with $a = 0.050$–0.086 fm. The connected three-point functions are computed for a large number of source-sink separations (between 9 and 17 values of τ, depending on the ensemble) where the largest $\tau = 1.4$–1.5 fm. The ground-state matrix elements are extracted employing two analysis strategies: one employing the summation method (with only the ground-state terms) and the other performing two-state fits to correlator ratios. For the latter, the mass gap to the first excited state is set with a prior equal to twice the pion mass. As both the light- and strange-quark masses vary in the simulations, $\sigma_{\pi N}$ and σ_s are fitted simultaneously with the quark-mass dependence parameterized by SU(3) $\mathcal{O}(p^3)$ covariant baryon χPT. Combined continuum, chiral and finite-volume fits are performed, where cuts are made on the data set entering the fit which depend on the lattice spacing, finite volume and pion mass. Akaike-information-criterion [139] averages of the results are computed for the two analysis choices separately. The two results are then combined to form the final values.

The χQCD 15A [57] study also qualifies for global averaging. In this mixed-action study, three RBC/UKQCD $N_f = 2+1$ domain-wall ensembles are analyzed comprising two lattice spacings, $a = 0.08$ fm with $M_{\pi,\text{sea}} = 300$ MeV and $a = 0.11$ fm with $M_{\pi,\text{sea}} = 330$ MeV and 139 MeV. Overlap fermions are employed with a number of nonunitary valence-quark masses. The connected three-point functions are measured with three values of τ in the range 0.9–1.4 fm. A combined chiral, continuum and volume extrapolation is performed for all data with $M_\pi < 350$ MeV. The leading-order expressions are taken for the lattice-spacing and volume dependence while partially quenched SU(2) HBχPT up to M_π^3-terms models the chiral behaviour for $\sigma_{\pi N}$. The strange-quark sigma term has a milder dependence on the pion mass and only the leading-order quadratic terms are included in this case.

MILC has also computed σ_s using a hybrid method [213] which makes use of the Feynman-Hellmann (FH) theorem and involves evaluating the nucleon matrix element $\langle N|\int d^4x\, \bar{s}s|N\rangle$.[5] This method is applied in MILC 09D [213] to the $N_f = 2+1$ asqtad ensembles with lattice spacings $a = 0.06$, 0.09, 0.12 fm and values of M_π ranging down to 224 MeV. A continuum and chiral extrapolation is performed including terms linear in the light-quark mass and quadratic in a. As the coefficient of the discretization term is poorly determined, a Bayesian prior is used, with a width corresponding to a 10% discretization effect between the continuum limit

[5] Note that in the direct method the matrix element $\langle N|\int d^3x\, \bar{s}s|N\rangle$, involving the spatial-volume sum, is evaluated for a fixed timeslice.

and the coarsest lattice spacing.[6] A similar updated analysis is presented in MILC 12C [212], with an improved evaluation of $\langle N|\int d^4x\,\bar{s}s|N\rangle$ on a subset of the $N_f = 2+1$ asqtad ensembles. The study is also extended to HISQ $N_f = 2+1+1$ ensembles comprising four lattice spacings with $a = 0.06$–0.15 fm and a minimum pion mass of 131 MeV. Results are presented for $g_S^s = \langle N|\bar{s}s|N\rangle$ (in the $\overline{\text{MS}}$ scheme at 2 GeV) rather than for σ_s. The scalar matrix element is renormalized for both three and four flavours using the 2-loop factor for the asqtad action [217]. The error incurred by applying the same factor to the HISQ results is expected to be small.[7]

Both MILC 09D and MILC 12C achieve green tags for all the criteria, see Tab. 72. As the same set of asqtad ensembles is utilized in both studies we take MILC 12C as superseding MILC 09D for the three-flavour case. The global averaging is discussed in Sec. 10.4.4.

10.4.3 Results for $g_S^{u,d,s}$ using the Feynman-Hellmann theorem

An alternative approach for accessing the sigma terms is to determine the slope of the nucleon mass as a function of the quark masses, or equivalently, the squared pseudoscalar meson masses. The Feynman-Hellman (FH) theorem gives

$$\sigma_{\pi N} = m_u\frac{\partial M_N}{\partial m_u} + m_d\frac{\partial M_N}{\partial m_d} \approx M_\pi^2\frac{\partial M_N}{\partial M_\pi^2}, \qquad \sigma_s = m_s\frac{\partial M_N}{\partial m_s} \approx M_{\bar{s}s}^2\frac{\partial M_N}{\partial M_{\bar{s}s}^2}, \tag{446}$$

where the fictitious $\bar{s}s$ meson has a mass squared $M_{\bar{s}s}^2 = 2M_K^2 - M_\pi^2$. In principle this is a straightforward method as the nucleon mass can be extracted from fits to two-point correlation functions, and a further fit to M_N as a function of M_π (and also M_K for σ_s) provides the slope. Nonetheless, this approach presents its own challenges: a functional form for the chiral behaviour of the nucleon mass is needed, and while baryonic χPT (BχPT) is the natural choice, the convergence properties of the different formulations are not well established. Results are sensitive to the formulation chosen and the order of the expansion employed. If there is an insufficient number of data points when implementing higher-order terms, the coefficients are sometimes fixed using additional input, e.g., from analyses of experimental data. This may influence the slope extracted. Simulations with pion masses close to or bracketing the physical point can alleviate these difficulties. In some studies the nucleon mass is used to set the lattice spacing. This naturally forces the fit to reproduce the physical nucleon mass at the physical point and may affect the extracted slope. Note that, if the nucleon mass is fitted as a function of the pion and kaon masses, the dependence of the meson masses on the quark masses also, in principle, needs to be considered in order to extract the sigma terms.

An overview of recent three- and four-flavour determinations of $\sigma_{\pi N}$ and σ_s is given in Tab. 73. All the results are eligible for global averaging, with RQCD 22 [221] being the sole new work. For details of earlier works (published before 2014) with at least one red square [38, 60, 132, 227–229] and all $N_f = 2$ [32, 59] works we refer the reader to the FLAG 21 report. Note that the renormalization criterion is not included in Tab. 73 as renormalization is not normally required when computing the sigma terms in the Feynman-Hellmann approach.[8] At present, a rating indicating control over excited-state contamination is also not considered since a wide range of source-sink separations are available for nucleon two-point functions

[6] This is consistent with discretization effects observed in other quantities at $a = 0.12$ fm.

[7] At least at 1-loop the renormalization factors for HISQ and asqtad are very similar, cf. Ref. [218].

[8] An exception to this is when clover fermions are employed. In this case one must take care of the mixing between quark flavours when renormalizing the quark masses that appear in Eq. (446).

Collaboration	Ref.	N_f	publication status	continuum extrapolation	chiral extrapolation	finite volume	$\sigma_{\pi N}$ [MeV]	σ_s [MeV]
BMW 20A	[219]	1+1+1+1	P	★‡	★	★	0.0398(32)(44)×m_N †	0.0577(46)(33)×m_N †
ETM 14A	[220]	2+1+1	A	★	○	○	64.9(1.5)(13.2)△	–
RQCD 22	[221]	2+1	A	★	★	★	43.9(4.7)	$16(^{58}_{68})$
BMW 15	[222]	2+1	A	★‡	★	★	38(3)(3)	105(41)(37)
Junnarkar 13	[223]	2+1	A	○	○	○	–	48(10)(15)
BMW 11A	[224]	2+1	A	○‡	★	○	$39(4)(^{18}_{7})$	$67(27)(^{55}_{47})$

△ Two results for $\sigma_{\pi N}$ are quoted arising from different fit ansätze to the nucleon mass. The systematic error is the same as in Ref. [225] for a combined $N_f = 2$ and $N_f = 2+1+1$ analysis [226].

‡ The rating takes into account that the action is not fully O(a) improved by requiring an additional lattice spacing.

† The quark fractions $f_{T_{ud}} = f_{T_u} + f_{T_d} = \sigma_{\pi N}/m_N$ and $f_{T_s} = \sigma_s/m_N$ are computed.

Table 73: Overview of results for $\sigma_{\pi N}$ and σ_s from the Feynman-Hellmann approach.

and ground-state dominance is normally achieved. This issue may be revisited in the future as statistical precision improves and this systematic is further investigated.

We first summarize the determinations of $\sigma_{\pi N}$. BMW have performed a $N_f = 1+1+1+1$ study BMW 20A [219] which follows a two-step analysis procedure: the dependence of the nucleon mass on the pion and kaon masses is determined on HEX-smeared clover ensembles with $a = 0.06$–0.1 fm and pion masses in the range $M_\pi = 195$–420 MeV. The meson masses as a function of the quark masses are evaluated on stout-staggered ensembles with a similar range in a and quark masses which bracket their physical values. As [219] is a preprint, their results (for both sigma terms) are not considered for global averaging.

Regarding $N_f = 2+1+1$, there is only one recent study. In ETM 14A [220], fits are performed to the nucleon mass utilizing SU(2) χPT for data with $M_\pi \geq 213$ MeV as part of an analysis to set the lattice spacing. The expansion is considered to $\mathcal{O}(p^3)$ and $\mathcal{O}(p^4)$, with two and three of the coefficients as free parameters, respectively. The difference between the two fits is taken as the systematic error. No discernable discretization or finite-volume effects are observed where the lattice spacing is varied over the range $a = 0.06$–0.09 fm and the spatial volumes cover $M_\pi L = 3.4$ up to $M_\pi L > 5$. The results are unchanged when a near-physical-point $N_f = 2$ ensemble is added to the analysis in Ref. [225].

Turning to $N_f = 2+1$, RQCD 22 [221] utilizes 49 nonperturbatively $\mathcal{O}(a)$-improved Wilson fermion CLS ensembles, with six lattice spacings in the range $0.04 \leq a \leq 0.1$ fm and $M_\pi \sim 130$–410 MeV. The ensembles lie on three trajectories in the quark-mass plane, two of which meet at the physical point. Simultaneous fits to the bayon octet are performed, employing SU(3) $\mathcal{O}(p^3)$ covariant baryon χPT, heavy baryon χPT and Taylor-expansion fit

forms for the quark-mass dependence. The final values at the physical point in the continuum and infinite-volume limits are obtained by performing an Akaike-information-criterion [139] average of the covariant baryon χPT fits to various reduced data sets. These fits include finite-volume terms to $\mathcal{O}(p^3)$ as well as terms quadratic in the lattice spacing in order to model cut-off effects.

In BMW 11A [224], stout-smeared tree-level clover fermions are employed on 15 ensembles with simulation parameters encompassing $a = 0.06$–0.12 fm, $M_\pi \sim 190$–550 MeV and $M_\pi L \gtrsim 4$. Taylor, Padé and covariant SU(3) BχPT fit forms are considered. Due to the use of smeared gauge links, discretization effects are found to be mild even though the fermion action is not fully $\mathcal{O}(a)$-improved. Fits are performed including an $\mathcal{O}(a)$ or $\mathcal{O}(a^2)$ term and also without a lattice-spacing-dependent term. Finite-volume effects were assessed to be small in an earlier work [230]. The final results are computed considering all combinations of the fit ansatz weighted by the quality of the fit. In BMW 15 [222], a more extensive analysis on 47 ensembles is presented for HEX-smeared clover fermions involving five lattice spacings and pion masses reaching down to 120 MeV. Bracketing the physical point reduces the reliance on a chiral extrapolation. Joint continuum, chiral and infinite-volume extrapolations are carried out for a number of fit parameterizations with the final results determined via the Akaike-information-criterion procedure. Although only $\sigma_{\pi N}$ is accessible in the FH approach in the isospin limit, the individual quark fractions $f_{T_q} = \sigma_q/M_N$ for $q = u, d$ for the proton and the neutron are also quoted in BMW 15, using isospin relations.[9]

With one exception, all of the above studies have also determined the strange-quark sigma term, while Junnarkar 13 [223] only presents results for σ_s. This quantity is difficult to access via the Feynman-Hellmann method since in most simulations the physical point is approached by varying the light-quark mass, keeping m_s approximately constant. While additional ensembles can be generated, it is hard to resolve a small slope with respect to m_s. Such problems are illustrated by the large uncertainties in the results from BMW 11A and BMW 15. Alternative approaches have been pursued where the physical point is approached along a trajectory keeping the average of the light- and strange-quark masses fixed [228], and where quark-mass reweighting is applied [60]. One can also fit to the whole baryon octet and apply SU(3) flavour-symmetry constraints as investigated in RQCD 22 [221] and Refs. [224, 227–229].

Junnarkar 13 [223] is a mixed-action study which utilizes domain-wall valence fermions on MILC $N_f = 2{+}1$ asqtad ensembles. The derivative $\partial M_N/\partial m_s$ is determined from simulations above and below the physical strange-quark mass for M_π around 240–675 MeV. The resulting values of σ_s are extrapolated quadratically in M_π. The quark fraction $f_{T_s} = \sigma_s/M_N$ exhibits a milder pion-mass dependence and extrapolations of this quantity were also performed using ansätze linear and quadratic in M_π. A weighted average of all three fits was used to form the final result. Two lattice spacings were analyzed, with a around 0.09 fm and 0.12 fm, however, discretization effects could not be resolved.

The global averaging of the results is discussed in the next section.

10.4.4 Summary of Results for $g_S^{u,d,s}$

We consider computing global averages of results determined via the direct, hybrid and Feynman-Hellmann (FH) methods. Beginning with $\sigma_{\pi N}$, Tabs. 72 and 73 show that for

[9] These isospin relations were also derived in Ref. [231].

$N_f = 2+1+1$ ETM 14A (FH) and PNDME 21 (direct) satisfy the selection criteria. The FLAG average for the four-flavour case reads

$$N_f = 2+1+1: \qquad \sigma_{\pi N} = 60.9(6.5)\ \text{MeV} \qquad \text{Refs. [106, 220].} \tag{447}$$

We remark that although the $N_f = 1+1+1+1$ BMW 20A study [219] also satisfies the criteria, it is not considered for averaging as it is a preprint. For $N_f = 2+1$ we form an average from the BMW 11A (FH), BMW 15 (FH), χQCD 15A (direct), RQCD 22 (FH) and Mainz 23 (direct) results, yielding

$$N_f = 2+1: \qquad \sigma_{\pi N} = 42.2(2.4)\ \text{MeV} \qquad \text{Refs. [57, 211, 221, 222, 224].} \tag{448}$$

Note that both BMW results are included as they were obtained on independent sets of ensembles (employing different fermion actions). The RQCD 22 and Mainz 23 studies both utilize CLS $N_f = 2+1$ ensembles (the latter utilizes a subset of the ensembles employed by the former). To be conservative we take the statistical errors for these two studies to be 100% correlated. The FLAG result for $N_f = 2$ can be found in the FLAG 21 report [1].

Moving on to σ_s and the calculations detailed in Tab. 72, for $N_f = 2+1+1$ MILC 12C (hybrid) and BMW 20A satisfy the quality criteria, however, the latter is a preprint and is not considered for averaging. In order to convert the result for $\langle N|\bar{s}s|N\rangle$ given in MILC 12C to a value for σ_s, we multiply by the appropriate FLAG average for m_s given in Eq. (35) of FLAG 19. This gives our result for four flavours, which is unchanged since the last FLAG report,

$$N_f = 2+1+1: \qquad \sigma_s = 41.0(8.8)\ \text{MeV} \qquad \text{Ref. [212].} \tag{449}$$

For $N_f = 2+1$ we perform a weighted average of BMW 11A (FH), MILC 12C (hybrid), Junnarkar 13 (FH), BMW 15 (FH), χQCD 15A (direct), RQCD 22 (FH) and Mainz 23 (direct). MILC 09D [213] also passes the FLAG selection rules, however, this calculation is superseded by MILC 12C. As for Eq. (449), the strangeness scalar matrix element determined in the latter study is multiplied by the three-flavour FLAG average for m_s given in Eq. (33) of FLAG 19. There are correlations between the MILC 12C and Junnarkar 13 results as there is some overlap between the sets of asqtad ensembles used in both cases. We take the statistical errors for these two studies to be 100% correlated and, similarly, for the Mainz 23 and RQCD 22 studies (as for $\sigma_{\pi N}$). The global average is

$$N_f = 2+1: \qquad \sigma_s = 44.9(6.4)\ \text{MeV} \qquad \text{Refs. [57, 211, 212, 221–224],} \tag{450}$$

where the error has been increased by around 10% because $\chi^2/dof = 1.2317$ for the weighted average. For all the other averages presented above, the χ^2/dof is less than one and no rescaling of the error is applied. There are no $N_f = 2$ studies of σ_s which pass the FLAG quality criteria, see the FLAG 21 report for further details.

We remark that it was not possible to determine $\delta(a_{\min})$ for the above works based on the information provided.

All the results for $\sigma_{\pi N}$ and σ_s are displayed in Figs. 46 and 47 along with the averages given above. Note that where $f_{T_{ud}} = f_{T_u} + f_{T_d}$ or f_{T_s} is quoted in Tabs. 72 and 73, we multiply by the experimental proton mass in order to include the results in the figures. For $\sigma_{\pi N}$, the averages are consistent with the respective FLAG 21 values, however, the errors are significantly reduced. For four flavours, this is due to the PNDME 21 direct result, which dominates the average. The results that enter the average for three flavours, are all

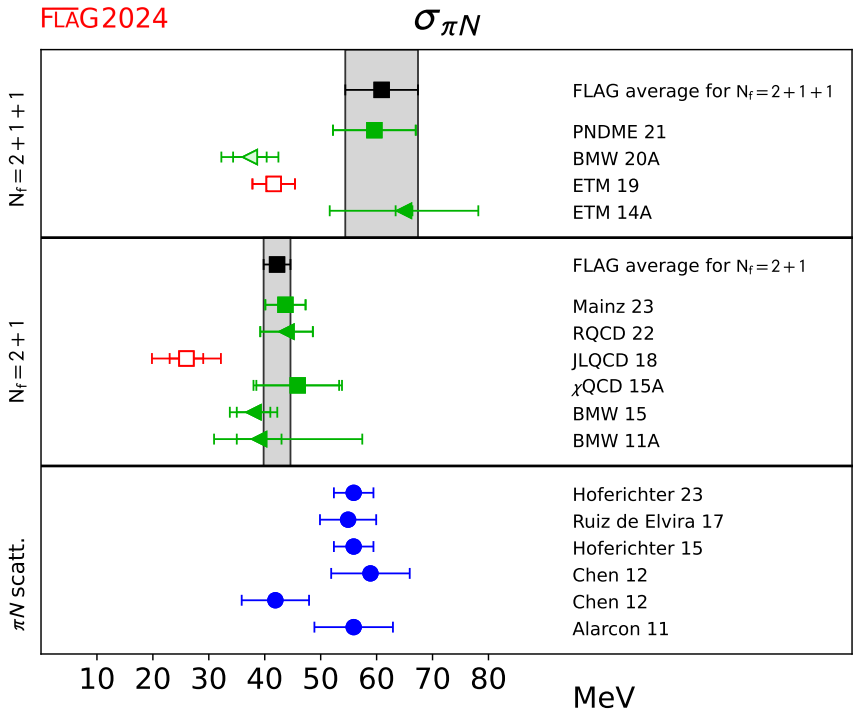

Figure 46: Lattice results and FLAG averages for the nucleon sigma term, $\sigma_{\pi N}$, for the $N_f = 2+1$, and $2+1+1$ flavour calculations. Determinations via the direct approach are indicated by squares and the Feynman-Hellmann method by triangles. Results from recent analyses of π-N scattering [214–216, 232, 233] (circles) are shown for comparison. Note that the charged pion is used to define the isospin limit in these phenomenological analyses, while the neutral pion with $M_\pi \sim 135$ MeV is usually used to define the physical point in lattice simulations. We adjust the results to be consistent with the latter, applying the correction for the different conventions determined in Ref. [233].

consistent with each other and the addition of the RQCD 22 and Mainz 23 studies reduces the uncertainty. The latter is the most precise result to date which passes all the FLAG quality criteria. Notably, there is now a 2.7σ difference between the $N_f = 2+1$ and $N_f = 2+1+1$ FLAG averages. This is unlikely to be due to the inclusion of charm quarks in the sea. The control of excited-state contributions remains an issue. In particular, the PNDME 21 study utilizes a narrow-width prior in their fitting analysis set to the lowest multi-hadron ($N\pi$ or $N\pi\pi$) excited-state energy. This is motivated by a χPT analysis which indicates that these multi-hadron contributions are significant at physical pion masses. If this constraint is relaxed then a sigma term of around 42 MeV is obtained. Mainz 23 also find an increase in the sigma term if such a prior is included in the fitting procedure; however, the shift is much less pronounced. Although progress is being made in terms of improving the statistical precision of the correlation functions and realising more source-sink separations (with the maximum separation currently around 1.5 fm), more work needs to be done in order to control excited-state contributions at close-to-physical pion masses. We caution the reader that as more results for both $\sigma_{\pi N}$ and σ_s become available the averages may change.

Also shown for comparison in the figures are determinations of $\sigma_{\pi N}$ from recent analyses of π-N scattering [214–216, 232, 233]. The $N_f = 2+1+1$ lattice average is in agreement with

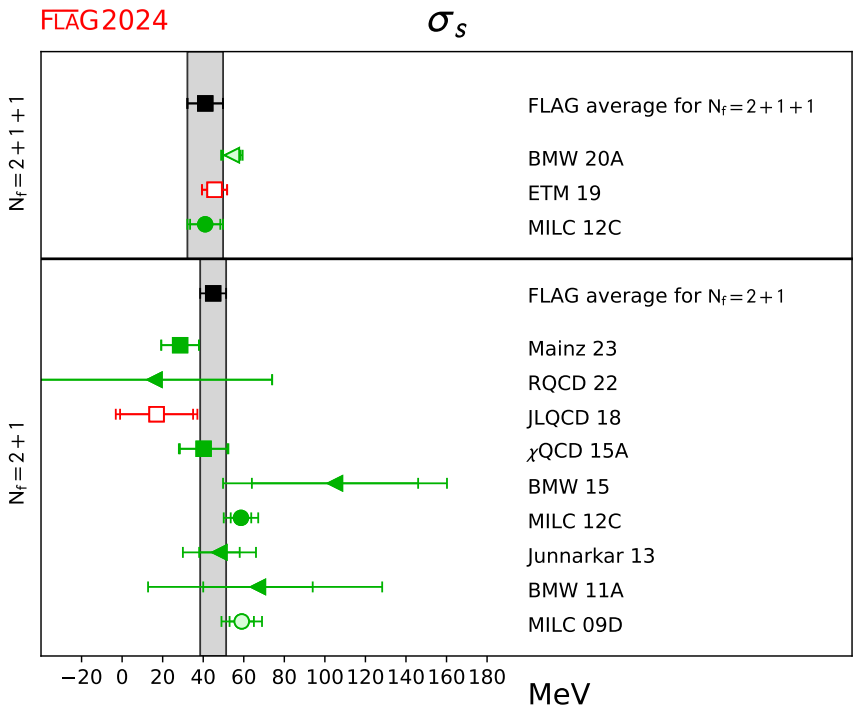

Figure 47: Lattice results and FLAG averages for σ_s for the $N_f = 2+1$, and $2+1+1$ flavour calculations. Determinations via the direct approach are indicated by squares, the Feynman-Hellmann method by triangles and the hybrid approach by circles.

Hoferichter et al. [233] (Hoferichter 23 in Fig. 46), while there is some tension, at the level of around three standard deviations, with the lattice average for $N_f = 2+1$.[10]

For the strangeness sigma term, the four-flavour average is unchanged from the previous FLAG report, while the three-flavour average has decreased by 1σ and there is a small reduction in the error. There is a slight tension between the Mainz 23 and MILC 12C $N_f = 2+1$ results, however, both FLAG averages are consistent with each other.

Finally we remark that, by exploiting the heavy-quark limit, the light- and strange-quark sigma terms can be used to estimate σ_q for the charm, bottom and top quarks [195–197]. The resulting estimate for the charm quark, see, e.g., the RQCD 16 $N_f = 2$ analysis of Ref. [36] that reports $f_{T_c} = 0.075(4)$ or $\sigma_c = 70(4)$ MeV, is consistent with the direct determinations of ETM 19 [160] for $N_f = 2+1+1$ of $\sigma_c = 107(22)$ MeV, ETM 16A [40] for $N_f = 2$ of $\sigma_c = 79(21)(^{12}_{8})$ MeV and χQCD 13A [56] for $N_f = 2+1$ of $\sigma_c = 94(31)$ MeV. BMW in BMW 20A [219] employing the Feynman-Hellmann approach obtain $f_{T_c} = \sigma_c/m_N = 0.0734(45)(55)$ for $N_f = 1+1+1+1$. MILC in MILC 12C [212] find $\langle N|\bar{c}c|N\rangle = 0.056(27)$ in the $\overline{\text{MS}}$ scheme at a scale of 2 GeV for $N_f = 2+1+1$ via the hybrid method. Considering the large uncertainty, this is consistent with the other results once multiplied by the charm-quark mass.

[10] We adjust the result of Ref. [233] such that it is consistent with defining the isospin limit using the mass of the neutral pion.

10.5 Isovector second Mellin moments $\langle x\rangle_{u-d}$, $\langle x\rangle_{\Delta u-\Delta d}$ and $\langle x\rangle_{\delta u-\delta d}$

This section introduces the basics of the calculation of the momentum fraction carried by the quarks and the transversity and helicity moments in the isovector channel. These moments of spin-independent (i.e., unpolarized), $q = q_\uparrow + q_\downarrow$, helicity (i.e., polarized), $\Delta q = q_\uparrow - q_\downarrow$, and transversity, $\delta q = q_\top + q_\perp$ distributions, are defined as

$$\langle x\rangle_q = \int_0^1 x\,[q(x)+\overline{q}(x)]\,dx\,, \tag{451}$$

$$\langle x\rangle_{\Delta q} = \int_0^1 x\,[\Delta q(x)+\Delta\overline{q}(x)]\,dx\,, \tag{452}$$

$$\langle x\rangle_{\delta q} = \int_0^1 x\,[\delta q(x)+\delta\overline{q}(x)]\,dx\,, \tag{453}$$

where $q_{\uparrow(\downarrow)}$ corresponds to quarks with helicity aligned (anti-aligned) with that of a longitudinally polarized target, and $q_{\top(\perp)}$ corresponds to quarks with spin aligned (anti-aligned) with that of a transversely polarized target. These alignments are shown pictorially in Fig. 48.

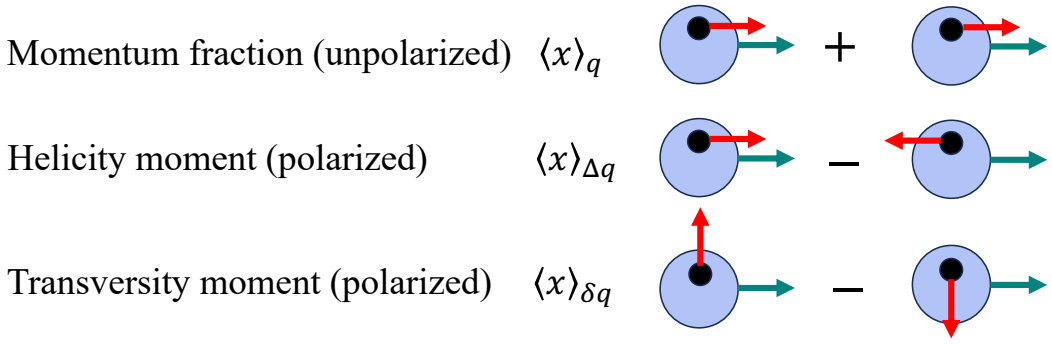

Figure 48: A pictorial description of the three moments showing the direction of the spin of the quark (red arrow) with respect to the nucleon momentum (green arrow).

At leading twist, these moments can be extracted from the forward matrix elements of one-derivative vector, axial-vector and tensor operators within ground-state nucleons. The complete set of the relevant twist-two operators are

$$\begin{aligned}
\mathcal{O}^{\mu\nu}_{V^a} &= \overline{q}\gamma^{\{\mu}\overleftrightarrow{D}^{\nu\}}\tau^a q\,,\\
\mathcal{O}^{\mu\nu}_{A^a} &= \overline{q}\gamma^{\{\mu}\overleftrightarrow{D}^{\nu\}}\gamma^5\tau^a q\,,\\
\mathcal{O}^{\mu\nu\rho}_{T^a} &= \overline{q}\sigma^{[\mu\{\nu]}\overleftrightarrow{D}^{\rho\}}\tau^a q\,,
\end{aligned} \tag{454}$$

where $q = \{u, d\}$ is the isodoublet of light quarks and $\sigma^{\mu\nu} = (\gamma^\mu\gamma^\nu - \gamma^\nu\gamma^\mu)/2$. The derivative $\overleftrightarrow{D}^\nu \equiv \frac{1}{2}(\overrightarrow{D}^\nu - \overleftarrow{D}^\nu)$ consists of four terms defined in Ref. [234]. Lorentz indices within { } in Eq. (454) are symmetrized and within [] are antisymmetrized. It is also implicit that, where relevant, the traceless part of the above operators is taken.

The methodology for nonperturbative renormalization of these operators is very similar to that for the charges. Details of these twist-two operators and their renormalization can be found in Refs. [107] and [87].

In numerical calculations, it is typical to set the spin of the nucleon in a given direction. Choosing the spin to be in the "3" direction and restricting to the isovector case, $\tau^a = \tau^3$, the explicit operators become

$$\mathcal{O}^{44}_{V^3} = \overline{q}(\gamma^4 \overleftrightarrow{D}^4 - \frac{1}{3}\boldsymbol{\gamma}\cdot\overleftrightarrow{\mathbf{D}})\tau^3 q\,, \tag{455}$$

$$\mathcal{O}^{34}_{A^3} = \overline{q}\gamma^{\{3}\overleftrightarrow{D}^{4\}}\gamma^5\tau^3 q\,, \tag{456}$$

$$\mathcal{O}^{124}_{T^3} = \overline{q}\sigma^{[1\{2]}\overleftrightarrow{D}^{4\}}\tau^3 q\,. \tag{457}$$

The isovector moments are then obtained from their forward matrix elements within the nucleon ground state using the following relations:

$$\langle 0|\mathcal{O}^{44}_{V^3}|0\rangle = -M_N\,\langle x\rangle_{u-d}\,, \tag{458}$$

$$\langle 0|\mathcal{O}^{34}_{A^3}|0\rangle = -\frac{iM_N}{2}\,\langle x\rangle_{\Delta u-\Delta d}\,, \tag{459}$$

$$\langle 0|\mathcal{O}^{124}_{T^3}|0\rangle = -\frac{iM_N}{2}\,\langle x\rangle_{\delta u-\delta d}\,. \tag{460}$$

10.5.1 Results for the isovector moments $\langle x\rangle_{u-d}$, $\langle x\rangle_{\Delta u-\Delta d}$ and $\langle x\rangle_{\delta u-\delta d}$

A summary of results for these three moments is given in Tabs. 74 and 75 and the values including the FLAG averages are shown in Fig. 49. Results from $N_f = 2$ simulations and publications prior to 2014 have been included as this is the first review of these quantities. For the momentum fraction and helicity moment, we have also included phenomenological estimates. Lattice values for the momentum fraction are consistent with phenomenology but have larger errors. Results for the helicity moment, $\langle x\rangle_{\Delta u-\Delta d}$, are consistent and have similar uncertainties. Lattice results for the transversity moment are a prediction.

We discuss results for these three moments together as the methodology for their calculations and the analysis is the same, and the systematics are similar. All results presented in this section are in the $\overline{\text{MS}}$ scheme at 2 GeV.

For the 2+1+1-theory, the PNDME 20A and ETM 22 results in [174, 234] qualify for the averages. The PNDME 20A results are from nine HISQ ensembles analyzed using clover fermions. The operators are renormalized nonperturbatively using the RI'-MOM scheme, and the chiral-continuum-finite-volume extrapolation is done keeping the leading-order corrections in each of the three variables. Analyses of excited-state contamination are done using three strategies that differ in the selection of the first excited-state mass. The final results are from a three-state fit to the three-point function with the spectrum taken from the two-point function, i.e., assuming no enhanced contribution from multihadron excited states. An additional systematic uncertainty is assigned to cover the spread of these three estimates.

The ETM collaboration has presented new results from three ensembles with 2+1+1-flavour twisted-mass fermions with close-to-physical pion masses at $a = 0.057$, 0.069 and 0.80 fm in [174]. These results supersede those in [235, 236] based on the single ensemble at $a = 0.080$ fm for the momentum fraction and the transversity moment. To control excited-state contamination, they compare results from the plateau, summation and two-state methods with the final values taken from the two-state fit. Operators are renormalized nonperturbatively via the RI'-MOM scheme supplemented by perturbative subtraction of lattice artefacts. The continuum extrapolation, which keeps the leading correction $\propto a^2$, shows a significant slope for $\langle x\rangle_{u-d}$, which reduces the continuum-limit value.

Collaboration	Ref.	N_f	publication status	continuum extrapolation	chiral extrapolation	finite volume	renormalization	excited states	$\langle x\rangle_{u-d}$	$\langle x\rangle_{\Delta u-\Delta d}$
ETM 22	[174]	2+1+1	A	★	★	★	★	○	0.126(32)	
PNDME 20A	[234]	2+1+1	A	★‡	★	★	★	○	0.173(14)(07)	0.213(15)(22)
ETM 20C	[235]	2+1+1	A	■	○	★	★	○	0.171(18)	
ETM 19A	[236]	2+1+1	A	■	○	★	★	○	0.178(16)	0.193(18)
Mainz 24	[161]	2+1	A	★‡	★	★	★	○	0.153(15)(10)	0.207(15)(06)
LHPC 24	[237]	2+1	A	■‡	★	★	★	○	0.200(17)	0.213(16)
NME 21A	[238]	2+1	C	★‡	★	★	★	○	0.156(12)(20)	0.185(12)(20)
NME 20	[239]	2+1	A	○‡	★	★	★	○	0.155(17)(20)	0.183(14)(20)
Mainz 19	[87]	2+1	A	★‡	○	★	★	○	$0.180(25)(^{14}_{6})$	$0.221(25)(^{10}_{0})$
χQCD 18A	[240]	2+1	A	○	★	★	★	○	0.151(28)(29)	
LHPC 12A	[170]	2+1	A	■‡	★	★	★	○	0.140(21)	
LHPC 10	[68]	2+1	A	■‡	○	■	★	■	0.1758(20)	0.1972(55)
RBC/UKQCD 10D	[55]	2+1	A	■	■	○	★	■	0.140–0.237	0.180–0.279
RQCD 18	[241]	2	A	○‡	★	★	★	■	0.195(7)(15)	0.271(14)(16)
ETM 17C	[42]	2	A	■	○	○	★	○	0.194(9)(11)	
ETM 15D	[39]	2	A	■	○	○	★	○	0.208(24)	0.229(30)
RQCD 14A	[242]	2	A	○‡	★	★	★	■	0.217(9)	

‡ The rating takes into account that the moments are not fully $\mathcal{O}(a)$-improved by requiring an additional lattice spacing.

Table 74: Overview of results for $\langle x\rangle_{u-d}$ and $\langle x\rangle_{\Delta u-\Delta d}$. The $N_f = 2$ results and publications prior to 2014 are included as this is the first review of these quantities.

When determining the final results to quote for the $2 + 1 + 1$ theory, we note the large difference between the results from Refs. [174, 234] for the momentum fraction. Our conservative approach is to construct the interval defined by the PNDME 20A value plus error and the ETM 22 value, i.e., 0.126–0.189, and then take the mean of the interval for the central value and half the spread for the error as shown in Fig. 49. For the transversity moment we perform the FLAG averaging assuming no correlations between the two calculations. For the helicity fraction we quote the PNDME 20A [234] values. The values of $\delta(a_{\min})$ for the three moments for the PNDME 20A calculation [234] are 0.6, 0.3 and 0.13, and those for ETM 22 are roughly 0.8 (momentum fraction) and 0.0 (transversity). The FLAG averages are

Collaboration	Ref.	N_f	publication status	continuum extrapolation	chiral extrapolation	finite volume	renormalization	excited states	$\langle x\rangle_{\delta u-\delta d}$
ETM 22	[174]	2+1+1	A	★	★	★	★	○	0.168(44)
PNDME 20A	[234]	2+1+1	A	★‡	★	★	★	○	0.208(19)(24)
ETM 19A	[236]	2+1+1	A	■	○	★	★	○	0.204(23)
Mainz 24	[161]	2+1	A	★‡	★	★	★	○	0.195(17)(15)
LHPC 24	[237]	2+1	A	■‡	★	★	★	○	0.219(21)
NME 21A	[238]	2+1	C	★‡	★	★	★	○	0.209(15)(20)
NME 20	[239]	2+1	A	○‡	★	★	★	○	0.220(18)(20)
Mainz 19	[87]	2+1	A	★‡	○	★	★	○	$0.212(32)\binom{20}{10}$
RQCD 18	[241]	2	A	○‡	★	★	★	■	0.266(8)(4)
ETM 15D	[39]	2	A	■	○	○	★	○	0.306(29)

‡ The rating takes into account that the moments are not fully $\mathcal{O}(a)$-improved by requiring an additional lattice spacing.

Table 75: Overview of results for $\langle x\rangle_{\delta u-\delta d}$. The $N_f = 2$ results and publications prior to 2014 are included as this is the first review of these quantities.

$$N_f = 2+1+1: \quad \langle x\rangle_{u-d} = 0.158(32) \quad \text{Refs. [174, 234]}, \tag{461}$$
$$N_f = 2+1+1: \quad \langle x\rangle_{\Delta u-\Delta d} = 0.213(27) \quad \text{Ref. [234]}, \tag{462}$$
$$N_f = 2+1+1: \quad \langle x\rangle_{\delta u-\delta d} = 0.195(25) \quad \text{Refs. [174, 234]}. \tag{463}$$

Five calculations qualify for averages for the 2+1-flavour theory: the Mainz [87, 161], the NME [238, 239], and χQCD [240]. Of these, the Mainz 24 [161] supercedes the Mainz 19 [87], and while the NME 21A [238] is an update of NME 20 [239], it is a conference proceeding.

The Mainz 24 results are based on fifteen $N_f = 2+1$ ensembles produced by the CLS collaboration covering the ranges $0.05 \le a \le 0.09$ fm and $130 \le M_\pi \le 360$ MeV. A two-state summation method is used to control excited-state contamination. In the continuum-chiral-finite-volume extrapolation, leading-order corrections are used for the continuum and finite-volume corrections and up to NNLO results from SU(2) baryon chiral perturbation theory for the chiral part.

The NME 20 [239] results are based on seven $N_f = 2+1$ clover ensembles produced by the JLab/W&M/LANL/MIT collaborations. They cover the range $0.07 \le a \le 0.13$ fm and $170 \le M_\pi \le 280$ MeV. The analysis methodology is the same as in Ref. [234] already

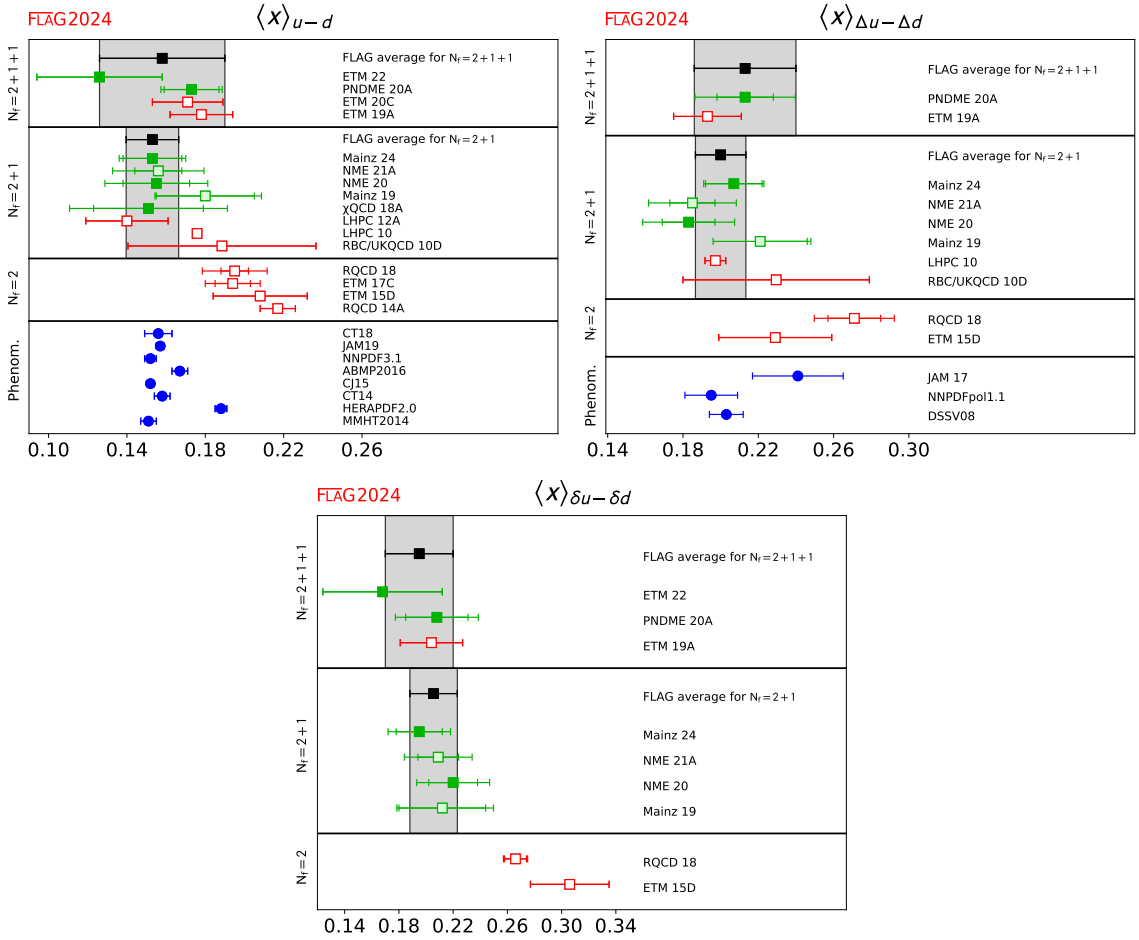

Figure 49: Lattice-QCD results for the second Mellin moments $\langle x \rangle_{u-d}$, $\langle x \rangle_{\Delta u-\Delta d}$ and $\langle x \rangle_{\delta u-\delta d}$. Results from $N_f = 2$ simulations and publications prior to 2014 have been included as this is the first review of these quantities. For the momentum-fraction and helicity moment, we have also included phenomenological estimates [243–253].

discussed above.

The χQCD [240] calculation uses four domain-wall ensembles that have been generated by the RBC/UKQCD collaboration that cover the range $0.08 \leq a \leq 0.14$ fm and $139 \leq M_\pi \leq 330$ MeV. A number of values of overlap-valence-quark masses, in addition to those close to the unitary point $M_\pi^{\rm sea} = M_\pi^{\rm valence}$, are used. The renormalization is carried out nonperturbatively. The continuum-chiral-finite-volume extrapolation is carried out using the leading corrections plus terms accounting for partial quenching, i.e., the leading terms in the difference $M_\pi^{\rm sea} - M_\pi^{\rm valence}$.

The three older calculations, LHPC 12A [170], LHPC 10 [68] and RBC/UKQCD [55], do not meet the criteria of control over the continuum limit. Similarly, the $N_f = 2$ calculations fail to satisfy one or more of the FLAG criteria.

The 2+1-flavour FLAG averages for the momentum fraction, $\langle x \rangle_{u-d}$, are constructed using the Mainz 24 [161], NME 20 [239] and χQCD 18A [240] values assuming zero correlations between them. The results for the helicity and transversity moments are the FLAG averages of the Mainz 24 [161] and NME 20 [239] values again assuming zero correlations. The values

of $\delta(a_{\min})$ for the Mainz 24 [161] for the three moments are 1.5, 0.2, 0.1 and those for the NME 20 are 0.5, 1.0 and 0.2. The χQCD 18A work does not provide enough information to determine $\delta(a_{\min})$. The FLAG averages are

$$N_f = 2+1: \quad \langle x \rangle_{u-d} = 0.153(13) \quad \text{Refs. [161, 239, 240]}, \tag{464}$$

$$N_f = 2+1: \quad \langle x \rangle_{\Delta u - \Delta d} = 0.200(13) \quad \text{Refs. [161, 239]}, \tag{465}$$

$$N_f = 2+1: \quad \langle x \rangle_{\delta u - \delta d} = 0.206(17) \quad \text{Refs. [161, 239]}. \tag{466}$$

References

[1] [FLAG 21] Y. Aoki et al., *FLAG Review 2021*, *Eur. Phys. J. C* **82** (2022) 869 [2111.09849].

[2] [FLAG 19] S. Aoki et al., *FLAG Review 2019: Flavour Lattice Averaging Group (FLAG)*, *Eur. Phys. J. C* **80** (2020) 113 [1902.08191].

[3] S. Syritsyn, *Review of Hadron Structure Calculations on a Lattice*, *PoS* **LATTICE2013** (2014) 009 [1403.4686].

[4] S. Capitani, M. Della Morte, D. Djukanovic, G. von Hippel, J. Hua, B. Jäger et al., *Nucleon electromagnetic form factors in two-flavor QCD*, *Phys. Rev.* **D92** (2015) 054511 [1504.04628].

[5] R.S. Sufian, Y.-B. Yang, A. Alexandru, T. Draper, J. Liang and K.-F. Liu, *Strange Quark Magnetic Moment of the Nucleon at the Physical Point*, *Phys. Rev. Lett.* **118** (2017) 042001 [1606.07075].

[6] R. Gupta, Y.-C. Jang, H.-W. Lin, B. Yoon and T. Bhattacharya, *Axial Vector Form Factors of the Nucleon from Lattice QCD*, *Phys. Rev. D* **96** (2017) 114503 [1705.06834].

[7] J. Green, N. Hasan, S. Meinel, M. Engelhardt, S. Krieg, J. Laeuchli et al., *Up, down, and strange nucleon axial form factors from lattice QCD*, *Phys. Rev.* **D95** (2017) 114502 [1703.06703].

[8] [CSSM/QCDSF/UKQCD 17] A. J. Chambers et al., *Electromagnetic form factors at large momenta from lattice QCD*, *Phys. Rev.* **D96** (2017) 114509 [1702.01513].

[9] C. Alexandrou, M. Constantinou, K. Hadjiyiannakou, K. Jansen, C. Kallidonis, G. Koutsou et al., *Nucleon electromagnetic form factors using lattice simulations at the physical point*, *Phys. Rev.* **D96** (2017) 034503 [1706.00469].

[10] C. Alexandrou, M. Constantinou, K. Hadjiyiannakou, K. Jansen, C. Kallidonis, G. Koutsou et al., *Strange nucleon electromagnetic form factors from lattice QCD*, *Phys. Rev.* **D97** (2018) 094504 [1801.09581].

[11] [PACS 18] K.-I. Ishikawa, Y. Kuramashi, S. Sasaki, N. Tsukamoto, A. Ukawa and T. Yamazaki, *Nucleon form factors on a large volume lattice near the physical point in 2+1 flavor QCD*, *Phys. Rev.* **D98** (2018) 074510 [1807.03974].

[12] C. Alexandrou, S. Bacchio, M. Constantinou, J. Finkenrath, K. Hadjiyiannakou, K. Jansen et al., *Proton and neutron electromagnetic form factors from lattice QCD*, *Phys. Rev. D* **100** (2019) 014509 [1812.10311].

[13] [PACS 18A] E. Shintani, K.-I. Ishikawa, Y. Kuramashi, S. Sasaki and T. Yamazaki, *Nucleon form factors and root-mean-square radii on a (10.8 fm)^4 lattice at the physical point*, *Phys. Rev. D* **99** (2019) 014510 [1811.07292], [Erratum: Phys.Rev.D 102, 019902 (2020)].

[14] [RQCD 19] G. S. Bali, L. Barca, S. Collins, M. Gruber, M. Löffler, A. Schäfer et al., *Nucleon axial structure from lattice QCD*, *JHEP* **05** (2020) 126 [1911.13150].

[15] [LHPC 19] N. Hasan, J. Green, S. Meinel, M. Engelhardt, S. Krieg, J. Negele et al., *Nucleon axial, scalar, and tensor charges using lattice QCD at the physical pion mass*, *Phys. Rev. D* **99** (2019) 114505 [1903.06487].

[16] C. Alexandrou et al., *Nucleon axial and pseudoscalar form factors from lattice QCD at the physical point*, *Phys. Rev. D* **103** (2021) 034509 [2011.13342].

[17] D. Djukanovic, T. Harris, G. von Hippel, P.M. Junnarkar, H.B. Meyer, D. Mohler et al., *Isovector electromagnetic form factors of the nucleon from lattice QCD and the proton radius puzzle*, *Phys. Rev. D* **103** (2021) 094522 [2102.07460].

[18] H.-W. Lin et al., *Parton distributions and lattice QCD calculations: a community white paper*, *Prog. Part. Nucl. Phys.* **100** (2018) 107 [1711.07916].

[19] M. Constantinou, *The x-dependence of hadronic parton distributions: A review on the progress of lattice QCD*, *Eur. Phys. J. A* **57** (2021) 77 [2010.02445].

[20] M. Constantinou et al., *Parton distributions and lattice QCD calculations: toward 3D structure*, *Prog. Part. Nucl. Phys.* **121** (2021) 103908 [2006.08636].

[21] K. Cichy and M. Constantinou, *A guide to light-cone PDFs from Lattice QCD: an overview of approaches, techniques and results*, *Adv. High Energy Phys.* **2019** (2019) 3036904 [1811.07248].

[22] C. Monahan, *Recent Developments in x-dependent Structure Calculations*, *PoS* **LATTICE2018** (2018) 018 [1811.00678].

[23] M.J. Savage, *Nuclear Physics from Lattice QCD*, *Prog. Part. Nucl. Phys.* **67** (2012) 140 [1110.5943].

[24] [NPLQCD 17] E. Chang, Z. Davoudi, W. Detmold, A.S. Gambhir, K. Orginos, M.J. Savage et al., *Scalar, Axial, and Tensor Interactions of Light Nuclei from Lattice QCD*, *Phys. Rev. Lett.* **120** (2018) 152002 [1712.03221].

[25] T. Iritani, *Two-baryon systems from HAL QCD method and the mirage in the temporal correlation of the direct method*, *EPJ Web Conf.* **175** (2018) 05008 [1710.06147].

[26] M.L. Wagman, F. Winter, E. Chang, Z. Davoudi, W. Detmold, K. Orginos et al., *Baryon-Baryon Interactions and Spin-Flavor Symmetry from Lattice Quantum Chromodynamics*, *Phys. Rev.* **D96** (2017) 114510 [1706.06550].

[27] [χQCD 18] J. Liang, Y.-B. Yang, T. Draper, M. Gong and K.-F. Liu, *Quark spins and Anomalous Ward Identity*, *Phys. Rev.* **D98** (2018) 074505 [1806.08366].

[28] Y.-C. Jang, R. Gupta, B. Yoon and T. Bhattacharya, *Axial Vector Form Factors from Lattice QCD that Satisfy the PCAC Relation*, *Phys. Rev. Lett.* **124** (2020) 072002 [1905.06470].

[29] H.W. Hamber, E. Marinari, G. Parisi and C. Rebbi, *Considerations on Numerical Analysis of QCD*, *Nucl. Phys.* **B225** (1983) 475.

[30] G.P. Lepage, *The Analysis of Algorithms for Lattice Field Theory*, in *Theoretical Advanced Study Institute in Elementary Particle Physics*, 6, 1989.

[31] [QCDSF 06] A. A. Khan, M. Göckeler, P. Hägler, T. Hemmert, R. Horsley et al., *Axial coupling constant of the nucleon for two flavours of dynamical quarks in finite and infinite volume*, *Phys.Rev.* **D74** (2006) 094508 [hep-lat/0603028].

[32] [QCDSF 12] G. Bali, P. Bruns, S. Collins, M. Deka, B. Glasle et al., *Nucleon mass and sigma term from lattice QCD with two light fermion flavors*, *Nucl.Phys.* **B866** (2013) 1 [1206.7034].

[33] [QCDSF 13] R. Horsley, Y. Nakamura, A. Nobile, P. Rakow, G. Schierholz et al., *Nucleon axial charge and pion decay constant from two-flavor lattice QCD*, *Phys. Lett.* **B732** (2014) 41 [1302.2233].

[34] [Mainz 12] S. Capitani, M. Della Morte, G. von Hippel, B. Jager, A. Jüttner et al., *The nucleon axial charge from lattice QCD with controlled errors*, *Phys.Rev.* **D86** (2012) 074502 [1205.0180].

[35] [RQCD 14] G. S. Bali, S. Collins, B. Glässle, M. Göckeler, J. Najjar, R.H. Rödl et al., *Nucleon isovector couplings from $N_f = 2$ lattice QCD*, *Phys. Rev.* **D91** (2015) 054501 [1412.7336].

[36] [RQCD 16] G. S. Bali, S. Collins, D. Richtmann, A. Schäfer, W. Söldner and A. Sternbeck, *Direct determinations of the nucleon and pion σ terms at nearly physical quark masses*, *Phys. Rev.* **D93** (2016) 094504 [1603.00827].

[37] [Mainz 17] S. Capitani, M. Della Morte, D. Djukanovic, G.M. von Hippel, J. Hua, B. Jäger et al., *Iso-vector axial form factors of the nucleon in two-flavor lattice QCD*, *Int. J. Mod. Phys.* **A34** (2019) 1950009 [1705.06186].

[38] [PACS-CS 09] K.-I. Ishikawa et al., *SU(2) and SU(3) chiral perturbation theory analyses on baryon masses in 2+1 flavor lattice QCD*, *Phys. Rev.* **D80** (2009) 054502 [0905.0962].

[39] [ETM 15D] A. Abdel-Rehim et al., *Nucleon and pion structure with lattice QCD simulations at physical value of the pion mass*, *Phys. Rev.* **D92** (2015) 114513 [1507.04936], [Erratum: Phys. Rev.D93,no.3,039904(2016)].

[40] [ETM 16A] A. Abdel-Rehim, C. Alexandrou, M. Constantinou, K. Hadjiyiannakou, K. Jansen, C. Kallidonis et al., *Direct Evaluation of the Quark Content of Nucleons from Lattice QCD at the Physical Point*, *Phys. Rev. Lett.* **116** (2016) 252001 [1601.01624].

[41] [ETM 17B] C. Alexandrou, M. Constantinou, K. Hadjiyiannakou, K. Jansen, C. Kallidonis, G. Koutsou et al., *Nucleon axial form factors using $N_f = 2$ twisted mass fermions with a physical value of the pion mass*, *Phys. Rev.* **D96** (2017) 054507 [1705.03399].

[42] [ETM 17C] C. Alexandrou, M. Constantinou, K. Hadjiyiannakou, K. Jansen, C. Kallidonis, G. Koutsou et al., *Nucleon Spin and Momentum Decomposition Using Lattice QCD Simulations*, *Phys. Rev. Lett.* **119** (2017) 142002 [1706.02973].

[43] [ETM 17] C. Alexandrou et al., *Nucleon scalar and tensor charges using lattice QCD simulations at the physical value of the pion mass*, *Phys. Rev.* **D95** (2017) 114514 [1703.08788], [Erratum: Phys. Rev.D96,no.9,099906(2017)].

[44] [PNDME 13] T. Bhattacharya, S.D. Cohen, R. Gupta, A. Joseph, H.-W. Lin and B. Yoon, *Nucleon Charges and Electromagnetic Form Factors from 2+1+1-Flavor Lattice QCD*, *Phys. Rev.* **D89** (2014) 094502 [1306.5435].

[45] [PNDME 15A] T. Bhattacharya, V. Cirigliano, S. Cohen, R. Gupta, A. Joseph, H.-W. Lin et al., *Iso-vector and Iso-scalar Tensor Charges of the Nucleon from Lattice QCD*, *Phys. Rev.* **D92** (2015) 094511 [1506.06411].

[46] [PNDME 15] T. Bhattacharya, V. Cirigliano, R. Gupta, H.-W. Lin and B. Yoon, *Neutron Electric Dipole Moment and Tensor Charges from Lattice QCD*, *Phys. Rev. Lett.* **115** (2015) 212002 [1506.04196].

[47] [PNDME 16] T. Bhattacharya, V. Cirigliano, S. Cohen, R. Gupta, H.-W. Lin and B. Yoon, *Axial, Scalar and Tensor Charges of the Nucleon from 2+1+1-flavor Lattice QCD*, *Phys. Rev.* **D94** (2016) 054508 [1606.07049].

[48] [CalLat 17] E. Berkowitz et al., *An accurate calculation of the nucleon axial charge with lattice QCD*, 1704.01114.

[49] [PNDME 18B] R. Gupta, B. Yoon, T. Bhattacharya, V. Cirigliano, Y.-C. Jang and H.-W. Lin, *Flavor diagonal tensor charges of the nucleon from (2+1+1)-flavor lattice QCD*, *Phys. Rev.* **D98** (2018) 091501 [1808.07597].

[50] [PNDME 18A] H.-W. Lin, R. Gupta, B. Yoon, Y.-C. Jang and T. Bhattacharya, *Quark contribution to the proton spin from 2+1+1-flavor lattice QCD*, *Phys. Rev.* **D98** (2018) 094512 [1806.10604].

[51] [PNDME 18] R. Gupta, Y.-C. Jang, B. Yoon, H.-W. Lin, V. Cirigliano and T. Bhattacharya, *Isovector Charges of the Nucleon from 2+1+1-flavor Lattice QCD*, *Phys. Rev.* **D98** (2018) 034503 [1806.09006].

[52] [CalLat 18] C. C. Chang et al., *A per-cent-level determination of the nucleon axial coupling from quantum chromodynamics*, *Nature* (2018) [1805.12130].

[53] [RBC/UKQCD 08B] T. Yamazaki et al., *Nucleon axial charge in 2+1 flavor dynamical lattice QCD with domain wall fermions*, *Phys.Rev.Lett.* **100** (2008) 171602 [0801.4016].

[54] [RBC/UKQCD 09B] T. Yamazaki, Y. Aoki, T. Blum, H.-W. Lin, S. Ohta, S. Sasaki et al., *Nucleon form factors with 2+1 flavor dynamical domain-wall fermions*, *Phys. Rev.* **D79** (2009) 114505 [0904.2039].

[55] [RBC/UKQCD 10D] Y. Aoki, T. Blum, H.-W. Lin, S. Ohta, S. Sasaki, R. Tweedie et al., *Nucleon isovector structure functions in (2+1)-flavor QCD with domain wall fermions*, *Phys. Rev.* **D82** (2010) 014501 [1003.3387].

[56] [χQCD 13A] M. Gong et al., *Strangeness and charmness content of the nucleon from overlap fermions on 2+1-flavor domain-wall fermion configurations*, *Phys. Rev.* **D88** (2013) 014503 [1304.1194].

[57] [χQCD 15A] Y.-B. Yang, A. Alexandru, T. Draper, J. Liang and K.-F. Liu, *πN and strangeness sigma terms at the physical point with chiral fermions*, *Phys. Rev.* **D94** (2016) 054503 [1511.09089].

[58] [χQCD 15] M. Gong, Y.-B. Yang, J. Liang, A. Alexandru, T. Draper and K.-F. Liu, *Strange and charm quark spins from the anomalous Ward identity*, *Phys. Rev.* **D95** (2017) 114509 [1511.03671].

[59] [JLQCD 08B] H. Ohki, H. Fukaya, S. Hashimoto, T. Kaneko, H. Matsufuru, J. Noaki et al., *Nucleon sigma term and strange quark content from lattice QCD with exact chiral symmetry*, *Phys. Rev.* **D78** (2008) 054502 [0806.4744].

[60] [JLQCD 12A] H. Ohki, K. Takeda, S. Aoki, S. Hashimoto, T. Kaneko, H. Matsufuru et al., *Nucleon strange quark content from $N_f = 2 + 1$ lattice QCD with exact chiral symmetry*, *Phys. Rev.* **D87** (2013) 034509 [1208.4185].

[61] [JLQCD 18] N. Yamanaka, S. Hashimoto, T. Kaneko and H. Ohki, *Nucleon charges with dynamical overlap fermions*, *Phys. Rev.* **D98** (2018) 054516 [1805.10507].

[62] R. Babich, J. Brannick, R.C. Brower, M.A. Clark, T.A. Manteuffel, S.F. McCormick et al., *Adaptive multigrid algorithm for the lattice Wilson-Dirac operator*, *Phys. Rev. Lett.* **105** (2010) 201602 [1005.3043].

[63] M. Lüscher, *Deflation acceleration of lattice QCD simulations*, *JHEP* **12** (2007) 011 [0710.5417].

[64] G.S. Bali, S. Collins and A. Schafer, *Effective noise reduction techniques for disconnected loops in Lattice QCD*, *Comput. Phys. Commun.* **181** (2010) 1570 [0910.3970].

[65] T. Blum, T. Izubuchi and E. Shintani, *New class of variance-reduction techniques using lattice symmetries*, *Phys. Rev.* **D88** (2013) 094503 [1208.4349].

[66] A. Stathopoulos, J. Laeuchli and K. Orginos, *Hierarchical probing for estimating the trace of the matrix inverse on toroidal lattices*, *SIAM J. Sci. Comput.* **35** (2013) S299 [1302.4018].

[67] A.S. Gambhir, A. Stathopoulos, K. Orginos, B. Yoon, R. Gupta and S. Syritsyn, *Algorithms for Disconnected Diagrams in Lattice QCD*, *PoS* **LATTICE2016** (2016) 265 [1611.01193].

[68] [LHPC 10] J. D. Bratt et al., *Nucleon structure from mixed action calculations using 2+1 flavors of asqtad sea and domain wall valence fermions*, *Phys.Rev.* **D82** (2010) 094502 [1001.3620].

[69] B. Yoon et al., *Controlling Excited-State Contamination in Nucleon Matrix Elements*, *Phys. Rev.* **D93** (2016) 114506 [1602.07737].

[70] T.A. DeGrand and S. Schaefer, *Improving meson two point functions in lattice QCD*, *Comput. Phys. Commun.* **159** (2004) 185 [hep-lat/0401011].

[71] L. Giusti, P. Hernandez, M. Laine, P. Weisz and H. Wittig, *Low-energy couplings of QCD from current correlators near the chiral limit*, *JHEP* **0404** (2004) 013 [hep-lat/0402002].

[72] R. Gupta, A. Patel, C.F. Baillie, G. Guralnik, G.W. Kilcup and S.R. Sharpe, *QCD With Dynamical Wilson Fermions*, *Phys. Rev.* **D40** (1989) 2072.

[73] C. Thron, S. Dong, K. Liu and H. Ying, *Pade - Z(2) estimator of determinants*, *Phys.Rev.* **D57** (1998) 1642 [hep-lat/9707001].

[74] S. Bernardson, P. McCarty and C. Thron, *Monte Carlo methods for estimating linear combinations of inverse matrix entries in lattice QCD*, *Comput. Phys. Commun.* **78** (1993) 256.

[75] J. Foley et al., *Practical all-to-all propagators for lattice QCD*, *Comput. Phys. Commun.* **172** (2005) 145 [hep-lat/0505023].

[76] S. Güsken, U. Löw, K.H. Mütter, R. Sommer, A. Patel and K. Schilling, *Nonsinglet Axial Vector Couplings of the Baryon Octet in Lattice QCD*, *Phys. Lett.* **B227** (1989) 266.

[77] C. Alexandrou, F. Jegerlehner, S. Gusken, K. Schilling and R. Sommer, *B meson properties from lattice QCD*, *Phys. Lett.* **B256** (1991) 60.

[78] D.S. Roberts, W. Kamleh, D.B. Leinweber, M.S. Mahbub and B.J. Menadue, *Accessing High Momentum States In Lattice QCD*, *Phys. Rev. D* **86** (2012) 074504 [1206.5891].

[79] M. Della Morte, B. Jäger, T. Rae and H. Wittig, *Improved interpolating fields for hadrons at non-zero momentum*, *Eur.Phys.J.* **A48** (2012) 139 [1208.0189].

[80] G.S. Bali, B. Lang, B.U. Musch and A. Schäfer, *Novel quark smearing for hadrons with high momenta in lattice QCD*, *Phys. Rev. D* **93** (2016) 094515 [1602.05525].

[81] B.C. Tiburzi, *Time Dependence of Nucleon Correlation Functions in Chiral Perturbation Theory*, *Phys. Rev.* **D80** (2009) 014002 [0901.0657].

[82] O. Bär, *Multi-hadron-state contamination in nucleon observables from chiral perturbation theory*, *EPJ Web Conf.* **175** (2018) 01007 [1708.00380].

[83] O. Bär, *Nucleon-pion-state contribution in lattice calculations of the nucleon charges g_A, g_T and g_S*, *Phys. Rev.* **D94** (2016) 054505 [1606.09385].

[84] O. Bär, *Nucleon-pion-state contribution in lattice calculations of moments of parton distribution functions*, *Phys. Rev.* **D95** (2017) 034506 [1612.08336].

[85] M.T. Hansen and H.B. Meyer, *On the effect of excited states in lattice calculations of the nucleon axial charge*, *Nucl. Phys.* **B923** (2017) 558 [1610.03843].

[86] B. Yoon et al., *Isovector charges of the nucleon from 2+1-flavor QCD with clover fermions*, *Phys. Rev.* **D95** (2017) 074508 [1611.07452].

[87] [Mainz 19] T. Harris, G. von Hippel, P. Junnarkar, H.B. Meyer, K. Ottnad, J. Wilhelm et al., *Nucleon isovector charges and twist-2 matrix elements with $N_f = 2+1$ dynamical Wilson quarks*, *Phys. Rev. D* **100** (2019) 034513 [1905.01291].

[88] L. Maiani, G. Martinelli, M.L. Paciello and B. Taglienti, *Scalar Densities and Baryon Mass Differences in Lattice QCD With Wilson Fermions*, *Nucl. Phys.* **B293** (1987) 420.

[89] S.J. Dong, K.F. Liu and A.G. Williams, *Lattice calculation of the strangeness magnetic moment of the nucleon*, *Phys. Rev.* **D58** (1998) 074504 [hep-ph/9712483].

[90] S. Capitani, B. Knippschild, M. Della Morte and H. Wittig, *Systematic errors in extracting nucleon properties from lattice QCD*, *PoS* **LATTICE2010** (2010) 147 [1011.1358].

[91] J. Bulava, M. Donnellan and R. Sommer, *On the computation of hadron-to-hadron transition matrix elements in lattice QCD*, *JHEP* **01** (2012) 140 [1108.3774].

[92] S. Güsken, K. Schilling, R. Sommer, K.H. Mütter and A. Patel, *Mass Splittings in the Baryon Octet and the Nucleon σ Term in Lattice QCD*, *Phys. Lett.* **B212** (1988) 216.

[93] R. Sommer, *Current matrix elements with quenched Wilson fermions*, *Nucl. Phys. Proc. Suppl.* **17** (1990) 513.

[94] C. Bouchard, C.C. Chang, T. Kurth, K. Orginos and A. Walker-Loud, *On the Feynman-Hellmann Theorem in Quantum Field Theory and the Calculation of Matrix Elements*, *Phys. Rev.* **D96** (2017) 014504 [1612.06963].

[95] [CSSM/QCDSF/UKQCD 14] A. J. Chambers et al., *Feynman-Hellmann approach to the spin structure of hadrons*, *Phys. Rev.* **D90** (2014) 014510 [1405.3019].

[96] A.J. Chambers et al., *Disconnected contributions to the spin of the nucleon*, *Phys. Rev.* **D92** (2015) 114517 [1508.06856].

[97] B.J. Owen, J. Dragos, W. Kamleh, D.B. Leinweber, M.S. Mahbub, B.J. Menadue et al., *Variational Approach to the Calculation of gA*, *Phys. Lett.* **B723** (2013) 217 [1212.4668].

[98] C. Egerer, D. Richards and F. Winter, *Controlling excited-state contributions with distillation in lattice QCD calculations of nucleon isovector charges g_S^{u-d}, g_A^{u-d}, g_T^{u-d}*, *Phys. Rev. D* **99** (2019) 034506 [1810.09991].

[99] G. Fox, R. Gupta, O. Martin and S. Otto, *Monte Carlo Estimates of the Mass Gap of the O(2) and O(3) Spin Models in (1+1)-dimensions*, *Nucl. Phys.* **B205** (1982) 188.

[100] C. Michael, *Adjoint Sources in Lattice Gauge Theory*, *Nucl. Phys.* **B259** (1985) 58.

[101] M. Lüscher and U. Wolff, *How to Calculate the Elastic Scattering Matrix in Two-dimensional Quantum Field Theories by Numerical Simulation*, *Nucl. Phys.* **B339** (1990) 222.

[102] B. Blossier, M. Della Morte, G. von Hippel, T. Mendes and R. Sommer, *On the generalized eigenvalue method for energies and matrix elements in lattice field theory*, *JHEP* **04** (2009) 094 [0902.1265].

[103] J. Dragos, R. Horsley, W. Kamleh, D.B. Leinweber, Y. Nakamura, P.E.L. Rakow et al., *Nucleon matrix elements using the variational method in lattice QCD*, *Phys. Rev.* **D94** (2016) 074505 [1606.03195].

[104] L. Barca, G. Bali and S. Collins, *Toward N to Nπ matrix elements from lattice QCD*, *Phys. Rev. D* **107** (2023) L051505 [2211.12278].

[105] C. Alexandrou, G. Koutsou, Y. Li, M. Petschlies and F. Pittler, *Investigation of pion-nucleon contributions to nucleon matrix elements*, 2408.03893.

[106] [PNDME 21] R. Gupta, S. Park, M. Hoferichter, E. Mereghetti, B. Yoon and T. Bhattacharya, *Pion–Nucleon Sigma Term from Lattice QCD*, *Phys. Rev. Lett.* **127** (2021) 242002 [2105.12095].

[107] M. Göckeler, R. Horsley, E.-M. Ilgenfritz, H. Perlt, P.E.L. Rakow, G. Schierholz et al., *Polarized and unpolarized nucleon structure functions from lattice QCD*, *Phys. Rev.* **D53** (1996) 2317 [hep-lat/9508004].

[108] K. Jansen, C. Liu, M. Luscher, H. Simma, S. Sint, R. Sommer et al., *Nonperturbative renormalization of lattice QCD at all scales*, *Phys. Lett.* **B372** (1996) 275 [hep-lat/9512009].

[109] M. Lüscher, S. Sint, R. Sommer and P. Weisz, *Chiral symmetry and O(a) improvement in lattice QCD*, *Nucl. Phys.* **B478** (1996) 365 [hep-lat/9605038].

[110] [RQCD 16A] G. S. Bali, E.E. Scholz, J. Simeth and W. Söldner, *Lattice simulations with $N_f = 2 + 1$ improved Wilson fermions at a fixed strange quark mass*, *Phys. Rev.* **D94** (2016) 074501 [1606.09039].

[111] A. Gerardin, T. Harris and H.B. Meyer, *Non-perturbative renormalization and $O(a)$-improvement of the non-singlet vector current with $N_{\rm f} = 2 + 1$ Wilson fermions and tree-level Symanzik improved gauge action*, *Phys. Rev.* **D99** (2019) 014519 [1811.08209].

[112] R. Frezzotti and G.C. Rossi, *Chirally improving Wilson fermions. I: O(a) improvement*, *JHEP* **08** (2004) 007 [hep-lat/0306014].

[113] R. Frezzotti and G.C. Rossi, *Twisted mass lattice QCD with mass nondegenerate quarks*, *Nucl. Phys. Proc. Suppl.* **128** (2004) 193 [hep-lat/0311008], [,193(2003)].

[114] S. Capitani, M. Göckeler, R. Horsley, H. Perlt, P.E.L. Rakow, G. Schierholz et al., *Renormalization and off-shell improvement in lattice perturbation theory*, *Nucl. Phys.* **B593** (2001) 183 [hep-lat/0007004].

[115] T. Bhattacharya, R. Gupta, W. Lee, S.R. Sharpe and J.M.S. Wu, *Improved bilinears in lattice QCD with non-degenerate quarks*, *Phys. Rev.* **D73** (2006) 034504 [hep-lat/0511014].

[116] M. Bochicchio, L. Maiani, G. Martinelli, G.C. Rossi and M. Testa, *Chiral symmetry on the lattice with Wilson fermions*, *Nucl.Phys.* **B262** (1985) 331.

[117] G. Martinelli, C. Pittori, C.T. Sachrajda, M. Testa and A. Vladikas, *A general method for nonperturbative renormalization of lattice operators*, *Nucl. Phys.* **B445** (1995) 81 [hep-lat/9411010].

[118] [RBC/UKQCD 14B] T. Blum et al., *Domain wall QCD with physical quark masses*, *Phys. Rev.* **D93** (2016) 074505 [1411.7017].

[119] S. Sint and P. Weisz, *Further results on O(a) improved lattice QCD to one loop order of perturbation theory*, *Nucl. Phys.* **B502** (1997) 251 [hep-lat/9704001].

[120] Y. Taniguchi and A. Ukawa, *Perturbative calculation of improvement coefficients to O(g**2a) for bilinear quark operators in lattice QCD*, *Phys. Rev.* **D58** (1998) 114503 [hep-lat/9806015].

[121] P. Korcyl and G.S. Bali, *Non-perturbative determination of improvement coefficients using coordinate space correlators in $N_f = 2 + 1$ lattice QCD*, *Phys. Rev.* **D95** (2017) 014505 [1607.07090].

[122] M. Constantinou, M. Hadjiantonis, H. Panagopoulos and G. Spanoudes, *Singlet versus nonsinglet perturbative renormalization of fermion bilinears*, *Phys. Rev.* **D94** (2016) 114513 [1610.06744].

[123] G.S. Bali, S. Collins, M. Göckeler, S. Piemonte and A. Sternbeck, *Non-perturbative renormalization of flavor singlet quark bilinear operators in lattice QCD*, *PoS* **LATTICE2016** (2016) 187 [1703.03745].

[124] S. Dinter, V. Drach, R. Frezzotti, G. Herdoiza, K. Jansen and G. Rossi, *Sigma terms and strangeness content of the nucleon with $N_f = 2 + 1 + 1$ twisted mass fermions*, *JHEP* **08** (2012) 037 [1202.1480].

[125] [ALPHA 12] P. Fritzsch, F. Knechtli, B. Leder, M. Marinkovic, S. Schaefer et al., *The strange quark mass and the Λ parameter of two flavor QCD*, *Nucl.Phys.* **B865** (2012) 397 [1205.5380].

[126] [BMW 12A] S. Borsanyi, S. Dürr, Z. Fodor, C. Hoelbling, S.D. Katz et al., *High-precision scale setting in lattice QCD*, *JHEP* **1209** (2012) 010 [1203.4469].

[127] E.E. Jenkins and A.V. Manohar, *Baryon chiral perturbation theory using a heavy fermion Lagrangian*, *Phys. Lett.* **B255** (1991) 558.

[128] V. Bernard, N. Kaiser and U.-G. Meissner, *Chiral dynamics in nucleons and nuclei*, *Int. J. Mod. Phys. E* **4** (1995) 193 [hep-ph/9501384].

[129] T.N. Truong, *Chiral Perturbation Theory and Final State Theorem*, *Phys. Rev. Lett.* **61** (1988) 2526.

[130] T. Becher and H. Leutwyler, *Baryon chiral perturbation theory in manifestly Lorentz invariant form*, *Eur. Phys. J.* **C9** (1999) 643 [hep-ph/9901384].

[131] T. Fuchs, J. Gegelia, G. Japaridze and S. Scherer, *Renormalization of relativistic baryon chiral perturbation theory and power counting*, *Phys. Rev.* **D68** (2003) 056005 [hep-ph/0302117].

[132] A. Walker-Loud et al., *Light hadron spectroscopy using domain wall valence quarks on an Asqtad sea*, *Phys. Rev. D* **79** (2009) 054502 [0806.4549].

[133] A. Torok, S.R. Beane, W. Detmold, T.C. Luu, K. Orginos, A. Parreno et al., *Meson-Baryon Scattering Lengths from Mixed-Action Lattice QCD*, *Phys. Rev.* **D81** (2010) 074506 [0907.1913].

[134] E.E. Jenkins, A.V. Manohar, J.W. Negele and A. Walker-Loud, *A Lattice Test of 1/N(c) Baryon Mass Relations*, *Phys. Rev.* **D81** (2010) 014502 [0907.0529].

[135] A. Walker-Loud, *Evidence for non-analytic light quark mass dependence in the baryon spectrum*, *Phys. Rev.* **D86** (2012) 074509 [1112.2658].

[136] V. Bernard, N. Kaiser, J. Kambor and U.G. Meissner, *Chiral structure of the nucleon*, *Nucl. Phys.* **B388** (1992) 315.

[137] S.R. Beane and M.J. Savage, *Baryon axial charge in a finite volume*, *Phys. Rev.* **D70** (2004) 074029 [hep-ph/0404131].

[138] R.E. Kass and A.E. Raftery, *Bayes factors*, *Journal of the American Statistical Association* **90** (1995) 773.

[139] H. Akaike, *A new look at the statistical model identification*, *IEEE Transactions on Automatic Control* **19** (1974) 716.

[140] M. Schmelling, *Averaging correlated data*, *Phys.Scripta* **51** (1995) 676.

[141] T. Bhattacharya, V. Cirigliano, S.D. Cohen, A. Filipuzzi, M. Gonzalez-Alonso et al., *Probing Novel Scalar and Tensor Interactions from (Ultra)Cold Neutrons to the LHC*, *Phys.Rev.* **D85** (2012) 054512 [1110.6448].

[142] UCNA collaboration, *Precision measurement of the neutron β-decay asymmetry*, *Phys.Rev.* **C87** (2013) 032501 [1210.7048].

[143] UCNA collaboration, *New result for the neutron β-asymmetry parameter A_0 from UCNA*, *Phys. Rev.* **C97** (2018) 035505 [1712.00884].

[144] D. Mund, B. Maerkisch, M. Deissenroth, J. Krempel, M. Schumann, H. Abele et al., *Determination of the Weak Axial Vector Coupling from a Measurement of the Beta-Asymmetry Parameter A in Neutron Beta Decay*, *Phys. Rev. Lett.* **110** (2013) 172502 [1204.0013].

[145] M. Ademollo and R. Gatto, *Nonrenormalization Theorem for the Strangeness Violating Vector Currents*, *Phys.Rev.Lett.* **13** (1964) 264.

[146] J.F. Donoghue and D. Wyler, *Isospin breaking and the precise determination of V_{ud}*, *Phys.Lett.* **B241** (1990) 243.

[147] V. Cirigliano, J. de Vries, L. Hayen, E. Mereghetti and A. Walker-Loud, *Pion-Induced Radiative Corrections to Neutron β Decay*, *Phys. Rev. Lett.* **129** (2022) 121801 [2202.10439].

[148] R. Alarcon et al., *Precise Measurement of Neutron Decay Parameters*, 2007.

[149] W. Wilburn et al., *Measurement of the neutrino-spin correlation Parameter b in neutron decay using ultracold neutrons*, *Rev. Mex. Fis.* **Suppl. 55** (2009) 119.

[150] Nab collaboration, *Nab: Measurement Principles, Apparatus and Uncertainties*, *Nucl.Instrum.Meth.* **A611** (2009) 211 [0810.0251].

[151] M. Gonzalez-Alonso and J. Martin Camalich, *Isospin breaking in the nucleon mass and the sensitivity of β decays to new physics*, *Phys. Rev. Lett.* **112** (2014) 042501 [1309.4434].

[152] [FLAG 13] S. Aoki, Y. Aoki, C. Bernard, T. Blum, G. Colangelo et al., *Review of lattice results concerning low-energy particle physics*, *Eur.Phys.J.* **C74** (2014) 2890 [1310.8555].

[153] J. Dudek et al., *Physics Opportunities with the 12 GeV Upgrade at Jefferson Lab*, *Eur. Phys. J.* **A48** (2012) 187 [1208.1244].

[154] Z. Ye, N. Sato, K. Allada, T. Liu, J.-P. Chen, H. Gao et al., *Unveiling the nucleon tensor charge at Jefferson Lab: A study of the SoLID case*, *Phys. Lett.* **B767** (2017) 91 [1609.02449].

[155] H.-W. Lin, W. Melnitchouk, A. Prokudin, N. Sato and H. Shows, *First Monte Carlo Global Analysis of Nucleon Transversity with Lattice QCD Constraints*, *Phys. Rev. Lett.* **120** (2018) 152502 [1710.09858].

[156] M. Radici and A. Bacchetta, *First Extraction of Transversity from a Global Analysis of Electron-Proton and Proton-Proton Data*, *Phys. Rev. Lett.* **120** (2018) 192001 [1802.05212].

[157] [ETM 23] C. Alexandrou, S. Bacchio, M. Constantinou, J. Finkenrath, R. Frezzotti, B. Kostrzewa et al., *Nucleon axial and pseudoscalar form factors using twisted-mass fermion ensembles at the physical point*, *Phys. Rev. D* **109** (2024) 034503 [2309.05774].

[158] [PNDME 23] Y.-C. Jang, R. Gupta, T. Bhattacharya, B. Yoon and H.-W. Lin, *Nucleon isovector axial form factors*, *Phys. Rev. D* **109** (2024) 014503 [2305.11330].

[159] [CalLat 19] A. Walker-Loud et al., *Lattice QCD Determination of g_A*, *PoS* **CD2018** (2020) 020 [1912.08321].

[160] [ETM 19] C. Alexandrou, S. Bacchio, M. Constantinou, J. Finkenrath, K. Hadjiyiannakou, K. Jansen et al., *Nucleon axial, tensor, and scalar charges and σ-terms in lattice QCD*, *Phys. Rev. D* **102** (2020) 054517 [1909.00485].

[161] [Mainz 24] D. Djukanovic, G. von Hippel, H.B. Meyer, K. Ottnad and H. Wittig, *Improved analysis of isovector nucleon matrix elements with $N_f = 2 + 1$ flavors of $O(a)$ improved Wilson fermions*, *Phys. Rev. D* **109** (2024) 074507 [2402.03024].

[162] [PACS 23] R. Tsuji, Y. Aoki, K.-I. Ishikawa, Y. Kuramashi, S. Sasaki, K. Sato et al., *Nucleon form factors in $N_f = 2+1$ lattice QCD at the physical point: Finite lattice spacing effect on the root-mean-square radii*, *Phys. Rev. D* **109** (2024) 094505 [2311.10345].

[163] [RQCD 23] G. S. Bali, S. Collins, S. Heybrock, M. Löffler, R. Rödl, W. Söldner et al., *Octet baryon isovector charges from Nf=2+1 lattice QCD*, *Phys. Rev. D* **108** (2023) 034512 [2305.04717].

[164] [QCDSF/UKQCD/CSSM 23] R. E. Smail et al., *Constraining beyond the standard model nucleon isovector charges*, *Phys. Rev. D* **108** (2023) 094511 [2304.02866].

[165] [PACS 22B] R. Tsuji, N. Tsukamoto, Y. Aoki, K.-I. Ishikawa, Y. Kuramashi, S. Sasaki et al., *Nucleon isovector couplings in $N_f = 2 + 1$ lattice QCD at the physical point*, *Phys. Rev. D* **106** (2022) 094505 [2207.11914].

[166] [Mainz 22] D. Djukanovic, G. von Hippel, J. Koponen, H.B. Meyer, K. Ottnad, T. Schulz et al., *Isovector axial form factor of the nucleon from lattice QCD*, *Phys. Rev. D* **106** (2022) 074503 [2207.03440].

[167] [NME 21] S. Park, R. Gupta, B. Yoon, S. Mondal, T. Bhattacharya, Y.-C. Jang et al., *Precision Nucleon Charges and Form Factors Using 2+1-flavor Lattice QCD*, *Phys. Rev. D* **105** (2022) 054505 [2103.05599].

[168] [RBC 08] H.-W. Lin, T. Blum, S. Ohta, S. Sasaki and T. Yamazaki, *Nucleon structure with two flavors of dynamical domain-wall fermions*, *Phys.Rev.* **D78** (2008) 014505 [0802.0863].

[169] [LHPC 05] R. G. Edwards et al., *The nucleon axial charge in full lattice QCD*, *Phys. Rev. Lett.* **96** (2006) 052001 [hep-lat/0510062].

[170] [LHPC 12A] J. R. Green, M. Engelhardt, S. Krieg, J.W. Negele, A.V. Pochinsky and S.N. Syritsyn, *Nucleon Structure from Lattice QCD Using a Nearly Physical Pion Mass*, *Phys. Lett.* **B734** (2014) 290 [1209.1687].

[171] [LHPC 12] J. R. Green, J.W. Negele, A.V. Pochinsky, S.N. Syritsyn, M. Engelhardt and S. Krieg, *Nucleon Scalar and Tensor Charges from Lattice QCD with Light Wilson Quarks*, *Phys. Rev.* **D86** (2012) 114509 [1206.4527].

[172] [χQCD 21A] L. Liu, T. Chen, T. Draper, J. Liang, K.-F. Liu, G. Wang et al., *Nucleon isovector scalar charge from overlap fermions*, *Phys. Rev. D* **104** (2021) 094503 [2103.12933].

[173] [RBC/UKQCD 19] M. Abramczyk, T. Blum, T. Izubuchi, C. Jung, M. Lin, A. Lytle et al., *Nucleon mass and isovector couplings in 2+1-flavor dynamical domain-wall lattice QCD near physical mass*, *Phys. Rev. D* **101** (2020) 034510 [1911.03524].

[174] [ETM 22] C. Alexandrou et al., *Moments of the nucleon transverse quark spin densities using lattice QCD*, *Phys. Rev. D* **107** (2023) 054504 [2202.09871].

[175] M. Constantinou, R. Horsley, H. Panagopoulos, H. Perlt, P.E.L. Rakow, G. Schierholz et al., *Renormalization of local quark-bilinear operators for N_f=3 flavors of stout link nonperturbative clover fermions*, *Phys. Rev. D* **91** (2015) 014502 [1408.6047].

[176] [ETM 15F] C. Alexandrou, M. Constantinou and H. Panagopoulos, *Renormalization functions for Nf=2 and Nf=4 twisted mass fermions*, *Phys. Rev. D* **95** (2017) 034505 [1509.00213].

[177] Particle Data Group collaboration, *Review of Particle Physics*, *PTEP* **2022** (2022) 083C01.

[178] A. Walker-Loud, C.E. Carlson and G.A. Miller, *The Electromagnetic Self-Energy Contribution to $M_p - M_n$ and the Isovector Nucleon MagneticPolarizability*, *Phys. Rev. Lett.* **108** (2012) 232301 [1203.0254].

[179] P.E. Shanahan, A.W. Thomas and R.D. Young, *Strong contribution to octet baryon mass splittings*, *Phys. Lett. B* **718** (2013) 1148 [1209.1892].

[180] S.R. Beane, K. Orginos and M.J. Savage, *Strong-isospin violation in the neutron proton mass difference from fully-dynamical lattice QCD and PQQCD*, *Nucl. Phys.* **B768** (2007) 38 [hep-lat/0605014].

[181] [QCDSF/UKQCD 12A] R. Horsley, J. Najjar, Y. Nakamura, D. Pleiter, P.E.L. Rakow, G. Schierholz et al., *Isospin breaking in octet baryon mass splittings*, *Phys. Rev. D* **86** (2012) 114511 [1206.3156].

[182] [RM123 13] G. M. de Divitiis, R. Frezzotti, V. Lubicz, G. Martinelli, R. Petronzio et al., *Leading isospin breaking effects on the lattice*, *Phys.Rev.* **D87** (2013) 114505 [1303.4896].

[183] [BMW 13A] Sz. Borsanyi et al., *Isospin splittings in the light baryon octet from lattice QCD and QED*, *Phys. Rev. Lett.* **111** (2013) 252001 [1306.2287].

[184] [BMW 14] Sz. Borsanyi et al., *Ab initio calculation of the neutron-proton mass difference*, *Science* **347** (2015) 1452 [1406.4088].

[185] [QCDSF/UKQCD 15] R. Horsley et al., *Isospin splittings of meson and baryon masses from three-flavor lattice QCD + QED*, *J. Phys.* **G43** (2016) 10LT02 [1508.06401].

[186] D.A. Brantley, B. Joo, E.V. Mastropas, E. Mereghetti, H. Monge-Camacho, B.C. Tiburzi et al., *Strong isospin violation and chiral logarithms in the baryon spectrum*, 1612.07733.

[187] M. Radici, A. Courtoy, A. Bacchetta and M. Guagnelli, *Improved extraction of valence transversity distributions from inclusive dihadron production*, *JHEP* **05** (2015) 123 [1503.03495].

[188] Z.-B. Kang, A. Prokudin, P. Sun and F. Yuan, *Extraction of Quark Transversity Distribution and Collins Fragmentation Functions with QCD Evolution*, *Phys. Rev.* **D93** (2016) 014009 [1505.05589].

[189] Z.-B. Kang, *private communication, Jun. 2015.*

[190] G.R. Goldstein, J.O. Gonzalez Hernandez and S. Liuti, *Flavor dependence of chiral odd generalized parton distributions and the tensor charge from the analysis of combined π^0 and η exclusive electroproduction data*, 1401.0438.

[191] M. Pitschmann, C.-Y. Seng, C.D. Roberts and S.M. Schmidt, *Nucleon tensor charges and electric dipole moments*, *Phys. Rev.* **D91** (2015) 074004 [1411.2052].

[192] J. Benel, A. Courtoy and R. Ferro-Hernandez, *A constrained fit of the valence transversity distributions from dihadron production*, *Eur. Phys. J. C* **80** (2020) 465 [1912.03289].

[193] U. D'Alesio, C. Flore and A. Prokudin, *Role of the Soffer bound in determination of transversity and the tensor charge*, *Phys. Lett. B* **803** (2020) 135347 [2001.01573].

[194] JAM collaboration, *Transversity Distributions and Tensor Charges of the Nucleon: Extraction from Dihadron Production and Their Universal Nature*, *Phys. Rev. Lett.* **132** (2024) 091901 [2306.12998].

[195] M.A. Shifman, A.I. Vainshtein and V.I. Zakharov, *Remarks on Higgs Boson Interactions with Nucleons*, *Phys. Lett.* **78B** (1978) 443.

[196] K.G. Chetyrkin, B.A. Kniehl and M. Steinhauser, *Decoupling relations to O (alpha-s**3) and their connection to low-energy theorems*, *Nucl. Phys.* **B510** (1998) 61 [hep-ph/9708255].

[197] R.J. Hill and M.P. Solon, *Standard Model anatomy of WIMP dark matter direct detection II: QCD analysis and hadronic matrix elements*, *Phys. Rev.* **D91** (2015) 043505 [1409.8290].

[198] European Muon collaboration, *A Measurement of the Spin Asymmetry and Determination of the Structure Function g(1) in Deep Inelastic Muon-Proton Scattering*, *Phys. Lett.* **B206** (1988) 364.

[199] X.-D. Ji, *Gauge-Invariant Decomposition of Nucleon Spin*, *Phys. Rev. Lett.* **78** (1997) 610 [hep-ph/9603249].

[200] R.L. Jaffe and A. Manohar, *The G(1) Problem: Fact and Fantasy on the Spin of the Proton*, *Nucl. Phys.* **B337** (1990) 509.

[201] M. Pospelov and A. Ritz, *Electric dipole moments as probes of new physics*, *Annals Phys.* **318** (2005) 119 [hep-ph/0504231].

[202] C. Abel et al., *Measurement of the Permanent Electric Dipole Moment of the Neutron*, *Phys. Rev. Lett.* **124** (2020) 081803 [2001.11966].

[203] C. Baker, D. Doyle, P. Geltenbort, K. Green, M. van der Grinten et al., *An Improved experimental limit on the electric dipole moment of the neutron*, *Phys.Rev.Lett.* **97** (2006) 131801 [hep-ex/0602020].

[204] C.-Y. Seng, *Reexamination of The Standard Model Nucleon Electric Dipole Moment*, *Phys. Rev.* **C91** (2015) 025502 [1411.1476].

[205] [PNDME 20] S. Park, T. Bhattacharya, R. Gupta, Y.-C. Jang, B. Joo, H.-W. Lin et al., *Nucleon charges and form factors using clover and HISQ ensembles*, *PoS* **LATTICE2019** (2020) 136 [2002.02147].

[206] [Mainz 19A] D. Djukanovic, H. Meyer, K. Ottnad, G. von Hippel, J. Wilhelm and H. Wittig, *Strange nucleon form factors and isoscalar charges with $N_f = 2 + 1$ $\mathcal{O}(a)$-improved Wilson fermions*, *PoS* **LATTICE2019** (2019) 158 [1911.01177].

[207] S. Park, T. Bhattacharya, R. Gupta, H.-W. Lin, S. Mondal and B. Yoon, *Update on flavor diagonal nucleon charges*, *PoS* **LATTICE2022** (2023) 118 [2301.07890].

[208] S. Park, T. Bhattacharya, R. Gupta, H.-W. Lin, S. Mondal and B. Yoon, *Update on flavor diagonal nucleon charges from clover fermions*, *PoS* **LATTICE2023** (2024) 328 [2401.00721].

[209] M. Engelhardt, *Strange quark contributions to nucleon mass and spin from lattice QCD*, *Phys. Rev.* **D86** (2012) 114510 [1210.0025].

[210] B.A. Kniehl and O.L. Veretin, *Bilinear quark operators in the RI/SMOM scheme at three loops*, *Phys. Lett. B* **804** (2020) 135398 [2002.10894].

[211] [Mainz 23] A. Agadjanov, D. Djukanovic, G. von Hippel, H.B. Meyer, K. Ottnad and H. Wittig, *Nucleon Sigma Terms with $N_f = 2 + 1$ Flavors of $O(a)$-Improved Wilson Fermions*, *Phys. Rev. Lett.* **131** (2023) 261902 [2303.08741].

[212] [MILC 12C] W. Freeman and D. Toussaint, *Intrinsic strangeness and charm of the nucleon using improved staggered fermions*, *Phys. Rev.* **D88** (2013) 054503 [1204.3866].

[213] [MILC 09D] D. Toussaint and W. Freeman, *The Strange quark condensate in the nucleon in 2+1 flavor QCD*, *Phys. Rev. Lett.* **103** (2009) 122002 [0905.2432].

[214] J.M. Alarcon, J. Martin Camalich and J.A. Oller, *The chiral representation of the πN scattering amplitude and the pion-nucleon sigma term*, *Phys. Rev.* **D85** (2012) 051503 [1110.3797].

[215] Y.-H. Chen, D.-L. Yao and H.Q. Zheng, *Analyses of pion-nucleon elastic scattering amplitudes up to $O(p^4)$ in extended-on-mass-shell subtraction scheme*, *Phys. Rev.* **D87** (2013) 054019 [1212.1893].

[216] M. Hoferichter, J. Ruiz de Elvira, B. Kubis and U.-G. Meissner, *High-Precision Determination of the Pion-Nucleon σ Term from Roy-Steiner Equations*, *Phys. Rev. Lett.* **115** (2015) 092301 [1506.04142].

[217] [HPQCD 05] Q. Mason, H. D. Trottier, R. Horgan, C. T. H. Davies and G. P. Lepage, *High-precision determination of the light-quark masses from realistic lattice QCD*, *Phys. Rev.* **D73** (2006) 114501 [hep-ph/0511160].

[218] C. McNeile, A. Bazavov, C.T.H. Davies, R.J. Dowdall, K. Hornbostel, G.P. Lepage et al., *Direct determination of the strange and light quark condensates from full lattice QCD*, *Phys. Rev.* **D87** (2013) 034503 [1211.6577].

[219] [BMW 20A] Sz. Borsanyi, Z. Fodor, C. Hoelbling, L. Lellouch, K. Szabo, C. Torrero et al., *Ab-initio calculation of the proton and the neutron's scalar couplings for new physics searches*, 2007.03319.

[220] [ETM 14A] C. Alexandrou, V. Drach, K. Jansen, C. Kallidonis and G. Koutsou, *Baryon spectrum with $N_f = 2 + 1 + 1$ twisted mass fermions*, *Phys. Rev.* **D90** (2014) 074501 [1406.4310].

[221] [RQCD 22] G. S. Bali, S. Collins, P. Georg, D. Jenkins, P. Korcyl, A. Schäfer et al., *Scale setting and the light baryon spectrum in $N_f = 2 + 1$ QCD with Wilson fermions*, *JHEP* **05** (2023) 035 [2211.03744].

[222] [BMW 15] S. Dürr et al., *Lattice computation of the nucleon scalar quark contents at the physical point*, *Phys. Rev. Lett.* **116** (2016) 172001 [1510.08013].

[223] P. Junnarkar and A. Walker-Loud, *Scalar strange content of the nucleon from lattice QCD*, *Phys. Rev.* **D87** (2013) 114510 [1301.1114].

[224] [BMW 11A] S. Dürr et al., *Sigma term and strangeness content of octet baryons*, *Phys. Rev.* **D85** (2012) 014509 [1109.4265], [Erratum: Phys. Rev.D93,no.3,039905(2016)].

[225] [ETM 17A] C. Alexandrou and C. Kallidonis, *Low-lying baryon masses using $N_f = 2$ twisted mass clover-improved fermions directly at the physical pion mass*, *Phys. Rev.* **D96** (2017) 034511 [1704.02647].

[226] C. Kallidonis, *private communication, Nov. 2018.*

[227] J. Martin Camalich, L.S. Geng and M.J. Vicente Vacas, *The lowest-lying baryon masses in covariant SU(3)-flavor chiral perturbation theory*, *Phys. Rev.* **D82** (2010) 074504 [1003.1929].

[228] [QCDSF/UKQCD 11] R. Horsley, Y. Nakamura, H. Perlt, D. Pleiter, P.E.L. Rakow, G. Schierholz et al., *Hyperon sigma terms for 2+1 quark flavours*, *Phys. Rev.* **D85** (2012) 034506 [1110.4971].

[229] P.E. Shanahan, A.W. Thomas and R.D. Young, *Sigma terms from an SU(3) chiral extrapolation*, *Phys. Rev.* **D87** (2013) 074503 [1205.5365].

[230] [BMW 08] S. Dürr et al., *Ab-initio determination of light hadron masses*, *Science* **322** (2008) 1224 [0906.3599].

[231] A. Crivellin, M. Hoferichter and M. Procura, *Accurate evaluation of hadronic uncertainties in spin-independent WIMP-nucleon scattering: Disentangling two- and three-flavor effects*, *Phys. Rev.* **D89** (2014) 054021 [1312.4951].

[232] J. Ruiz de Elvira, M. Hoferichter, B. Kubis and U.-G. Meissner, *Extracting the σ-term from low-energy pion-nucleon scattering*, *J. Phys.* **G45** (2018) 024001 [1706.01465].

[233] M. Hoferichter, J.R. de Elvira, B. Kubis and U.-G. Meißner, *On the role of isospin violation in the pion–nucleon σ-term*, *Phys. Lett. B* **843** (2023) 138001 [2305.07045].

[234] [PNDME 20A] S. Mondal, R. Gupta, S. Park, B. Yoon, T. Bhattacharya and H.-W. Lin, *Moments of nucleon isovector structure functions in $2 + 1 + 1$-flavor QCD*, *Phys. Rev. D* **102** (2020) 054512 [2005.13779].

[235] [ETM 20C] C. Alexandrou, S. Bacchio, M. Constantinou, J. Finkenrath, K. Hadjiyiannakou, K. Jansen et al., *Complete flavor decomposition of the spin and momentum fraction of the proton using lattice QCD simulations at physical pion mass*, *Phys. Rev. D* **101** (2020) 094513 [2003.08486].

[236] [ETM 19A] C. Alexandrou et al., *Moments of nucleon generalized parton distributions from lattice QCD simulations at physical pion mass*, *Phys. Rev. D* **101** (2020) 034519 [1908.10706].

[237] [LHPC 24] M. Rodekamp, M. Engelhardt, J.R. Green, S. Krieg, S. Liuti, S. Meinel et al., *Moments of nucleon unpolarized, polarized, and transversity parton distribution functions from lattice QCD at the physical point*, *Phys. Rev. D* **109** (2024) 074508 [2401.05360].

[238] [NME 21A] S. Mondal, T. Bhattacharya, R. Gupta, B. Joó, H.-W. Lin, S. Park et al., *Nucleon isovector momentum fraction, helicity and transversity moment using Lattice QCD*, *PoS* **LATTICE2021** (2021) 513 [2201.00067].

[239] [NME 20] S. Mondal, R. Gupta, S. Park, B. Yoon, T. Bhattacharya, B. Joó et al., *Nucleon momentum fraction, helicity and transversity from 2+1-flavor lattice QCD*, *JHEP* **21** (2020) 004 [2011.12787].

[240] [χQCD 18A] Y.-B. Yang, J. Liang, Y.-J. Bi, Y. Chen, T. Draper, K.-F. Liu et al., *Proton Mass Decomposition from the QCD Energy Momentum Tensor*, *Phys. Rev. Lett.* **121** (2018) 212001 [1808.08677].

[241] [RQCD 18] G. S. Bali, S. Collins, M. Göckeler, R. Rödl, A. Schäfer and A. Sternbeck, *Nucleon generalized form factors from two-flavor lattice QCD*, *Phys. Rev. D* **100** (2019) 014507 [1812.08256].

[242] [RQCD 14A] G. Bali, S. Collins, B. Gläßle, M. Göckeler, J. Najjar, R.H. Rödl et al., *The moment $\langle x\rangle_{u-d}$ of the nucleon from $N_f = 2$ lattice QCD down to nearly physical quark masses*, *Phys. Rev.* **D90** (2014) 074510 [1408.6850].

[243] L.A. Harland-Lang, A.D. Martin, P. Motylinski and R.S. Thorne, *Parton distributions in the LHC era: MMHT 2014 PDFs*, *Eur. Phys. J. C* **75** (2015) 204 [1412.3989].

[244] H1, ZEUS collaboration, *Combination of measurements of inclusive deep inelastic $e^{\pm}p$ scattering cross sections and QCD analysis of HERA data*, *Eur. Phys. J. C* **75** (2015) 580 [1506.06042].

[245] S. Dulat, T.-J. Hou, J. Gao, M. Guzzi, J. Huston, P. Nadolsky et al., *New parton distribution functions from a global analysis of quantum chromodynamics*, *Phys. Rev. D* **93** (2016) 033006 [1506.07443].

[246] A. Accardi, L.T. Brady, W. Melnitchouk, J.F. Owens and N. Sato, *Constraints on large-x parton distributions from new weak boson production and deep-inelastic scattering data*, *Phys. Rev. D* **93** (2016) 114017 [1602.03154].

[247] S. Alekhin, J. Blümlein, S. Moch and R. Placakyte, *Parton distribution functions, α_s, and heavy-quark masses for LHC Run II*, *Phys. Rev. D* **96** (2017) 014011 [1701.05838].

[248] NNPDF collaboration, *Parton distributions from high-precision collider data*, *Eur. Phys. J. C* **77** (2017) 663 [1706.00428].

[249] JAM collaboration, *Strange quark suppression from a simultaneous Monte Carlo analysis of parton distributions and fragmentation functions*, *Phys. Rev. D* **101** (2020) 074020 [1905.03788].

[250] T.-J. Hou et al., *New CTEQ global analysis of quantum chromodynamics with high-precision data from the LHC*, *Phys. Rev. D* **103** (2021) 014013 [1912.10053].

[251] D. de Florian, R. Sassot, M. Stratmann and W. Vogelsang, *Extraction of Spin-Dependent Parton Densities and Their Uncertainties*, *Phys. Rev. D* **80** (2009) 034030 [0904.3821].

[252] NNPDF collaboration, *A first unbiased global determination of polarized PDFs and their uncertainties*, *Nucl. Phys. B* **887** (2014) 276 [1406.5539].

[253] J.J. Ethier, N. Sato and W. Melnitchouk, *First simultaneous extraction of spin-dependent parton distributions and fragmentation functions from a global QCD analysis*, *Phys. Rev. Lett.* **119** (2017) 132001 [1705.05889].